# ANTAL KERPELY DOCTORAL SCHOOL OF MATERIALS SCIENCE & TECHNOLOGY


## Development of ceramic particle reinforced SAC305 lead-free solder composite material

A Ph.D. dissertation submitted to Antal Kerpely Doctoral School for the degree of

Doctor of Philosophy in the subject of Material Science and Technology

By

**Manoj Kumar Pal**

Supervisors

**Prof. Zoltán Gácsi (Professor)**

**Dr. Gergely Gréta (Associate Professor)**

Head of the Doctoral School

**Prof. Zoltán Gácsi**

Institute of Metallurgy, Metal Forming, and Nanotechnology

Faculty of Material Science and Engineering

University of Miskolc, Hungary-3515

November 2020

# List of abbreviation

The symbols are listed according to the order of appearance in the text.

| Symbol | Description | Units |
|---|---|---|
| $t_o$ | Spreading time | s |
| $E_a$ | Activation energy | kJ/mol |
| $R$ | Universal gas constant | J/K.mol |
| $T$ | Absolute temperature | K |
| $\Gamma^k$ | Amount of adsorption | $cm^3$ |
| $c$ | Total concentration | mol/L |
| $\gamma^k$ | Surface energy of molten solder k | N/m |
| $\rho$ | Density | g/cc |
| g | Weight | g |
| $P_c$ | Contact perimeter | µm |
| $P_{nc}$ | Non–contact perimeter | µm |
| β | Skewness | |
| $q$ | Total number of quadrats | |
| $N_{qi}$ | Number of reinforcement particles in the $i^{th}$ quadrat ($i$ = 1,2,..,$q$), | |
| $N_q^{mean}$ | Mean number of reinforcement particles/ quadrat | |
| σ | Standard deviation | |
| $x_t$ | Average thickness | µm |
| $A$ | Area of the IMCs | $µm^2$ |
| $L$ | Length | µm |
| $x_t$ | IMCs layer thickness at time t | µm |
| $t$ | Aging time | s |
| $x_0$ | Initial layer thickness | µm |
| $D$ | Diffusion coefficient | $µm^2/s$ |
| $n$ | Time exponent | |
| F | Applied load | g |

| | | |
|---|---|---|
| $d$ | Sample diameter | mm |
| $S_f$ | Spread factor | |
| h | Sample height | mm |
| $S_r$ | Spread ratio | |
| $\theta$ | Contact angle | $^{o}$ |

# 1. CHAPTER 1: Introduction

Customer demand has shown the industry to progress for smaller, faster, and low-cost electronics products. People need always smaller and faster devices with good performance and integrity by utilizing minimum energy and materials. The manufacturer starts to produce smaller mechanical, optical, and electronic products and devices (for example mobile phones, chips, and computers). Thus, electronics miniaturization has challenged to fabricate materials, processing conditions, and reliability of the product. Cost and performance are important technological keys for product evaluation **[1].**

The execution of lead-free solders is generated remarkable new challenges in the microelectronics sector **[2]**. Soldering is a metallurgical process that is used to join two (or more) materials by using a third material, which is called solder alloy that has a lower melting temperature than materials to be joint. Solder alloys are usually eutectic (63Sn–37Pb) or near-eutectic (60Sn–40Pb) alloys consisting of an Sn matrix with reinforcements of one or more elements used to reach certain desired physical, mechanical, and chemical properties of the alloy **[3].**

However, in the 1950s, the United States Environmental Protection Agency (EPA) considered Pb to be one of the dangers that posed the greatest risk to humans and the environment **[4].** When lead released into the atmosphere, the kidneys, brain, and nervous system directly affected it. Lead not only affects humans, but also the environment. Two types of risk (direct and indirect) are possible from the lead. The direct risk includes workers who are working in the electronics industry to whom solder fumes and fine lead-retaining particles are exposed during the manufacture of electronic components. The indirect risk is caused by the leaching of the electronic waste components by the effect of rain and groundwater contamination **[2].** To prevent environmental pollution, the European Union (EU) banned Pb material after 2006 and it is proposed the Waste for Electronic and Electrical Equipment (WEEE) and the Restriction of Hazardous Substance (RoHS) directive in January 2008 **[5][6][7][8]**. The purpose of these directives is to reduce waste electrical and electronic equipment and to minimize the hazardous substances in electrical and electronic equipment. This directive stated that electronic products sold to European consumers must be Pb–free and this is called lead-free for electronics **[9]**.

Sn–Pb solders require lead-free (green) replacement. Higher melting temperature (~ 220°C) and the cost of the metals are the main problems in the transformation to lead-free solders. High temperatures can propagate in lamination, low thermal fatigue, and crack formation in solder joints

**[10][11]**. For Pb–free soldering, several potential alloys have been developed, most of the alloys which contain Sn as the primary element. Sn–based solder alloys are a good choice because they have excellent wetting and spreading properties. Combining Sn with copper (Cu) and silver (Ag) looks like a probable Pb-free applicant **[12]**.

New solders are usually Sn-based and the main benchmark for the selection of lead–free solder is that the alloy should be eutectic alloy close. The Sn–Ag–Cu (SAC) is the strongest opponent of Pb-free soldering because it is near to eutectic. NEMI (National Electronics Manufacturing Initiative), Japan Electronics and Information Technology Industries Association (JEITA) suggested an Ag rich composition Sn–3.9Ag–0.6Cu(SAC396), Sn–3.0Ag–0.5Cu(SAC305), and Sn–3.5Ag–0.7Cu(SAC357), and The European Consortium – BRITE-EURAM recommended 95.5wt%Sn–3.8wt%Ag–0.7wt%Cu; Sn–3.8Ag–0.7Cu(SAC387), etc. **[13][14].**

To improve dimensional stability and mechanical reliability of electronic interconnections, there were several attempts to incorporate suitable reinforcement (including metal, ceramic, IMCs, and carbon nanomaterials, etc.) into lead-free solder matrices to prepare the composite solders and it's interconnection. The existence of different reinforcement added could refine the morphology of composite solders and its interfacial IMCs between solder joints and substrate. The added reinforcements could improve the wettability of the composite solder. The refinement of the IMCs greatly improves the reliability of the solder joint and mechanical properties of the solders it might also help to improve the creep resistance and mechanical properties of composite solder joints under harsh service conditions (including high temperature, large temperature gradient, and high current density) when compared with the plain solder joints.

The present dissertation is concentrated on the preparation and characterization of 96.5Sn–3Ag–0.5Cu(SAC305) composite solders containing reinforcement (SiC and SiC–Ni) and the investigation of the microstructural and mechanical properties of composite solder and its joints under the conditions of isothermal aging. The formation of IMCs in lead-free solders with weight variation during the reflow process due to lack of proven data. This research is examined the distribution of the reinforcement in the solder matrix, optimal reflow settings for lead–free solder, and the factor that influences the process are investigated.

# 2. CHAPTER 2: Literature review

## 1.1 Composite solder material

For many years, solder alloys containing the combinations of tin (Sn), lead (Pb), antimony (Sb), copper (Cu), silver (Ag), bismuth (Bi), indium (In), zinc (Zn), gold (Au), silicon (Si) and germanium (Ge) have been used in many industrial applications. Among these, tin-lead (Sn–Pb) solder alloys, particularly with compositions ranging between Sn95-Pb5 and Sn2-Pb98 (wt.%) have been attracted much attention due to their low cost and low/moderate melting temperatures (183 to 316°C) **[4]**.

Even it has been already commercialized; the Sn–Ag–Cu alloy system has several problems to be solved. One of the major problems is the formation of large intermetallic compounds (IMC) in these alloys **[15]**. The presence of large IMCs greatly reduces the reliability of the solder joint. These IMCs act as stress concentrators and negatively affects the mechanical properties of the solders. Another problem is the poor wetting of the solder alloys. To have a reliable solder joint, there must be a strong bonding between the solder and the surfaces to be jointed. To achieve this strong bond with the smallest amount of solder volume, the solder alloy must wet the largest possible area. The importance of wetting of the solder alloy has increased vitally in the past decade since the sizes of the microelectronic devices have decreased drastically.

There are many different lead-free alloys available nowadays. A solder alloy that is being proposed for the replacement of the traditional Sn–Pb eutectic composition should have its melting point as close as possible to the tin-lead eutectic temperature. The selections are based on a variety of considerations, including toxicity, physical properties (melting temperature, surface tension, wettability, thermal and electrical conductivity), mechanical properties, microstructure characteristics, electrochemical properties (corrosion, oxidation and dross formation, and compatibility with non-clean fluxes), manufacturability, cost, and availability **[16][17][3].** The preference is given to the Sn–Ag–Cu (SAC) alloy family, followed by alloys containing, silver, copper, bismuth, antimony, indium, zinc, and aluminum.

Among all the requirements, wettability (bondability) and suitable melting temperature are the two basics. First, the solder must be capable of wet and bond which indicates that it should be able to form intermetallic compounds with Cu. Second, the melting temperature should be sufficiently low enough to be reflowed as a paste and high enough to avoid the defects due to operating temperatures. Currently, the replacement alloys candidates include ternary, binary, and some

quaternary alloys of Sn with Ag, Zn, In, Sb, Bi, and Cu **[4]**. Solder composites developed by other investigators have been summarized in **Table 2.1.**

*Table 2.1 Existing solder composites*

| Matrix | Reinforcement | Author | Conclusions |
|---|---|---|---|
| Sn–3.5Ag–0.5Cu | ZnO | **[18]** | • The results showed a slightly increased melting temperature, increased the tensile strength, and inhibited the growth of the grain size as well as the IMCs $Ag_3Sn$ and $Cu_6Sn_5$. |
| | $ZrO_2$ | **[19]** | • The results showed the improvement of the wettability. |
| | $Y_2O_3$ | **[20]** | • The results showed the refinement of the IMCs grains and improved the shear strength. |
| | $Al_2O_3$ | **[21]** | • The results showed exhibit lower density, CTE, refined the Ag3Sn, Increased the YS and UTS, increased ductility of the composite solders. |
| | | **[22]** | • The results indicated the refinement of the IMCs grains, improved shear strength and the thickness of the IMC layer increased continuously with increasing numbers of reflow cycles. |
| | | **[23]** | • The results displayed the refinement of the Ag3Sn, improved the microhardness and wetting behavior. |
| Sn–3.7Ag–0.9Zn | SiC | **[24]** | • The results indicated the decrease of the β-Sn dendrites, IMCs, and increase the microhardness. |
| Sn–3.5Ag–0.25Cu | $TiO_2$ | **[25]** | • The results showed the increase in the liquidus temperature, refine both the grain size and morphology of Ag3Sn, increase the microhardness, 0.2YS, and UTS of the composite solder. |
| Sn–0.7Cu–0.05Ni | $TiO_2$ | **[26]** | • The results indicated the decrease of wetting properties, suppressing the growth of the $Cu_6Sn_5$ IMC layer, improved the shear strength, and decreased the CTE value. |
| Sn–1.0Ag–0.5Cu | $Fe_2O_3$ | **[27]** | • The results showed the refinement of the β-Sn grain and reduce the CTE, the suppressing formation, and growth |

| | | | |
|---|---|---|---|
| | SiC | **[28]** | of interfacial IMCs during reflowing and thermal cycling (TC), enhancing the shear strength of the solder joints. |
| | | **[29]** | • The results showed the improvement of the plasticity and refinement of the primary β-Sn grain.<br>• The results displayed smaller β-Sn sub-grains, refined IMCs with the greater eutectic area, an improvement in the 0.2 % YS and UTS, and decreased ductility. |
| Sn–3.5Ag–0.7Cu | $TiO_2$ | **[30]** | • The results displayed the suppression of the IMC layer and improved the wetting. |
| Sn–3.5Ag | $SnO_2$ | **[31]** | • The results showed the improvement of the hardness and tensile strength. |
| | | **[32]** | • The results showed the lower porosity, improvement of microhardness, higher 0.2% YS and UTS. |
| Sn–3.8Ag–0.7Cu | SiC | **[33]** | • The results displayed the lower melting, improvement of microhardness, and refined IMCs grains. |
| | SWCNT | **[34]** | • The results indicated an increase in tensile strength, hardness, better melting characteristics, and a slight decrement in elongation to failure. |
| Sn–4In–4.1Ag–0.5Cu | $Al_2O_3$ | **[35]** | • The results showed lower density and CTE values and increasing both 0.2% YS and UTS. |
| Sn–3.5Ag | $ZrO_2$ | **[36]** | • The results showed the refinement of the IMCs grains and the improvement of the microhardness. |
| Sn–9Zn | $Al_2O_3$ | **[37]** | • The results indicated the improvement of the microhardness and the shear strength. |
| Sn–3.0Ag–0.5Cu | $SiO_2$ | **[38]** | • The results displayed improved the wettability and refined microstructure. |
| | ZnO | **[39]** | • The results showed the refinement of the β-Sn, improvement of the shear strength, and microhardness. |
| | | **[40]** | • The results showed the improvement of the wettability, behavior, and reduction of the thickness of IMCs layers**.** |
| | $CeO_2$ | **[41]** | • The results indicated the reduction of the IMCs layer thickness. |
| | $SrTiO_3$ | **[42]** | • The results indicated the improvement of the shear strength and the reduction of the IMCs layer thickness. |

| | | | |
|---|---|---|---|
| | $TiO_2$ | **[43]** | • The results showed the refinement of the microstructure and the reduction of the IMCs layer. |
| | TiC | **[44]** | • The results displayed the lower CTE value, improved the wettability, and the reduction of the IMCs' growth. |
| | $La_2O_3$ | **[45]** | • The results showed improved Wettability, refined microstructure. |
| | NiO | **[46]** | • The results displayed the reduction of the IMCs layer thickness, improved hardness, and refined morphology. |
| | $Fe_2NiO_4$ | **[47]** | • The results showed the improved hardness and the reduction of the IMC thickness. |
| | SiC | **[48]** | • The results showed the refined IMCs grains, slightly decrement of the melting temperature, and improvement of the tensile strength. |
| | Ni-coated GNS | **[49]** | • The results displayed the improvement of the hardness and shear strength. |
| Sn–3.5Ag | NiTi Shape memory alloy | **[50]** | • The results indicated a significant reduction of the creep rates and strain ranges. |
| Sn–3.5Ag–0.7Cu | $TiB_2$ | **[51]** | • The results indicated an improvement in wettability, 0.2% YS, UTS, and reduction in ductility. |
| | MWCNT | **[52]** | • The results showed an improvement in wettability, 0.2% YS, UTS, and reduction in ductility. |
| Sn–3.5Ag–0.7Cu | $ZrO_2$ + 8 mol. % $Y_2O_3$ | **[53]** | • The results showed the lower density and ductility improved, however, improved the 0.2% YS, UTS, and CTE values. |
| Sn–0.7Cu | $Al_2O_3$ | **[54]** | • The results indicated the improvement of the microhardness, 0.2% YS and UTS, an increasing number of pores, pore size, and irregularity. |
| | Geopolymer Ceramic | **[55]** | • The results showed the improvement of the hardness and the compressive strength. |
| Sn–58Bi | $Y_2O_3$ | **[56]** | • The results indicated the improvement of the wetting properties, the shear strength; however, the growth rate of the IMC layer decreases slightly. |
| Sn–Ag | $CeO_2$ | **[57]** | • The results showed the improvement of the wear, friction resistance, and microhardness. |

According to **Table 2.1**, various researchers have used the ceramics reinforcements in the lead–free solder matrix and prepared the different types of solder composites. Ceramic reinforcements have some favorable properties (ex. chemical stability, abrasion and wear resistance, high strength, hardness, high melting point (thus high-temperature capability), low density) which makes a promising candidate for the reinforcements. Apart from this, they have poor wetting behavior and due to the brittle nature, high hardness, resistance to creep, and high strength, conventional machining methods are difficult to perform because of cracks, brittle fractures, and edge chipping.

#### *1.1.1 Type of reinforcements*

Due to the reactive properties of reinforcement and molten solder, it can be divided into three parts: (1) non–reactive (2) reactive, and (3) composite reinforcement. The advantages and disadvantages of reinforcement are listed in **Table 2.2**.

*Table 2.2: Type of reinforcements*

| ***Type*** | ***Materials*** | ***Reinforcement*** | ***Advantages*** | ***Disadvantages*** |
|---|---|---|---|---|
| **Non-reactive** | Oxide | $Al_2O_3$, $TiO_2$, $Fe_2O_3$, ZnO [58][23] **[37] [21][43][26][27] [59] [40][18][39]** | Stable physical and Chemical properties during the reflow process | Poor wetting |
| | Carbide | TiC, SiC **[60][29]** | | |
| | Carbon-based nano-materials | CNT, GNS **[61][34][62][63][56]** | | |
| **Reactive** | Metals | Ag, Cu, Fe, Ni, Al, Cr, Mn, Co **[64][65][66][67][68][69][70][71]** | Good wetting | Corrosive, Coarsening during reflow and aging |
| **Hybrids** | Metal/*X* | Ni–coated CNT, Ag–coated GNS **[62][72][73]** | Good dispersibility | Potential risk on reliability; high cost |

Carbon–based materials, Metal oxide, carbide, and nonmetallic elements are non–reactive reinforcements because they do not react with the solder matrix during the aging and reflow process, and they do not coarsen during their service life. However, such types of reinforcements cannot be wetted by the molten solder, during the reflow process generally reveals that they are expelled from the molten solder **[74][49].**

The reactive reinforcement, which is mainly metal (or alloy) materials and IMCs. This type of reinforcements is easily reacted with molten solder during the reflow process and preserved in the solder joint in the form of IMCs layers. Reactive reinforcement is likely to be coarsening during service life, resulting in a decreasing reinforcing effect. Recently, L. Ma et al. **[75]** produced novel reinforcement (polyhedral oligomeric silsesquioxanes polyhedral oligomeric silsesquioxane (POSS)) and composite reinforcement; these types of reinforcements were shown good stability in a soldering process. However, the relatively poor thermal and electrical conductivity of such reinforcement can affect the electrical performance of the solder joint. Also, complexity, high energy consumption, and high costs have limited the practical progress of such reinforcement.

SiC is used because of its low cost and the wide range of sizes and grades available. The addition of SiC increases Young's modulus and tensile strength of the composite materials and it is also increased in wear resistance **[76].** Aqeeli et al. **[76]** reported that SiC can help transfer the shear load at the matrix/reinforcement interface, strengthen the matrix and at the same time retain some ductility. However, while the yield and ultimate strength of the matrix increase with increasing concentration of ceramic particles, the ductility of the composites deteriorate significantly at higher concentrations. SiC has the self-organized dispersive systems property and it can help to formation of the heterogeneous nucleation, thereby distributing stress homogeneously in the solder joints **[77]**. The addition of SiC particles can also improve the sinterability of processed powders. Woo and Zhang **[78]** investigated the SiC-reinforced Al–7Si–0.4Mg composite powders and an increase in the sintering rate of the composite powder was reported due to the increased diffusion rate.

Some researchers **[29][48][24][33]** are prepared for the lead-free solder composites (SAC105/SiC, SAC305/SiC, Sn–3.7Ag–0.9Zn/SiC and SAC387/SiC) with the addition of SiC by mechanically mixing. SiC particles were found to provide additional nucleation places for the formation of the primary β–Sn phase and $Ag_3Sn$ IMCS. The strengthening effect of the composite solders is dependent on the reinforcements and the refined IMCs because these prevent dislocation slipping. Tsao and Chang **[79]** produced Sn–3.5Ag–90.25Cu composite solders with the addition of *x*–$TiO_2$ nanoparticles; it shows that 1wt%$TiO_2$ is the best composition and significant improvements in the mechanical properties. Nai et al. **[32]** also produced the Sn–0.7Cu/$Al_2O_3$ and Sn–3.5Ag/$SnO_2$ lead-free solders composites and evaluated mechanical and physical properties; however, the best results are obtained on the 1.5vol% $Al_2O_3$ and 0.7vol% $SnO_2$, which are better than the Sn–Pb solder. They have also investigated the microstructure of the pores because it is most that the

morphology of pores was observed to be one of the most influencing factors which can affect the strength of composite solder.

As mentioned above, non–reactive reinforcements are evicted from the molten solder during reflow, so it needs to form a bridge between solder and matrix. Au and Ni are considered ideal bridge materials because they are capable to react with Sn-based soldered alloys to form IMCs in a soldering process **[49][49].** Mokhtari et al. **[80]** and Yang et al. **[81][82]** produced the solder composite with the addition of Au coated Silica and Ni–coated carbon nanotubes (Ni–CNT); Their experimental results showed that the addition of coated reinforcements provided to the improvement of the microstructure, mechanical properties and wetting behavior of the solder alloys.

## 1.2 Fabrication of composite solders by PM (powder metallurgy) method

### *1.2.1 Mixing method*

In the current literature, researchers have described several processing methods for synthesizing complex composite solders. These methods can be broadly divided into two parts: (i) powder metallurgy technique and (ii) liquid metallurgy technique. The powder metallurgy technique was applied in the present work. In the mechanical mixing process, reinforcement particles are added as reinforcement to a solder powder, solder paste, or molten solder alloys to produce composite solders. **Figure 2.1a** shows a schematic diagram of the reinforcement and matrix powder mixture and **Figure 2.1b** the homogeneous distribution.

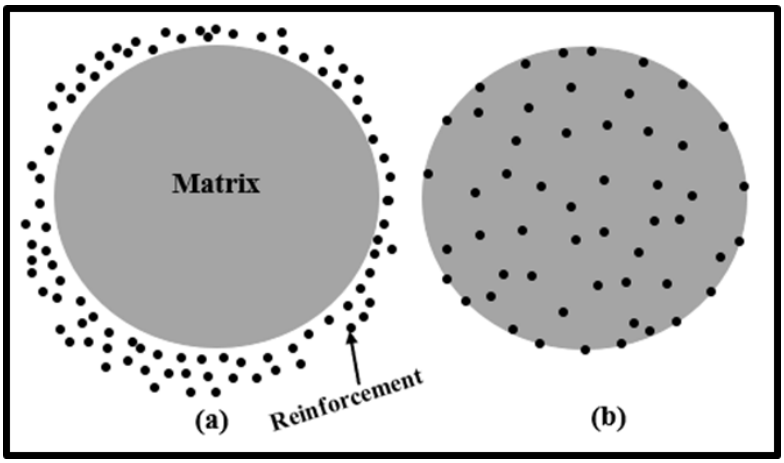


*Figure 2.1 Schematic diagram of reinforcement and matrix powder (modified): (a) before milling (zero-hour milling) and (b) after milling (homogeneous distribution)* ***[83]***

However, it is not easy to achieve a homogeneous and fine dispersion by the liquid metallurgy method due to the dispersion of the oxide particles is uneven due to the counter diffusion of alloying elements towards the surface and sometimes, large oxide particles precipitate at the grain boundaries leading to degradation in the mechanical properties of the composite.

But this method also has some advantages. Because the particles formed in this method are thermodynamically stable, the matrix–particle surfaces are generally clean, free of adsorbed gases, oxide films, and harmful reaction products, and thus much stronger. From the above discussion, it becomes clear that composites are difficult to produce by liquid processing methods, and therefore solid–state processing methods are the most suitable for this purpose **[84].** The advantages of the solid-state processing method are reduced pollution, low costs, and simplicity in process and handling. Also, these factors are especially important in the industry. Parts can be made from a variety of compositions. It is therefore much easy to have parts of desired mechanical and physical properties like density, hardness toughness, stiffness, damping, and specific electrical or magnetic properties. However, this method has some limitations such as the high cost of metal powders compared to the cost of raw material used for casting or forging a component. A few powders are even difficult to store without some deterioration. Large or complex shaped parts are difficult to produce by the solid-state process.

#### *1.2.2 Mechanical mixing method (Powder metallurgy)*

Powder metallurgy (PM) is the most popular manufacturing process. In general, Metal powders are used in the PM process with the specific characteristics of size and shape and then changes it into strong, accurate, and high–performance finished products. There are three main steps to this approach, mixing, compressing, and sintering.

The three main steps (mixing, compacting, and sintering) in the powder metallurgy process are illustrated in **Figure 2.2**. The process employs automated operations with low relative energy consumption, high material consumption, and low cost of capital. The PM method can cost–effectively synthesize complex components, such as automotive components. Accuracy and cost are very important in the casting process; however, the casting process poses several issues such as segregation, machining, and maintaining accuracy. Alloy powders can be fabricated below the melting temperature, segregation and other defects can be eliminated. PM technique can be used to produce porous metals, oxide dispersion alloys, ceramic–metal composites, and cemented

carbides. The powder metallurgy technique is popular because all processes can be performed in the solid-state and microstructural damage caused by elevated temperatures can be avoided. The important properties which lead to the continued development of the PM method are given below **[85][84][86]**:

I. Production of high-quality precision structural and complex parts.
II. Production of difficult–to–process materials where fully dense, high–performance alloys can be produced with uniform microstructure.
III. Economical consolidation of high-performance materials including composites containing mixed/non–equilibrium phases.
IV. Synthesis of non–equilibrium materials such as amorphous, microcrystalline, or metastable alloys.

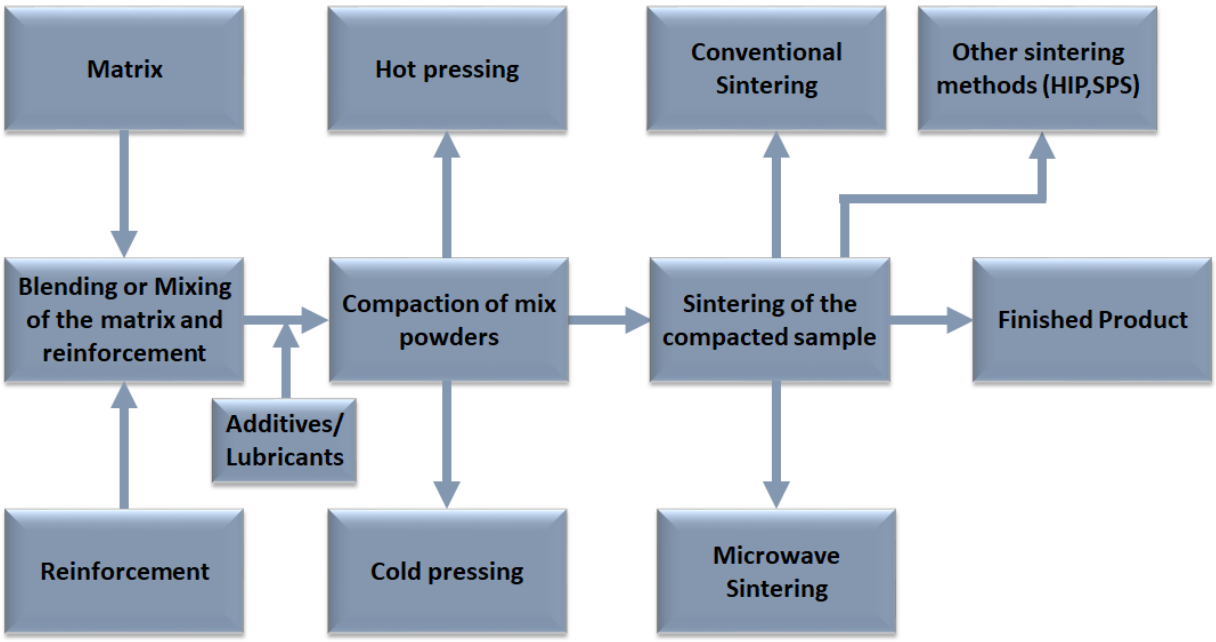


*Figure 2.2 Process of powder metallurgy technique*

A more efficient method is to mix each particle (reinforcements and matrix) by solid-state processing methods, such as mechanical grinding of a mixture of metal particles and ceramic nanoparticles. Sintering is an important step in the PM method in which densification and bond formation takes place. Sintering can be done by conventional heating methods, such as resistance heating, or by microwaves or by plasma, etc. **[87][88][89].**

## 1.3 Selection of Materials for Investigation

### 1.3.1 Solder Matrix Material

As discussed in section 2.1, Sn–3.0Ag–0.5Cu has superior mechanical properties compared to the other lead-free solders and particularly conventional eutectic Sn–Pb, Therefore, commercial lead-free solder alloy, Sn–3.0Ag–0.5Cu (SAC305) was selected as a matrix material.

### 1.3.2 Reinforcement Materials

In comparison to other ceramic reinforcing particles, SiC is also a typical ceramic material with excellent chemical stability, low density (3.21 g/cm$^3$), and high melting temperature (2,730 ºC); it also exhibits good mechanical properties. Additionally, it has also high electrical and thermal conductivity; so for this reason, SiC a potential reinforcement for composite solders without affecting significantly their performance. SiC is supported to form self-organized dispersive systems that can help to formation of the heterogeneous nucleation so that stress can be distributed homogeneously in the solder joints. SiC particles were found to provide additional nucleation places for the formation of the primary β–Sn phase and $Ag_3Sn$ IMCS. The strengthening effect of the composite solders is dependent on the reinforcements and the refined IMCs because these prevent dislocation slipping **[29][48][24][33]. Table 2.3** shows the advantages of SiC ceramic reinforcement.

*Table 2.3 Advantages of the SiC ceramic reinforcement*

| ***Reinforcement*** | ***Advantages*** | **Reference** |
|---|---|---|
| **SiC** | • Low cost and a wide range of sizes and grades available.<br>• It increases Young's modulus, tensile, and wear resistance.<br>• It can be helped the transfer the shear load at the matrix/reinforcement interface,<br>• Strengthen the matrix and at the same time retain some ductility.<br>• It has a self-organized dispersive systems property.<br>• It can help to formation of the heterogeneous nucleation.<br>• It can improve the sinterability of processed powders. | **[76]**<br><br><br><br>**[24][77][33][78]** |

## 1.4 Main problems in the composite solders studied

### *1.4.1 Distribution of reinforcements in a solder matrix*

Generally, the reinforcements are found at the grain boundaries of solder alloys and enhance the mechanical properties of the solder and joint. However, the addition of excessive reinforcement is probably to accumulate and agglomerated in the solder matrices, which can reduce the mechanical strength of composite solders. Therefore, the reinforcement must be homogeneously distributed in the matrix during the mixing process.

However, it is practically difficult to make a composite solder with homogeneously distributed reinforcements. The mixtures (solder powder and reinforcement particles) are milled for a long period and agglomeration is formed in the composite solder matrices. Some researchers have been used the mechanically mixing method to solve this problem and this method is provided a relatively uniform distribution of reinforcement particles in the matrix; however, some fractures are developed at the surface between reinforcement and the matrix due to plastic deformation during a long time mixing **[90][91]**. Various researchers have been successfully fabricated a composite solder with a uniform distribution of reinforcement particles **[92][93][94][55][36].**

In their experiments, an inert gas was used to remove the oxidation of the molten alloy. Due to different densities of reinforcement and solder matrix, the contact of the reinforcement particles will cause the non-uniform distribution in the solidification. Hence, to obtain a homogeneous distribution of the reinforcement within the composite solder, the composite alloy needs to be mixed in a proper method. The powder metallurgy technique would be a better option for the homogeneous distribution of the reinforcing particles in the solder matrix since the reinforcing particles can be formed by the precipitation of the IMC phase particles during the melting process. These reinforcing particles are homogeneously distributed in the solder matrix or at the interface of solder/copper without agglomeration.

### *1.4.2 Reliability of the bonding between the solder matrices and the reinforcements*

To enhance the performance of the solder, it is needed the strong bonding between reinforcement and solder matrix particles during the soldering process. If the bonding will be poor between the solder matrices and reinforcement particles, pores, cracks, and other impurities will easily be existed at the surface of particles during melting.

Also, cracks, pores, poor bonds, and interfacial strength will be normally developed due to mechanical deformation and it is directly affected the performance of the composite solder. Metallic and IMC particles have a strong bond with the solder matrix because these are the reactive reinforcement and it can be easy to react with the solder matrix and form a strong bond during the melting process. However, inert particles (ceramics and carbon-based materials) are non-reactive material and these do not react with the solder matrix and form a reliable bonding. Therefore, wetting or reaction of non-reactive particles and soldered alloy matrices is a very serious concern. It should be noted that reinforcement must be successfully embedded and homogeneously distributed into the solder matrices, most of the researchers studied that non–reactive reinforcement particles were expelled from the solder matrix during the soldering process. To solve this problem, the coating of the Au and Ni has been used by some researchers because these are formed a bridge between solder and non–reactive reinforcements and it can be easily reached with the solder particles during the melting process **[49].**

#### *1.4.3 Stability of the reinforcements and IMCs*

Another important problem is the stability of the reinforcement in the reflow and aging process. Non-reactive reinforcement particles will not be coarsened in the solder alloy. The same problem happens with the metal reinforcement particles; however, they usually coarsen at high temperatures.

It is very important to define the morphology of the composite solder before and after melting. Some researchers explained that $Ag_3Sn$ IMC particles formed in the solder matrix after solidification will not be nano–sized particles but in the form of platelet shapes **[95] [96].** Due to the brittle properties of the IMCs, they can directly influence the mechanical properties of the solder joints. Hwang et al. **[96]** reported that the $Cu_6Sn_5$ IMC particles were homogeneously distributed in the bulk area but did not re-melted during reflow because the melting temperature of these IMC particles was higher than the reflow temperature. In the general case, most nano–sized IMC particles dissolve in the solder matrix during reflow and coarsen after aging. However, when using solid-state bonding techniques, these IMC particles can be kept in the solder matrix with initial size and it can affect directly the strength of the solder. Therefore, further research on new solid–state bonding techniques is required to solve this issue.

### *1.4.4 Poor wettability*

The soldering process and the strength of the joint depend on the contact and the formation of the bond between the liquid material and the solid substrate material. Wettability tends to spread the liquid on a solid substrate and is generally considered by the contact angle. A liquid that spreads on a substrate and does not react by the substrate material is called non-reactive wetting, while the wetting process affected by the reaction between the spreading liquid and the substrate is called reactive wetting **[97]**. Young's equation gives the contact angle concerning the triple point. Young's equation provides the contact angle in terms of the interfacial energy or interfacial tensions occurring at the three-point interface. Several factors (For example system conditions, liquid properties, roughness, heterogeneity of the surface, atmospheric conditions, and substrate properties) can be influenced by the wetting property. On the other hand, the reactive wetting process is influenced by a few more factors, such as soldering temperature, flux, the addition of impurities, etc. However, the correct mechanism which can control the kinetics of wetting is very difficult to predict because reactive wetting is influenced by a lot of the factors, such as interfacial reactions, chemical reaction, diffusion of components, dissolution of the substrate, etc. Whenever the solidified liquid is spread on the solid substrate interface, the various condition of the solidified liquid as shown in **Figure 2.3.**

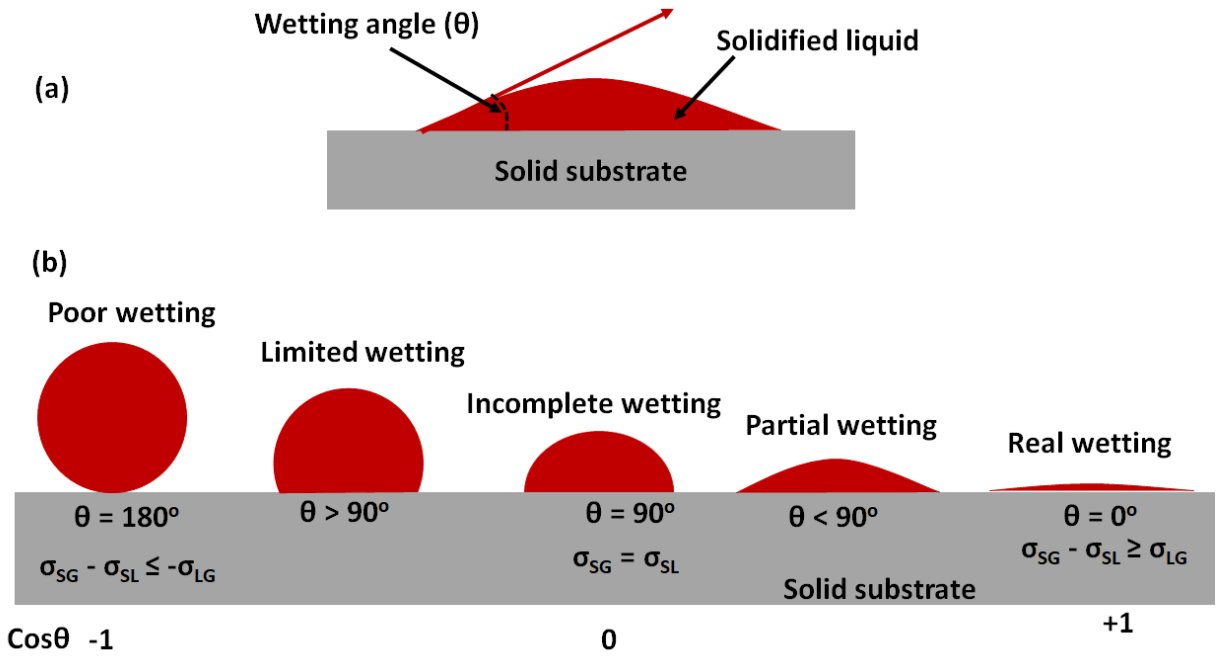


*Figure 2.3 Schematic diagram of different wetting phases on the solid substrate*

***(a)*** ***Surface roughness:*** The rough surface can create the new surface area for the solidified liquid and the actual contact angle would be different from the nominal contact angle. The new surface area is given by the rough surface and it increases the surface energy. Surface cleanliness is an important parameter that can affect the wettability property of the composite solder. Surface roughness is unavoidable because of the impurities on the surface of the substrate. Rough surfaces create a metastable state of equilibrium for the joints and it provides multiple contact angles **[97].**

***(b)*** ***Flux:*** The key role of the flux is to overcome the oxidation in the solidification process. The reduction of the oxide layer can obtain the real wetting on the solid substrate and it can change the interfacial properties of the solder joint. It can provide oxidize–free surface and help the solder particles to wet on the solid substrate. It can also protect from re-oxidation and directly affect the surface tension of the solidified solder in the direction of solder spreading **[98]**.

***(c)*** ***Temperature:*** Temperature plays a key role in the solidification process and it can affect the solidified liquid as well as a solid substrate. Oxidation behavior, reaction rate, surface tension, and viscosity are influenced by temperature. It is a general phenomenon that the viscosity and surface tension of a liquid decrease with increasing temperature. Therefore, wettability in all systems should improve with increasing temperature **[99]**. The diffusion rate increases with increasing temperature in reactive wetting. However, in some cases, it may be attributed to adverse effects because of oxidation, changes in reactivity, and phase changes. As a result. This kind of trend is often noticed during the solidification of solders in the existence of flux at different temperatures. Lopez and Kennedy **[100]** reported that the wetting process is showed a temperature dependence and it is followed by the spreading time and temperature dependence Arrhenius eq. (2.1).

$$\frac{1}{t_0} = K\ exp\left(\frac{-E_a}{RT}\right) \qquad Eq.(2.1)$$

Where, $t_o$ = Spreading time (s), $K$ = Pre-exponential factor, $E_a$ = Activation energy (kJ/mol), $R$ = Universal gas constant (J/K.mol) and, $T$ =Absolute temperature (K)

$E_a$ can be calculated by plotting the graph between $ln(1/t_o)$ vs $1/T$ and slope of the graph achieved as activation energy. On other hand, the activation energy of the spread liquid can also be obtained by applying the base radius, contact angle, and the height of the solidified liquid.

## 1.5 Achievements with the composite solders developed

### *1.5.1 Microstructural modification & growth of IMC particles*

In recent studies, most of the added reinforcement particles may have changed the microstructure of the solder matrices, and these variations have generally been positive and have contributed to improving the mechanical properties of the composite **[33][48][101][102][52][51][36].** This theory was based on the added reinforcement, because this is helped to the reduction of the particle size of the solder matrices and improved the strength of the solder alloy according to the Hall–Petch relationship **[103]**.

Kumar et al. **[34]** described the refinement of the $Cu_6Sn_5$ and $Ag_3Sn$ in the lead-free solder matrix. It was about 3.75 to 4.25 μm and 0.5 to 0.8 μm with (1wt% SWCNT) and without reinforcement. Various researchers have reported similar results with the addition of reinforcements into the lead-free solder matrix **[36][28] [101][33][104][105][106][90].** Lin et al. **[101]** investigated, the addition of $TiO_2$ nanoparticles in the lead-free solder has formed some agglomeration due to different microstructure than the conventional lead-based solder. However, for Sn–3.0Ag–0.5Cu solder alloy, two types of IMCs ($Ag_3Sn$ and $Cu_6Sn_5$) were observed, and SiC and Ni-coated SiC dispersed homogeneously in the β-Sn matrix.

### *1.5.2 Variations in wettability*

Sharma et al. **[45][107] [108]** reported that wetting behavior enhanced with the addition of $La_2O_3$, Graphene Nano-platelets, and Copper–Coated Carbon Nanofibers in the SAC305 and Sn–3.5Ag solder alloy. Lee et al. **[109]** also reported the wettability of an Sn–0.7Cu solder with the addition of 0.5% Ag nano-particles and it found the better wettability than the monolithic solder. Ni and $Ni_3Sn_4$ reinforced composite solder showed an enhanced wettability when compared with the unreinforced solder paste **[96]**. The addition of an appropriate amount of MWCNT improved the wettability of Sn–Ag–Cu composite solders **[52][110]**. However, Nai et al. **[51]** found the maximum contact angle on the 1.5vol.% of $TiB_2$ in then Sn–Ag–Cu composite solders and on the 5vol.% of $TiB_2$, the wettability was degraded. This phenomenon was attributed to the amount of

reinforcement in the matrix, the presence of too many reinforcement particles repressed the flow of molten solders by increasing its viscosity, and further reducing the spread-ability of the solder on the substrate. Sharma et al. **[45]** reported that the reinforcement of the $La_2O_3$ into the matrix reduces the interfacial energy and thus achieves better wetting because the wettability depends on the surface tension and the surface tension depends on the surface energy of the material.

However, it is not clear an exact mechanism for the variations of wettability between molten solder alloys and substrates with the addition of minor alloying elements. Therefore, further research is needed to explain the mechanism of wetting change.

#### *1.5.3 Effect on the growth of IMC particles*

The growth of IMCs grains and the IMCs layers in solder matrices (bulk area) and at the interface has been studied by many authors **[36][28] [101][33][104][105][106][90] [52][110] [45][107] [108].** IMC phases are formed between the grains and IMCs layers are developed due to interfacial and chemical reaction between the solder and substrate

According to the current literature, most of the ceramics and carbon nanomaterials **[58][111][112][113][44][48][114][115][63][116][62][33][105][101][110][52][34][51][117]** have been shown that these are very useful in suppressing the growth of IMC phases in solder matrices and interfaces during reflow or the thermal aging process.

Some researchers have studied the growth of the IMCs on the lead-free solder by using metal reinforcement particles (Co, P, Cu, In, Sb, Pt, Al, Zn, Ge, Ni, Ag, and Au). Amagai [118] indicated that Ni, Co, and Pt nano-particles were very beneficial in refining the growth of IMCs grains and layers because these are reactive reinforcements and it can be reacted easily with the lead-free solder particles. The microstructural analysis of the IMCs layers between Sn–3.5Ag and Sn–3.5Ag–0.7Cu and pure Cu and Ni substrates were investigated by Yu et al**. [119]**. It was found that during solidification, $Ag_3Sn$ nanoparticles were presented on the surface of the IMC layer, which would reduce the interfacial energy and suppress the excessive growth of the IMC layer. Shen et al. **[36]**, Liu et al. **[33]**, and El-Daly et al. **[120]** added $ZrO_2$ and SiC nanoparticles into an Sn–Ag and Sn–Ag–Cu lead-free solder and found the refinement of the IMCs.

Problems are developed with inert particles (non-reactive particles) because they do not react with the solder material (metallic elements) and it is agglomerated at the grain boundaries or IMC layers in the solder alloys. Surface absorption theory can be helped to describe the mechanism of

refinement (suppression) of the growth of IMCs in the solder during the reflow and aging process. According to the surfactant adsorption theory, the amount of absorption of reinforcement particles on the molten solder *k* is explained as follows Eq. (2.2) **[19][117][121]**:

$$\Gamma^k = \frac{-c}{RT}\frac{d\gamma^k}{dc} \qquad Eq.(2.2)$$

Where, $\Gamma^k$ is the amount of adsorption of reinforcement particles on molten solder k, *c* is the total concentration of reinforcement particles in the solder, *R* is the ideal gas constant, *T* is the absolute temperature and $\gamma^k$ is the surface energy of molten solder k without reinforcement particles.

When molten solder *k* adsorbed a layer of ceramic particles, the surface tension can be explained from the integral of the Eq. (2.3):

$$\sum_k \gamma_{(c)}^k A_k = \sum_k \left(\gamma_0^k - RT\int_0^c \frac{\Gamma^k}{c}dc\right) A_k \qquad Eq.(2.3)$$

Here, $A_k$ is the area of the crystal planes *k*, $\gamma_0^k$ is the surface tension of the initial crystal planes *k* without adsorption, $\gamma_{(c)}^k$ is the surface tension of crystal planes k with adsorption, $\Gamma^k$ is the adsorption of surface-active material at crystal planes *k*, *c* is the concentration of the surface-active material, T is the absolute temperature, R is the gas constant. If the crystal volume is constant; the surface energy of the crystal planes can be kept to a minimum in the equilibrium state. As shown in Eq. (2.4):

$$\sum_k \gamma_{(0)}^k A_k - RT\sum_K A_k \int_0^c \frac{\Gamma^k}{c}dc \rightarrow min. \qquad Eq.(2.4)$$

Where, $\sum_k \gamma_{(0)}^k A_k$ is assumed to be constant because of the independence of the concentration of surface-active materials. So $RT\sum_k A_k \int_0^c \frac{\Gamma^k}{c}dc$ should be maximized, which means the effect of the crystal plane with the maximum amount of adsorption, is most active.

In general, the crystal plane with maximum surface energy increases rapidly while the adsorption amount of surfactant is maximized. However, reinforcement particles, which are considered to be effective surfactants, can significantly reduce the surface energy of the crystal and therefore reduce the growth rate of the crystal plane. In this regard, this nano or micron-sized reinforcement can be adsorbed on the surface of the IMC particles or IMC layers to suppress their uncontrolled growth. The development of the IMCs involves various theories, including volume diffusion, grain boundary diffusion, dissolution, and coarsening into the solder **[122]**. Hence, these elements need

to be seriously investigated to recognize how the reinforcements are influenced by the solder matrix. Gain et al. **[121]** and Liu et al. **[33]** reported that $TiO_2$ and SiC particles suppress the $Ag_3Sn$ and $Cu_6Sn_5$ phase because adsorption of $TiO_2$ and SiC nanoparticles reduces the surface energy of primary $Ag_3Sn$ crystals. So, SiC and $TiO_2$ is a powerful surface–active agent that can be absorbed on the surface of IMCs particles and refine excessive growth.

#### *1.5.4 Enhancement of mechanical properties*

Most of the researchers are reported that reinforcement (metal, ceramic, IMC nanoparticles and carbon nanomaterials (such as carbon nanotube and graphene) or the reinforcement particles increased the mechanical properties of the solder composites and it has shown the desirable performance (such as high hardness, high tensile strength, and high shear strength) compared with monolithic solders. Liu et al. **[33]** and El–Daly et al. **[92]** reported that the tensile and yield strength of solder joints enhanced with SiC nanoparticles addition than that of monolithic SAC solder joints. Oher researchers also investigated the addition of ceramic nanoparticles, such as $ZrO_2$ **[36],** $Al_2O_3$ **[123][124][58][35]**, $TiO_2$ **[101][125][126]**, that these particles significantly enhanced the hardness, tensile strength and creep resistance of nano-composite solders. However, CNTs added composite solders disclosed that the reinforcement of MWCNTs and SWCNTs in solder matrices increased the yield strength (YS) ultimate tensile strength (UTS), and micro-hardness of solder joints while the ductility of composite solders decreased significantly **[102][110][52][34]**.

Also, MWCNTs and SWCNTs were established dimensionally stable in the lead-free solder due to the low coefficient of thermal expansion (CTE). According to the classical theory of strengthening dispersion **[127]**, the improvement of the mechanical properties of composite solders depends on the distribution of reinforcement particles in the solder matrices and at the grain boundaries. These reinforcement particles try to change deformation by preventing the grain-boundary sliding as well as obstructing dislocation movement in the solder matrix **[127][128]**. To understand the dependency of the size and mechanical properties, Shi et al. **[106]** studied the result of the reinforcement particle size scale on the mechanical properties of the solders. They investigated the thermal creep resistance with the addition of Cu and Ag particles in the Sn–Pb, and Sn–Cu solder alloys, and results show that tensile shear strength with the addition of nano–size particles are higher than the micro-size particles; however, micro–sized particles have shown better creep strength than the nanoparticles. The reason for this improvement was that nano–sized

particles refine the alloy grains and the fine grain size causes a decrease of the creep strength, which was more effective than the increase of creep resistance by impeding grain boundaries sliding.

However, to produce composite solders with high overall properties, more in–depth studies are needed to understand the optimal size of the reinforcing particles for solder alloys of different compositions and structures.

## 1.6 Research aims and objectives

Several studies have demonstrated that the SAC series is the most promising alternative for the lead-free solder alloy due to its excellent overall properties **[129][130][131].** Although some studies have indicated that the mechanical properties and microstructural defects of the SAC solder under different experimental conditions, further work is needed to eliminate these disadvantages. Sn–3.0Ag–0.5Cu (SAC305) was selected for the current study because it is a widely used Pb–free solder in the assembly of electronic devices. Unfortunately, SAC solder has lower reliability and mechanical properties than the Pb–solders. The joint strength of the SAC305 solder alloy can be improved with various modifications of reinforcement and the solder contents. Hence, optimal composition and process condition must be consider during soldering process **[132]**.

### *1.6.1 Knowledge gap*

Most of the previous and recent investigations are preliminary studies to identify mechanical properties and interfacial microstructures of composite interconnect with the addition of alloying elements under thermal aging and reflow condition.

Just a few studies investigated the distribution of the reinforcement particles, optimum composition, and connection between the reinforcement matrix particles. There is a gap in understanding the effect of the connection between the reinforcement and matrix particles. The knowledge is also missing in the systematic qualitative examination of average neighboring particles distance and morphological mosaic analysis of the ceramic reinforcement in the solder matrix.

In addition to this, IMCs layer growth was confirmed with various reflow, aging time, and temperature. The development of the IMCs layer is due to the higher diffusion of the Cu atoms. However, some literature is provided that the growth of the IMCs layers is surpassed with an

increase in temperature. There is a need to clarify the behavior of the IMCs layer of the Different time and temperature under reflow and aging condition.

### *1.6.2 Scientific goals*

Based on these, the present dissertation is emphasized on the preparation and characterization of Sn–3.0Ag–0.5Cu (SAC305) composite solder with various content (0.5, and 1.5 wt. %) of SiC and Ni–coated SiC reinforcements and the examination of physical, microstructural and hardness of a lead-free solder Sn–3.0Ag–0.5Cu. After careful literature review and finding of the knowledge gap, the following scientific aims have been defined:

(1) Identify the optimum composition of the reinforcement in the solder matrix.
(2) Investigate the relative contact perimeter between the reinforcement and lead–free solder particles.
(3) To investigate the average neighboring particle distance and morphological mosaic analysis of the ceramic reinforcement in the solder matrix.
(4) Observe the change in the thickness of the IMCs layer at the Cu–Sn interface and establish the relation between the growth thickness, time, and temperature under reflow and aging condition.
(5) How does the SiC and nickel-coated SiC reinforcements affect the microstructural evolution?
(6) How does the SiC affect the wettability and how does the nickel coating change this?
(7) What effect does increasing the amount of SiC have on wettability and hardness as well as on microstructure?
(8) What changes occur in the microstructure as a result of aging in the case of the composites?
(9) Does nickel coating matter for aging?
(10) What kind of processes takes place during reflow and aging?
(11) How does the thickness of the IMC layer change as a function of time and temperature during reflow and aging?

# 3 CHAPTER 3: Development of lead–free Sn–3.0Ag–0.5Cu/SiC and Sn–3.0Ag–0.5Cu/SiC(Ni) solder composite

## 3.1 Introduction

The recent research trends in lead–free solders moved in the direction of reinforcement by a fourth alloying element in the ternary solder alloy. This is devised to improve their mechanical properties, electrical properties, and also improve the microstructural stability. Tsao et al. **[133]** investigated the mechanical properties of SAC solder reinforced by ceramic particles like $TiO_2$ and $Al_2O_3$ nanoparticles. They found an improvement in the mechanical properties of the quaternary solder. Rare earth oxides were used as reinforcing particles with a marked improvement in obtained microstructure and properties of SAC solders **[134]**. However, the scientific community moved towards reinforcing carbide-based reinforcement owing to its low cost and ease of production. Some researchers have shown the reinforcement of SiC has significantly improved the microstructure, mechanical properties, and wetting behavior of the SAC solder alloy **[24][33] [120][135][136].**

Fathian et al. **[93]**, Chellvarajoo et al. **[47],** and El–daly et al**. [120]** concluded that the best way to prepare the solder composite is the powder metallurgy method. They stated that this method gives the best distribution of the reinforcement in the matrix. SAC305 lead-free solder powder was purchased as prepared from Cobar Europe B.V., Breda, the Netherland with an average particle size of 20–24 µm and SiC particles used in this study were procured as prepared from SIKA TECH (Switzerland) with an average particle size of 1–3 µm.

### *3.1.1 Synthesis of nickel-coated silicon carbide (SiC-Ni) particles by EN (Electroless nickel) method*

The electroless plating method is employed here for the coating of Ni on to SiC particles for the simplicity and non-hassle freedom associated with the process. Metallic Ni is obtained from the EN method by reduction of the nickel sulphate solution using a reducing agent. The entire process is carried out in presence of SiC particles being used as carriers.

As stated above, the SiC particles are preferred as carriers for Ni electroless plating. Vaezi et al. **[137]**, Pavlatou et al. **[138]**, Zimmerman et al. **[139],** and Ahmad **[140]** studied the effects of co-precipitation and co–deposition mechanisms involving SiC. As stated, Ni is reduced from its salt solution by using Sodium hypophosphite as a reducing agent **[140]**. The three–step used in the research work for the deposition of Ni onto SiC using EN plating method is shown below in **Figure**

**3.1**. The steps contain (i) ultrasonic cleaning, (ii) acidic pre–treatment (sensitization and activation), and (iii) EN plating.

The first step was purified the SiC in an acetone bath for about 30 min. The concentration of SiC particles with acetone was used 4*g*/100 ml during this study. In the second step, dried SiC powders were mixed with the solution of Sodium hypophosphite (60*g*/*l*), Lactic acid 98% (40*ml*), and distilled water, and this process was accomplished with a magnetic stirring speed of 300 rpm at 85°C for 40 min. After that, the solution was dried in the furnace at 120°C. In the third step, the solution was prepared for 56*g*/*l* nickel sulfate ($NiSO_4.7H_2O$), 60*g*/*l* sodium hypophosphite ($NaH_2PO_2$ .H2O), 40*ml* lactic acid 98% ($C_3H_6O_3$), and distilled water. The solution was stirred at the temperature of 85°C for 40min, and the pH value of the solution was adjusted at 4-5. One hour later, the solution was washed/rinsed with distilled water four to five times. Finally, the solution was dried at room temperature in the air. Complexing agents are added to prevent nickel oxidation and pH control. Thus, Ni coating on SiC particles was achieved before imparting them into the solder matrix.

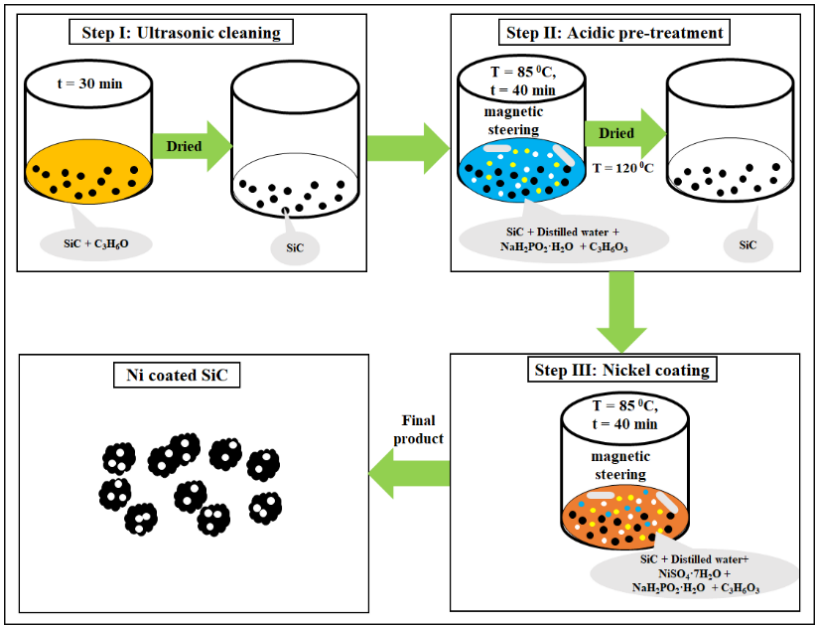


*Figure 3.1 Schematic diagram for Ni-coated SiC process*

**Figure 3.2(a–d)** shows an SEM image of Ni–coated SiC and the corresponding elemental maps, and the elemental maps were confirmed that nickel particles were deposited on the surface of SiC. However, the existence of Si, Ni, O, and P was determined by EDS **(Figure 3.3)** analysis.

The main reason for Ni–coated SiC is to avoid unnecessary reactions between ceramic SiC reinforcement and SAC solder matrix. Jiaqiang, Gao et al. **[141]** reported that reaction temperature was dependent on the size of the SiC particle because nickel atoms easily diffuse on the surface of the SiC particles. During electroless plating, firstly, nickel atoms are deposited as a form of clusters on the SiC particles surface. During the heating process, Ni atoms diffuse on the interface of the silicon carbide particle because clusters of the Ni atom are thermodynamically metastable.

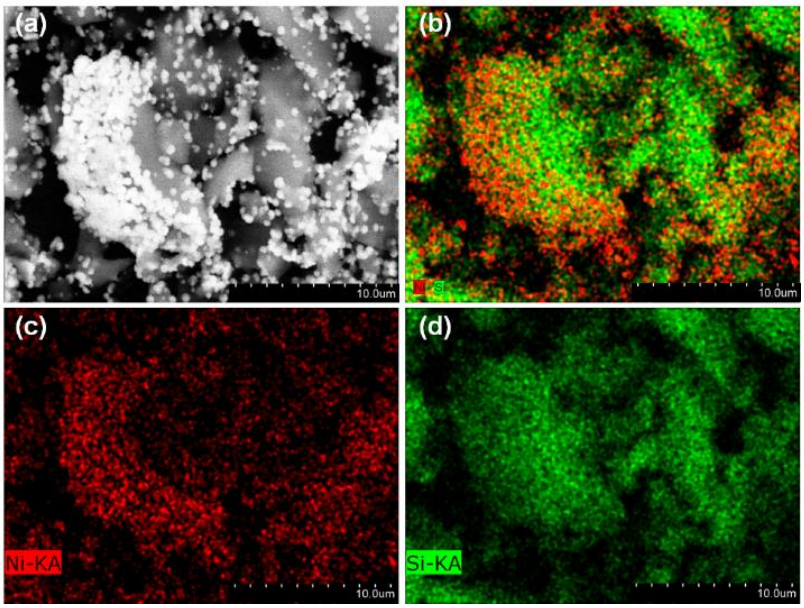


*Figure 3.2 (a) SEM image of Ni-coated SiC and corresponding elemental maps (b) Ni and Si (c) Ni (d) Si*

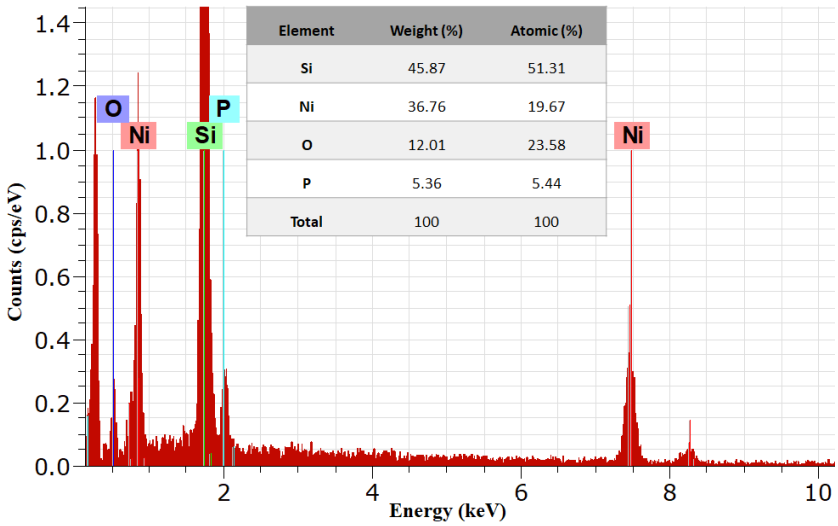


*Figure 3.3 EDS analysis of the SiC(Ni)*

## 3.2 Preparation of composite solders

Once the SiC particles are coated with Ni particles, the next logical step is to reinforce these particles into the lead-free SAC305 solder matrix. For this purpose, the powder metallurgy method was chosen. The SAC305 powder is blended with SiC and SiC(Ni) powders at various weight fractions. The composite lead–free solders from here on would be marked as SAC–*x*%SiC(Ni), where *x* stands for 0, 0.5, 1, and 1.5wt% for SiC and SiC(Ni). As stated above, we employed a powder metallurgy route for its consistency and homogeneous distribution of the reinforcements in the matrix. The SAC305 powder and reinforcements (SiC and SiC–Ni) powder particles were pre-weighed and put in a milling jar. They are mixed to achieve homogenization in a planetary ball mill for 1 hour. The rotational speed of the milling process was 200rpm and the ball to powder ratio is 10:1 (BPR). The steel balls used in this process were 3mm in diameter. Ethanol was used as milling media (40 ml). **Figure 3.4(a) and Figure 3.4 (b)** indicate the schematic view of the ball milling process and SEM picture of SAC305/SiC after 60 min of ball milling. Once this process is completed, we get a homogenously mixed SiC/SAC305 and SiC(Ni)/SAC305 powder. This powder is then compacted under a pressure of 200MPa in a cylindrical die of 15mm diameter. Oil lubricant was used to make the ejection and densification of the post process sample smoother. Following the compaction, the substrate was sintered in a furnace for 3 hours at 200°C under Ar inert gas environment.

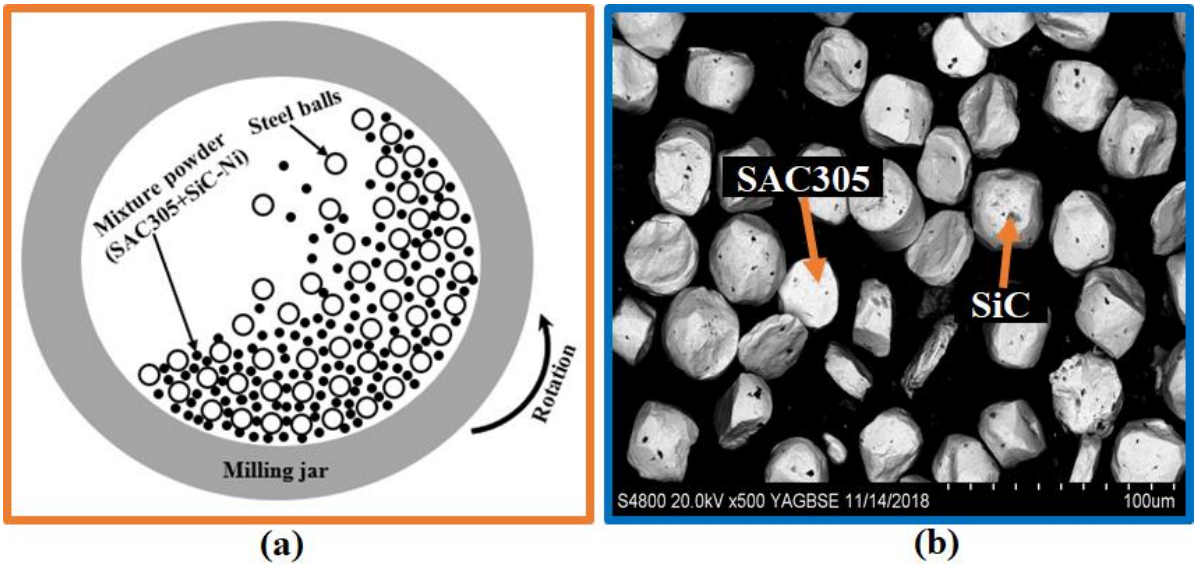


*Figure 3.4 (a) Schematic diagram of ball milling with mixture powder (matrix and reinforcement)*[142] *(b) SEM micrograph of SAC305/SiC after ball milling*

## 3.3 Results and discussion

### *3.3.1 Microstructural evolution of lead- free solder composite*

Post-processing and experimentation on coating Ni on SiC particles and reinforcing the SiC and SiC(Ni) into SAC305 solder matrix and mounting, the microstructural examinations were conducted by using SEM. The first investigation is the microstructure of the SiC reinforced SAC305 matrix. **Figure 3.5 (a–b)** shows the distribution of the SiC in the SAC305 solder matrix at lower and higher magnification; however, EDS analysis confirmed the presence of the SiC in the matrix.

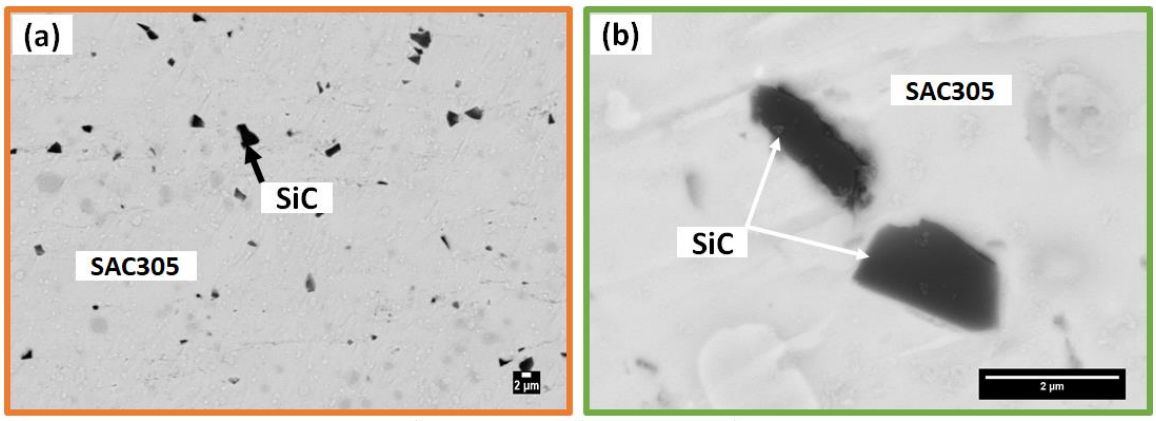


| Element | Weight (%) |
|---|---|
| Sn L | 1.26 |
| C K | 11.60 |
| Si K | 87.14 |

*Figure 3.5 Distribution of SiC in the SAC305 solder matrix (a) lower magnification (b) higher magnification (c) EDS data*

**Figure 3.6 (a–d)** shows the SEM micrograph of the SAC305 solder composite with addition of 0, 0.5, 1.0 and 1.5%SiC(Ni). The SAC matrix with 0 wt% SiC showed no defects or cracks. However, with the inclusion of ceramic Sic particles, cracks, and defects are developed in the solder matrix. Pores and agglomerates of SiC reinforcements were noticed in the matrix which did not join completely with SAC particles. As the concentration of SiC increased in the matrix, more pores, more agglomerates, and thicker grain boundaries are visible due to the SiC agglomeration. The first observation from microstructural examinations shows that by increasing the content of SiC(Ni) above a certain limit in the matrix, the bonding between the lead-free solder and

reinforcement particles decreases which would have adverse effects on the final mechanical properties of the composite. **Figure 3.6 (b–d)** attached below, shows the composite microstructure with pores associated with the SiC(Ni) reinforcements. Porosity is of significant interest for research as the mechanical properties depend directly on the porosity in the matrix. The least amount of defects were found in the pore lead-free solder (**Figure 3.6 (a)**).

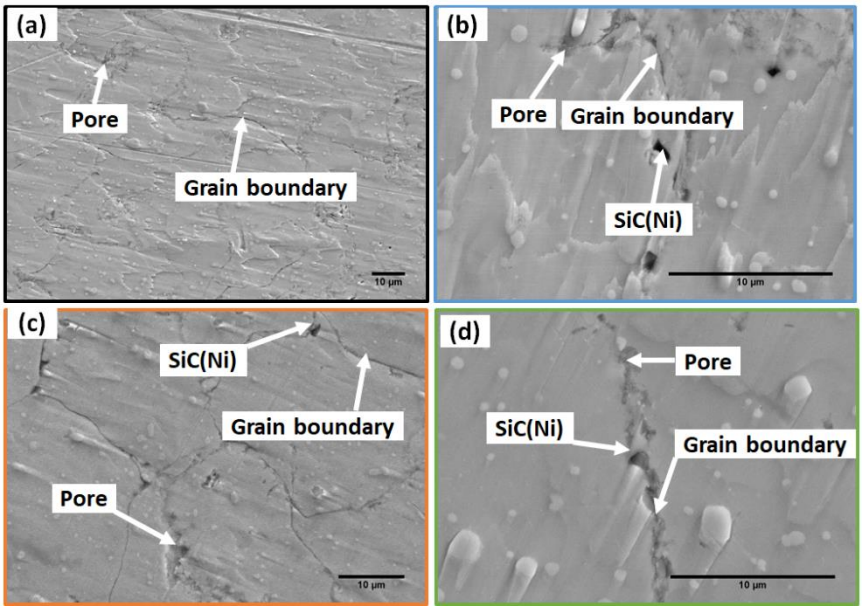


*Figure 3.6 SEM micrographs of SAC305 solder with addition of (a) 0 (b) 0.5 (c) 1.0 and (d) 1.5 wt% of SiC(Ni)*

### 3.3.2 Physical properties

#### *3.3.2.1 Relative density*

Density is an important parameter to be considered while selecting a solder material. Hence, it is considered before carrying on further investigations with ceramic reinforced lead-free solders. The particles come into contact, a neck growth develops, and the neck then becomes larger in the early stages of heating the sintering process. As the sintering time is extended, the particles are completely merged to form larger particle grains that are about 1.26 times larger than the diameter of the original particles. Also, the pores that are initially trapped between the particles are reduced during sintering **[143]**.

**Figure 3.7 and Figure 3.8** shows the relative density of SAC305 PM composite samples with varying composition of Sic and SiC(Ni). The following equation is used for the calculation, Eq. (3.1).

$$\rho = \frac{(g_2 - g_1) - (g_3 - g_4)}{(g_2 - g_1) \cdot (\frac{1}{\rho_f} 0.0012)} \qquad Eq.(3.1)$$

Where, $g_1$ *(g)* is the weight of hook in air, $g_2$ *(g)* is the total weight (weight of hook and weight of sample) in the air, $g_3$ *(g)* is the total weight (weight of hook and weight of sample) in the water and $g_4$ *(g)* is the weight of hook in the water, $\rho_f$ *(g/cc)* is the density of water.

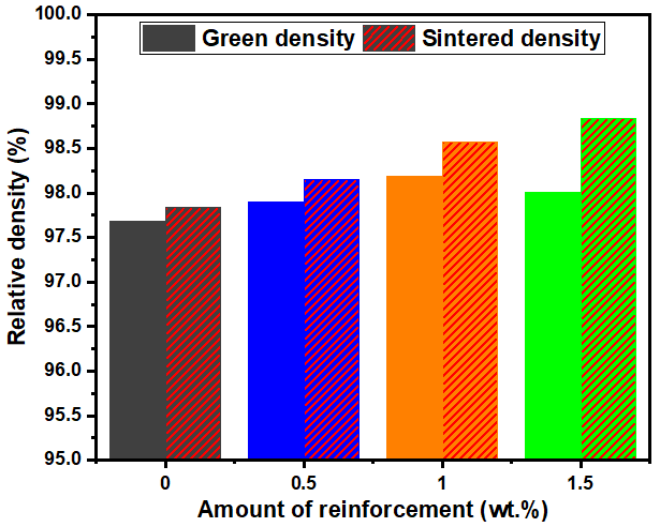


*Figure 3.7 Relative density of SAC305 lead-free solder PM composite samples with the addition of SiC*

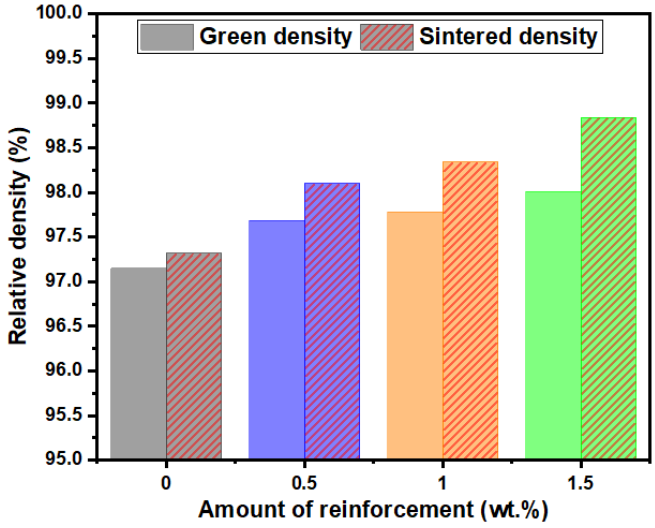


*Figure 3.8 Relative density of SAC305 lead-free PM solder composite samples with the addition of Ni coated Sic*

Monolithic lead–free solder shows a small difference of relative density between green and sintered lead-free solder as shown in **Figure 3.7 and Figure 3.8**. In other compositions (0.5%, 1%,

and 1.5%) of lead-free solder composites, the relative densities were varied with the weight percentage of reinforcement. The green density is affected by its micro-porosity. The sintered density can be increased by adding much smaller particles (reinforcement) providing the gap between the larger ones. In general, the sintered density increases with the range of particle size distribution, and this trend is more pronounced in more densely arrangements than in loosely packaged ones **[144]**. Ni-coated SiC is more homogeneously distributed in the lead-free solder matrix than the SiC reinforcement and it filled the gap more than the SiCparticles due to metallic bonding. All samples are pressed at 200 MPa and provide high-density values (both green and sintered) and indicate the higher relative density in all compositions.

#### *3.3.2.2 Porosity analysis*

As mentioned in the above sections, porosity is a really important parameter in the fabrication of lead–free solders as it directly affects the mechanical properties. Porosity depends on the grain refinement of the matrix and hence we assume naturally that porosity would have a negative effect on grain refinement. The pores are understood to form as a result of the agglomeration of particles on the surface coupled with non-uniform distribution of SiC particles in the SAC305 powder matrix.

In addition, the pores that are initially trapped between the particles are reduced during sintering. The porosity reduction during sintering where the pores between the grain boundaries are reduced, resulting in a denser sintered material. These initial large pores become spherical and smaller after sintering **[143]**. Hence, after a series of careful trial and error run of experiments, the reinforcement composition was limited to 1wt% of both SiC or SiC(Ni) particles.

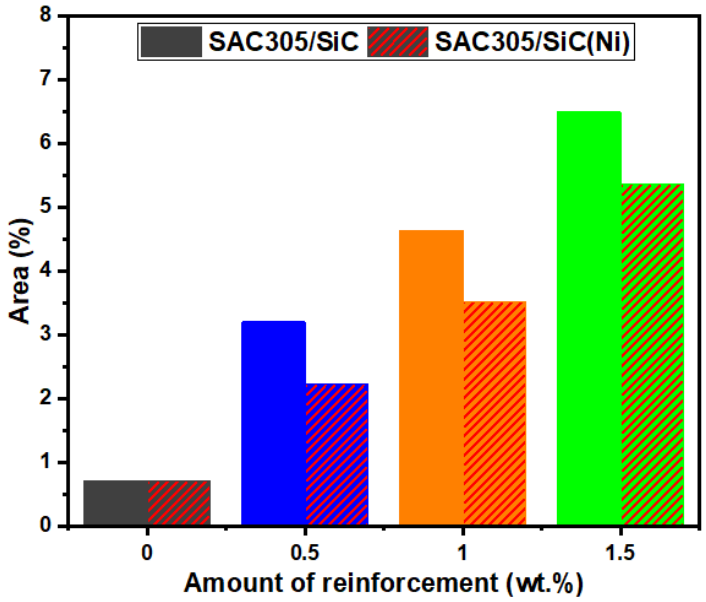


*Figure 3.9 Porosity analysis of the SAC305 solder composite with the addition of SiC and SiC(Ni)*

We can observe higher porosity for the samples at 1.5wt% reinforcement **(Figure 3.9)**. We can also observe the trend that the larger the content of reinforcement, the greater is the pore size (avg). The increasing number of reinforcement particles leads to a higher irregularity of pores **[145]**. In the present work, **Figure 3.9** which has 1.5wt%SiC(Ni) reinforcement in SAC305 solder showed the highest ratio of porosity. All other samples show pores and agglomerates of SiC(Ni) particles in between the SAC305 matrix. There is no complete bond between these agglomerates and matrix particles. The percentage of pores in composite increase with an increase in the amount of reinforcements and monolithic lead-free solder is showing the least amount of agglomerates and porosity and 1.5 wt% reinforced SAC305 solder composite showing the highest amount of agglomerates and porosity. Fine microstructure and reduces the porosity which may translate into increased solder reliability. SiC is a ceramic bonded material and it is not contacted directly to the lead-free solder material, however, Ni is a metallic material and it is easily contacted to the lead-free solder particles during the sintering process and fill the gap between the reinforcement and the matrix.

### 3.3.3 Compressive strength of the PM solder composite

Compressive strength is another mechanical property that needs measurement to effectively determine the solder composite strength. Homogeneous distribution of reinforcement particles means more refined phases which inhibit mechanical deformation more effectively.

The compressive strength of SiC and Ni–coated SiC reinforced lead-free solder composite are shown in **Figure 3.10**. The increase in reinforcement content increased the strength of the solder under compression. The maximum value for SiC and Ni–coated SiC addition was obtained at 1.0wt% but beyond this, the compressive strength decreased again. The average compressive strength for monolithic SAC305 solder was 34.21MPa while for 1wt% reinforced composite the compressive strength was 42.75MPa for SiC and 45.29MPa for Ni–coated SiC.

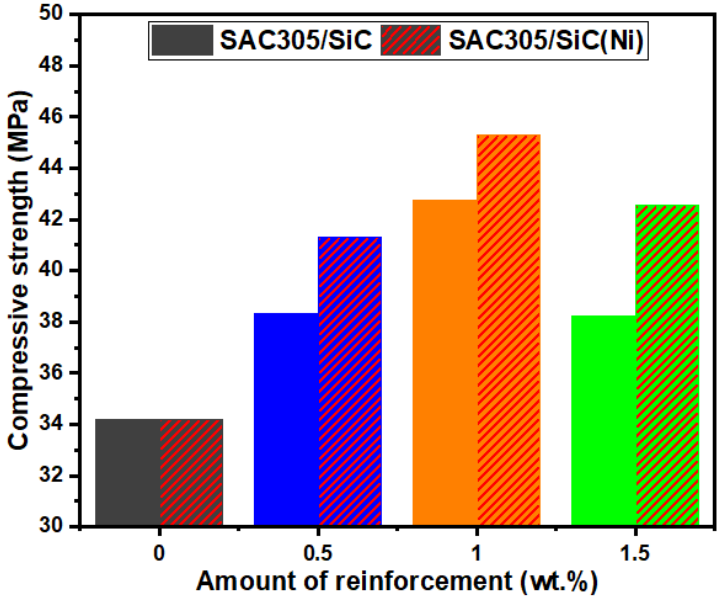


*Figure 3.10 Compressive strength of the SAC305 lead–free solder composite with the addition of SiC and SiC(Ni)*

Strength is increased due to the addition of ceramic particles because ceramic particles have a higher hardness. In general, the strength of metal matrix composites increases due to the decrease in elongation **[93]**. However, the strength is still higher than the monolithic sample. For a 1% added reinforcement sample, the strength decreased compared to 1.5% by weight because of the presumed increased porosity.

However, the addition of reinforcement particles has some negative effects, including increased porosity in liquid processes. On the other hand, it has been reported that in powder metallurgy

methods, the addition of reinforcement particles should not exceed a certain limit, otherwise the properties will decrease as in this study in 1% reinforced sample because of the increased number of reinforced particles may increase the number of micro-pores. Microscopic pores determine the strength because these are potential zones of crack initiation that ultimately lead to failure **[110][51] [93]**.

### 3.3.4 Relative contact perimeter (RCP) of reinforcement and matrix

Contact perimeter is defined as a contact surface between metallic solder and ceramic reinforcement particles. Some reinforcement particles are not fully connected with the surface of the metallic solder i.e non-contact perimeter. The contact and non-contact perimeter of SiC and SiC(Ni) particles are determined by ImageJ software. In **Figure 3.11(a),** the black line indicated the non-contact perimeter, and the rest of the portion is the contact perimeter. Following these analyses carried out for all the samples, the relative contact perimeter follows from following Eq. (3.2).

$$RCP = \frac{P_c}{P_c + P_{nc}} \cdot 100 \qquad Eq.(3.2)$$

Where, RCP is relative contact perimeter, $P_c$ (µm), and $P_{nc}$ (µm) are contact and non-contact perimeter respectively. The maximum RCP was found at 1.5wt% of reinforcement while the minimum RCP was found for 0.5wt%SiC reinforcement. **Figure 3.11(a)** shows the RCP of the matrix and the reinforcement particle. **Figure 3.11(b–c)** shows the SEM micrograph of lead–free solder composite with contact and non-contact interfaces between the matrix and reinforcement.

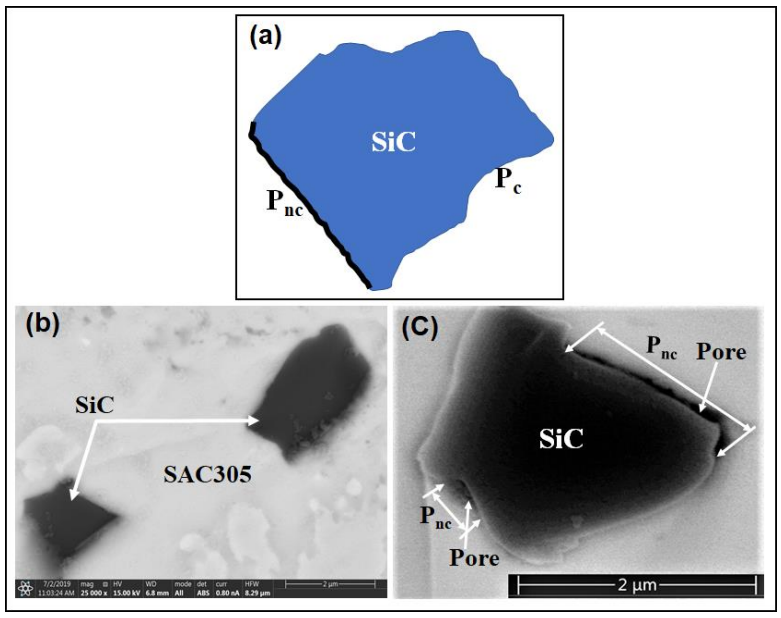


*Figure 3.11 (a) Schematic diagram of contact and non–contact perimeter analysis (b) SEM image of SAC305/SiC composite solder (c) SEM micrograph of SAC305 solder composite with contact and non–contact interface*

**Figure 3.12(a)** shows the SEM micrograph of the lead-free solder composite with the reinforcement (SiC or Ni–SiC) particle and **Figure 3.12(b)** indicates the segmented reinforcement particles in the matrix, which was measured the RCP. The process of evaluating the RCP is shown in **Figure 3.13.**

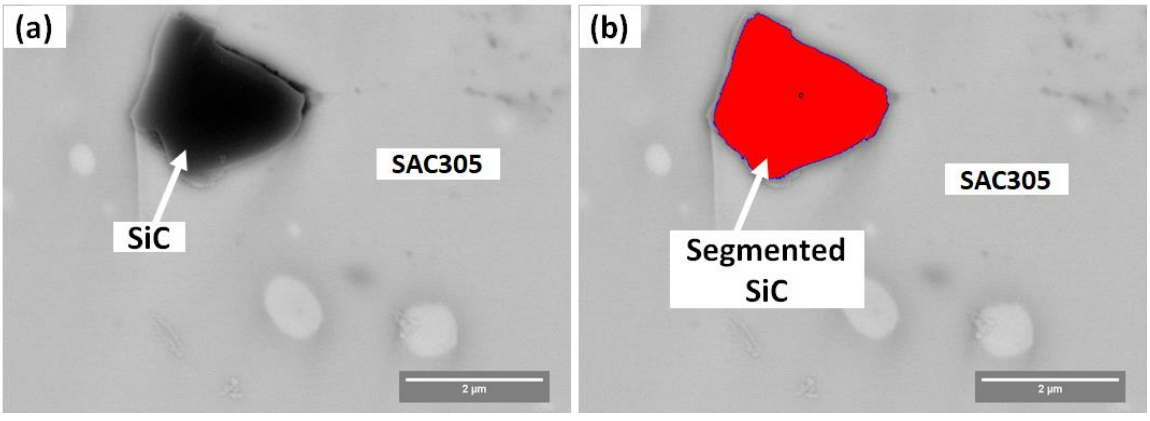


*Figure 3.12 (a) SEM micrograph of the SAC305 lead–free solder with the addition of SiC particle (b) Segmented SiC particle in the solder matrix*

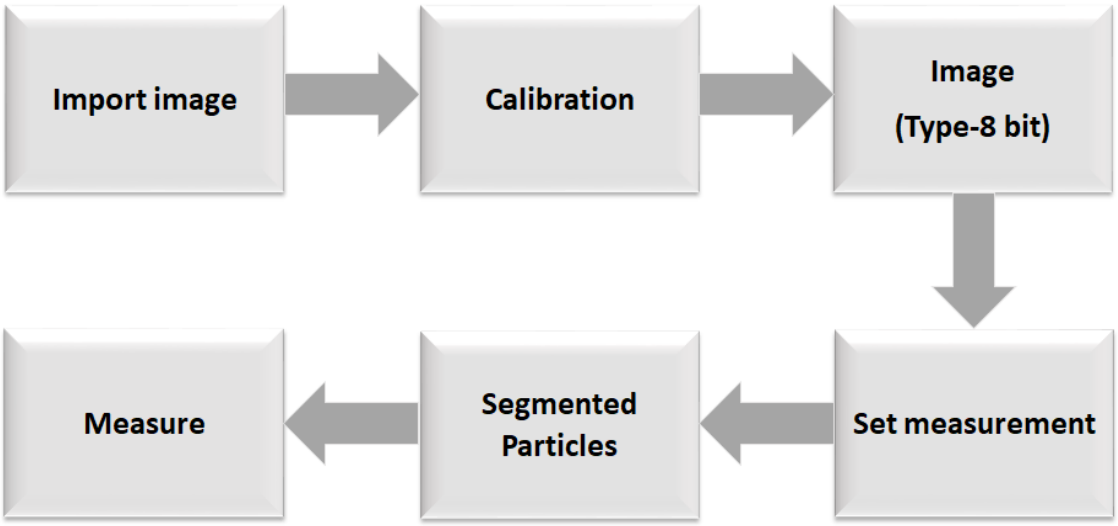


*Figure 3.13 Process of measurement of the RCP of the reinforcement particles*

**Figure 3.14** shows the results of the RCP of lead–free solder composites at a different weight fraction of SiC and SiC(Ni). The interface of SiC and SAC305 has poor mechanical bonding which is a direct effect on the result of weak adhesion and additionally agglomeration of SiC particles was also observed. To reduce the agglomeration and to improve the adhesion between SiC and SAC305, the coating of SiC with Ni was carried. Some portion of the reinforcement (SiC and SiC–Ni) was found not to be incomplete contact with the lead-free solder i.e. loss of adhesion (deadhesion). Compared to SiC reinforcement, SiC(Ni) reinforcement has shown improved adhesion with SAC305.

During this study, Ni surface coating was applied on SiC to overcome the weak bonding between lead-free solder and SiC particles. Silicon carbide consists of two types of atoms, the first is silicon atoms and the second is tetrahedral carbon atoms which have strong bonds in the crystal structure. Silicon carbide is a ceramic material with a covalent bond and has stable chemical properties. Ni is a metallic bonded material and it has good wetting characteristics with Sn-based solder because SAC solder has also metallic bonding. In these solder composites, SiC(Ni) is reacted with the SAC305 solder and forms a strong metallic–metallic bond at the interface between reinforcement and solder matrix.

**Figure 3.11(c)** shows that the matrix particle was not filled between the two SiC particles. Therefore, it is concluded that stress concentration has existed between the two particles easily under external load, which reduces the interfacial bond strength of the composite. The result of

**Figure 3.14** shows that the SiC content decreases the contact between the particles and Ni appears at the appropriate position. It is presumed that the Ni particles promotes the RCP of SiC in the solder matrix and avoids direct contact between two or more SiC particles due to metallic bonding. Therefore, micropore formation and agglomeration are significantly reduced. The highest RCP was measured in SiC(Ni) reinforced samples (1.5wt%), while the lowest is in the case of 0.5wt% SiC reinforcement. It is also observed that with the addition of Ni–coated silicon carbide, the relative contact perimeter of composite solders increased drastically.

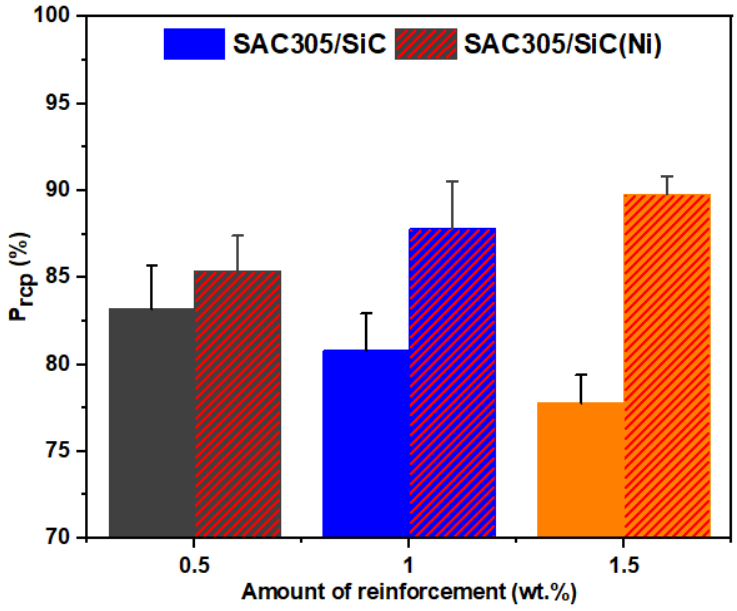


*Figure 3.14 Relative contact perimeter of SAC305 lead–free solder composite with the addition of SiC and SiC(Ni)*

### 3.3.5 Average neighboring particles distance

The average neighbor's particle distance, $d_{mn}$, is defined as the distance between the centers of gravity between neighboring particles in a matrix. It is not analogous with the mean free path between the particles and closest neighbor distance. In estimating the impact on the matrix of the reinforced particles, the distribution of both SiC and SiC(Ni) reinforcement particles were analyzed by Cprob. **Figure 3.15 (a)** demonstrates a schematic outline of estimating the average neighbor's particle distance and **Figure 3.15 (b)** shows the average neighbor's particle distance image generated by software Cprob.

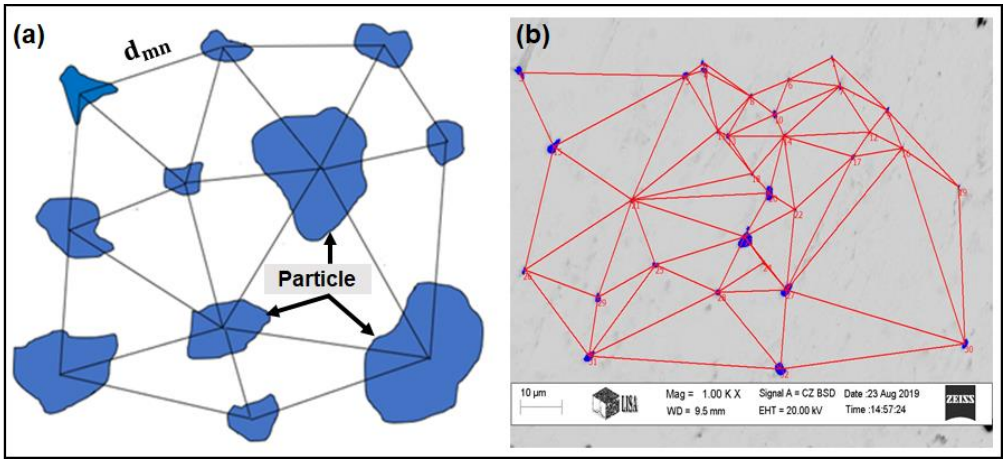


*Figure 3.15 (a) Schematic diagram of the neighbor's particle distance (b) Average neighbor's particle distance image generated by software (Cprob)*

**Figure 3.16 (a)** depicts the variation in average neighbor particle distance, $d_{mn}$ between the reinforcement and matrix particles for various weight fractions. Overall, the distribution of $d_{mn}$ values suggests a consistent pattern with processing. The parameter $d_{mn}$ is used to distinguish the different MMC. Thus, it is an identifier for measuring the dispersion of the reinforcement in the solder matrix. However a useful technique average neighbor particle distance has proven, it has certain drawbacks. For instance, if the neighbor's particle distance technique is applied to a composite system in which the particles are bunched together in gatherings of at least two, the subsequent closest neighbor's distance tends to the particle diameter, erroneously indicating best clustering, if the second, third, fourth, and so on neighbor's distances are considered **[146] [147].**

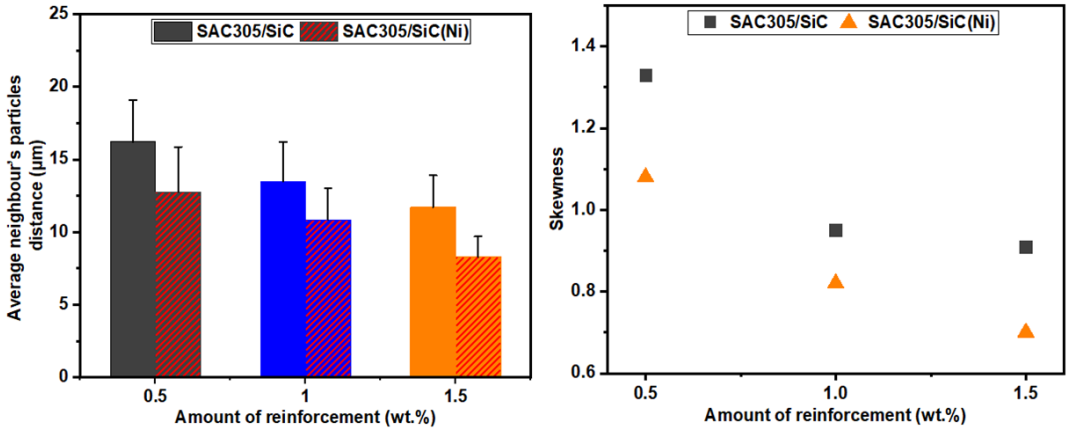


*Figure 3.16 (a) Average neighbor's particle distance of SAC305 solder composites with the addition of SiC and SiC(Ni) (b) Skewness of SAC305 solder composites*

Where, $d_{mn}$ is the distance between neighbor's particles, m is the first particle, and n is the neighbour's particle. Higher average inter-particle distance inside the matrix might affect the mechanical properties of the composite. The quadrat analysis of the lead-free solder composite is shown as a skewness diagram of the number of SiC & SiC(Ni) particles/quadrant, $N_q$ in **Figure 3.16 (b)**. Skewness diagram reveals that the overall shape of the $N_q$ distribution varies significantly with the degree of clustering. An increase in the amount of reinforcement particle clusters has skewed the $N_q$ distribution further. Skewness (β) indicates the degree of asymmetry in the statistical distribution, which is represented by the Eq. (3.3) below **[146].**

$$\beta = {(q)}\Big/{[(q-1)(q-2)]}\sum\left[{\left(N_{qi} - N_q^{mean}\right)}\Big/{(\sigma)}\right]^3 \qquad Eq.(3.3)$$

Where, β = Skewness

$q$ = Total number of quadrats studied,

$N_{qi}$ = Number of SiC or SiC(Ni) particles in the $i^{th}$ quadrat ($i$ = 1,2,..,$q$),

$N_q^{mean}$ = Mean number of SiC or SiC(Ni) particles per quadrat, and

σ = Standard deviation of the $N_q$ distribution

An increase in β indicates the increase in SiC and SiC(Ni) clusters. **Figure 3.16 (b)** shows a variation in β with the varying weight fraction of SiC and SiC(Ni) clusters. The skewness ranges between 1.3 to 0.91 for SAC305/SiC composite and between 1.08 to 0.7 for SAC305/SiC(Ni) composite. We see the skewness for SAC305/SiC(Ni) is much broader compared to SAC305/SiC composite solder, which is in agreement with the dissemination of reinforcement particles in lead–free solder. Exact statistical relation can be utilized comfortably for determining the cluster distribution using the quadrant analysis. In conclusion, the analysis of reinforcement distribution is an important factor because it is improved the dispersion of reinforcement particles in the MMCs. In both reinforcements, it is small changes in skewness i.e. impact of Ni coated SiC is more than SiC.

### 3.3.6 Morphological mosaic analysis

The general definition of a mosaic picture is a segmented picture of a plane. Each class of the segment has a mark. Segments are usually produced under object-oriented image coding where the image is partitioned into homogenous zones. The clustering of particles in the matrix is

demonstrated by cell size appropriation and the segmented binary was investigated further. Another technique is the morphological mosaic analysis. Under this method, there arises the issue of characteristic point and it generally overlooks object form. This method requires a constant dilation of the objects, tessellation based on the size and state of the object. However, analyzing the size of the cell carrying from mosaic would reveal the cluster of objects.

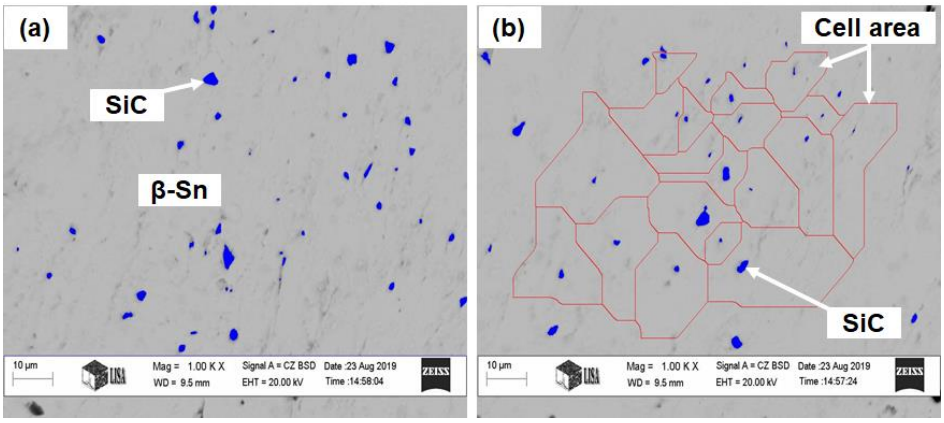


*Figure 3.17 (a) Analyzed segmented SEM micrograph of SAC305 solder with the reinforcement (b) Morphological mosaic of the image.*

FIB-SEM micrographs are taken from the polished samples of the inspected tests of SAC305 solder with the addition of Sic and Ni-coated SiC. The blue colored particles belong to reinforcements (SiC and Ni–SiC) in the micrograph. The cells in which the reinforcement's particles are distributed are visible in **Figure 3.17(a) and Figure 3.17(b)**. Larger and smaller mosaic structures can be seen. In this manner, the size (region) dissemination of the cells is considered and the size (area) distribution of cells is studied. **Figure 3.18(a)** shows the larger effect in SAC305/Ni–SiC solder composite. The average cell area of both composite solders seen to increase as the weight fraction of reinforcement increased, **Figure 3.18(b)** shows the skewness variation of both composites and Ni–coated SiC reinforced composite skewness is much lower than SiC composites i.e. Ni is very effective in the distribution of the particles in the SAC305 solder matrix.

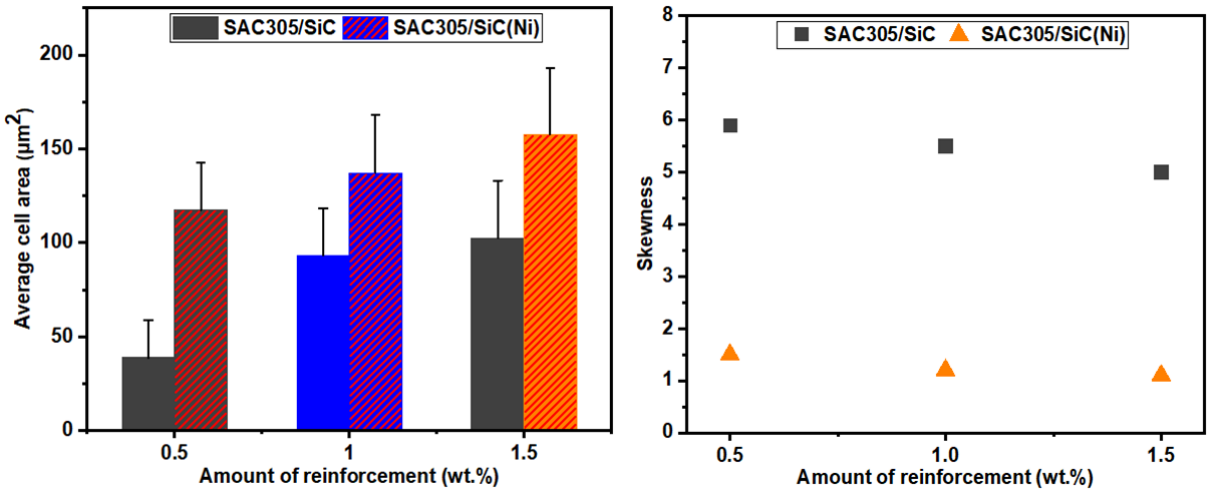


*Figure 3.18(a) Average cell area of SAC305 solder composites with the addition of SiC and Ni–coated SiC (b) Skewness of SAC305 solder composites*

## 3.4 Summary

The homogeneous distribution of the reinforcements in the matrix is very important for the composite material because it is directly affected the mechanical properties of the composite. It was achieved by the powder metallurgy method, Ni–coated silicon carbide (SiC–Ni) are synthesized by EN (Electroless nickel) method, and PM composites were fabricated. Microstructural analysis, physical and mechanical properties were comparatively studied of lead–free solder composite. RCP (relative contact perimeter), average neighboring particles distance, and morphological mosaic are investigated by the Cprob and ImageJ software. SiC particles were perfectly coated with Ni particles by electroless nickel plating method (Figure 3.2) and SiC and SiC(Ni) particles were homogeneously distributed in lead–free solder matrix by ball milling (Figure 3.5). The relative density of sintered and green samples was increased with the increase of the reinforcement composition, however, Ni–coated SiC composite solder samples have higher relative density than SiC reinforced samples. Ni–coated SiC reinforced composite solder has a lower porosity than SAC305/SiC composites and porosity was increased with an increase of composition. SAC305/SiC(Ni) solder composite has higher compressive strength than the SAC305/SiC and the maximum is shown at 1% composition. RCP (relative contact perimeter) was increased with an increase of Ni–coated SiC reinforcement in the solder, however, in the case of SiC reinforcement, it was decreased with an increase of composition. The average neighbour's particle was decreased with the addition of reinforcements.

# 4 CHAPTER 4: Morphology and IMCs of composite solders under reflow and thermal aging

## 4.1 Introduction

Thermal aging and reflow testing at low and high temperatures are the main approaches to evaluate the reliability of solder joints, as the microstructure and mechanical properties of solder joints deteriorate at relatively high operating temperatures. In this chapter, we evaluated and discussed morphology (including solder matrices and interfacial IMCs) and microhardness as a mechanical property to understand the performance of composite solders fabricated under reflow and isothermal aging conditions.

## 4.2 Experimental procedures

### *4.2.1 Preparation of samples for reflow and thermal aging*

To perform the reflow and thermal aging test, a cylindrical sample (3:3 mm in diameter and height) containing two different reinforcements with different compositions were soldered on the Cu substrate. These two types of composite solders were SAC/SiC and SAC/SiC(Ni). **Figure 4.1** shows the top and front view of the specified tool, which was used for preparing the samples. This tool was specifically designed and fabricated by the Institute of Physical Metallurgy, Metal forming, and Nanotechnology, University of Miskolc. The weight of the powder and the compaction pressure was 0.1g and 200MPa. (SAC305)100–$x$(SiC) solder powder was uniaxially compacted in a die (cold pressing at room temperature) to form a cylindrical bar of 3 mm in diameter. The base/substrate was a square copper plate (15 × 15mm) was grinded from sandpaper to achieve a smooth surface for the measurement of contact angle (θ), spread factor ($S_f$), and spread ratio ($S_r$) of the solder, 2mm thick copper sheet. Acetone was used to clean and polish the copper plate. A small amount (0.02g) of activated rosin (RA) flux was used on the surface of the sample and in between the solder sample and the Cu substrate. The main objective of the flux is to eliminate oxidation and other contaminants before and during the melting process.

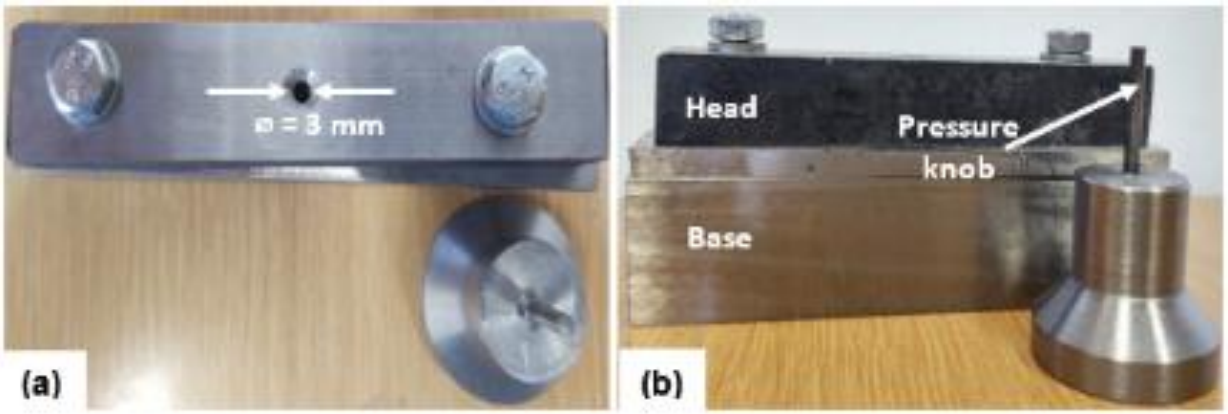


*Figure 4.1 Specific tool for preparation of samples (a) top view (b) front view*

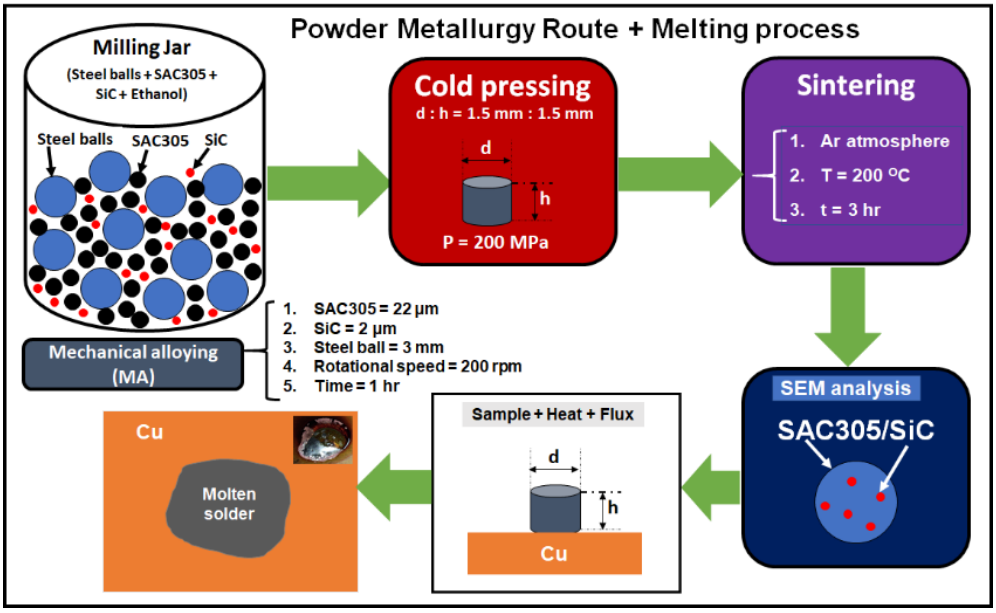


*Figure 4.2 The schematic diagram of the powder metallurgy and melting process of the composite solder*

**Figure 4.2** depicts the schematic diagram of the powder metallurgy and melting process of the composite solder. The solder sample was put on the center of the copper substrate and then the reflow process was conducted. Then, the samples were put in the furnace for melting. In chapter 2, it is proven that 1%SiC composition is optimal as compared to other weight percentages (0, 0.5, 1, and 1.5). SAC305/1%SiC is melted at various reflow temperature (240°C, 260°C, 280°C, and 300°C) at different time (30, 60, 90, & 120min.). When performing the thermal aging test, the thermal aging temperature was set to 140℃, 150℃, 160℃, and 170℃, while the thermal aging times were 0, 25, 50, 75, and 100h. Different samples that perform at different thermal aging times

were studied concerning the evolution and hardness of their microstructure. The detail of experimental conditions can be seen in **Table 4.1, Table 4.2, and Table 4.3**

*Table 4.1 Experimental analysis of SAC305/SiC and SAC305/ SiC(Ni) composite solder*

| **Composite solder** | **Atmosphere** | **Reflow temperature (°C)/Time (min.)** | **Aging temperature (°C)/Time (h)** | **Aim** |
|---|---|---|---|---|
| SAC305/*x*SiC, *x* = 0, 0.5, 1 & 1.5 | Room temperature | 260, 30 | 140, 100 | • Microstructures (Fig. 4.3 and Fig. 4.4)<br>• Microstructures at interfaces (fig.4.6-Fig. 4.8)<br>• IMCs layer thickness (fig. 4.11-Fig. 4.13) (Table 4.4 and Table 4.5)<br>• Hardness (Fig. 4.15)<br>• Contact angle (wettability) (Fig. 4.17)<br>• Spread ratio, spread factor (Fig. 4.18 and Fig. 4.19) |
| SAC305/*x*SiC(Ni, *x* = 0, 0.5, 1 & 1.5 | | | | |

*Table 4.2 Experimental analysis of SAC305/1%SiC composite solder at different reflow time and temperature*

| **Composite solder** | **Atmosphere** | **Reflow temperature (°C)** | **Reflow time (min.)** | **Aim** |
|---|---|---|---|---|
| SAC305/1% SiC | Room temperature | 240°C | 30, 60, 90, & 120 | • Microstructures at interfaces (Fig.4.21)<br>• IMCs layer thickness [multiple reflows (Fig. 4.22 and Table 4.6)]<br>• IMCs layer thickness (Table 4.7, Fig. 4.23-Fig.4.25)<br>• The activation energy (Table 10 and Fig. 4.31) |
| | | 260°C | | |
| | | 280°C | | |
| | | 300°C | | |

*Table 4.3 Experimental analysis of SAC305/1%SiC composite solder at different aging time and temperature*

| Composite solder | Atmosphere | Aging temperature (°C) | Aging time (h) | Aim |
|---|---|---|---|---|
| SAC305/1%SiC | Room temperature | 140°C | 25, 50, 75, & 100 | • Microstructures at interfaces (Fig. 4.26)<br>• IMCs layer thickness (Table 4.8, Fig. 4.27-Fig.4.29 )<br>• The activation energy (Table 11 and Fig. 4.32) |
| | | 150°C | | |
| | | 160°C | | |
| | | 170°C | | |

## 4.3 Results and discussion

### *4.3.1 Microstructural evolution in the solder matrix*

For microstructural observation, all samples were first mounted in epoxy before being grinding and polishing after different reflow and aging process. All polished samples were etched with etching reagent; the metallographic etching reagent consists of a mixture of ethanol and hydrochloric acid. The morphologies of the solder matrix and solder joints at the solder/Cu interface were examined using a FIB–SEM (Focus ion beam-scanning electron microscope).

All the composite solders with different composition (0, 0.5, 1, and 1.5%) reinforcement and 100h aging at 140°C were determined for a comparative study of the microstructural examination of the solder matrix; the morphology of the matrix structures of the different solder with the addition of SiC and SiC(Ni) are shown in **Figure 4.3 and Figure 4.4**.

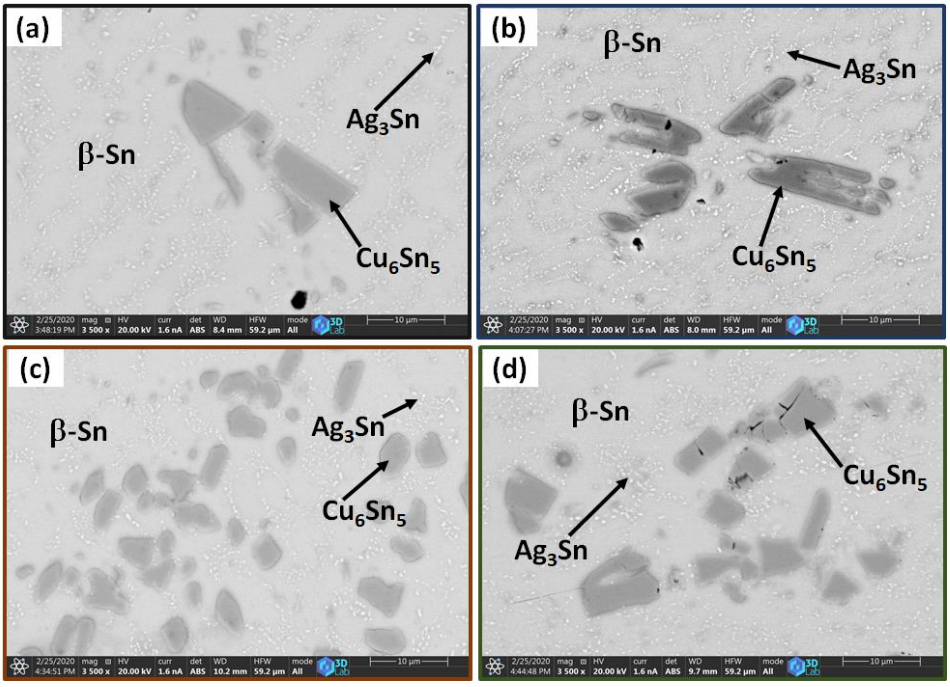


*Figure 4.3 Microstructure of SAC305/xSiC solder composites after 100 h aging (a) monolithic SAC305 (b) 0.5% (c) 1.0% (d) 1.5%*

After 100h aging, it can be observed that the grain boundary of the β–Sn phase disappeared, while the $Ag_3Sn$ IMC showed coarsening and $Cu_6Sn_5$ has a rod-like structure in the monolithic SAC305 solder matrix. It can be seen that after the addition of SiC and Ni–coated SiC, the size of $Ag_3Sn$ IMC and $Cu_6Sn_5$ IMC decreased significantly compared to monolithic SAC305 solder. As discussed in the literature **[9]** that the added reinforcement particles tend to adsorb to the IMC surface during the melting process; interatomic diffusion is thus reduced. After 100h of aging, the grain boundary of the β–Sn phase also becomes disappeared in the SAC305/1.0%SiC matrix; however, the total size of the IMCs range was smaller than for monolithic SAC305 alloy. In addition, the size of $Ag_3Sn$ and $Cu_6Sn_5$ IMCs showed an increasing trend in the aged composite solder matrix; however, the rate of increase was smaller than that of the monolithic SAC305 sample. In the SAC305/1.0%SiC matrix, it was also observed that the growth of $Ag_3Sn$ and $Cu_6Sn_5$ IMC was suppressed and their size was smaller than that of the monolithic SAC305 solder. In the case of SAC/SiC(Ni), the most obvious phenomenon is that after 100h of aging, abundant bulky $(Ni, Cu)_6Sn_5$ IMCs were formed in the solder matrix. This may be due to nickel atoms that were not fully reacted in the solder matrix in the reflow process and some atoms are continued to

participate in the inter-diffusion reaction with the copper substrate and tin atoms in the aging process, thereby $Cu_6Sn_5$ IMC layers were formed.

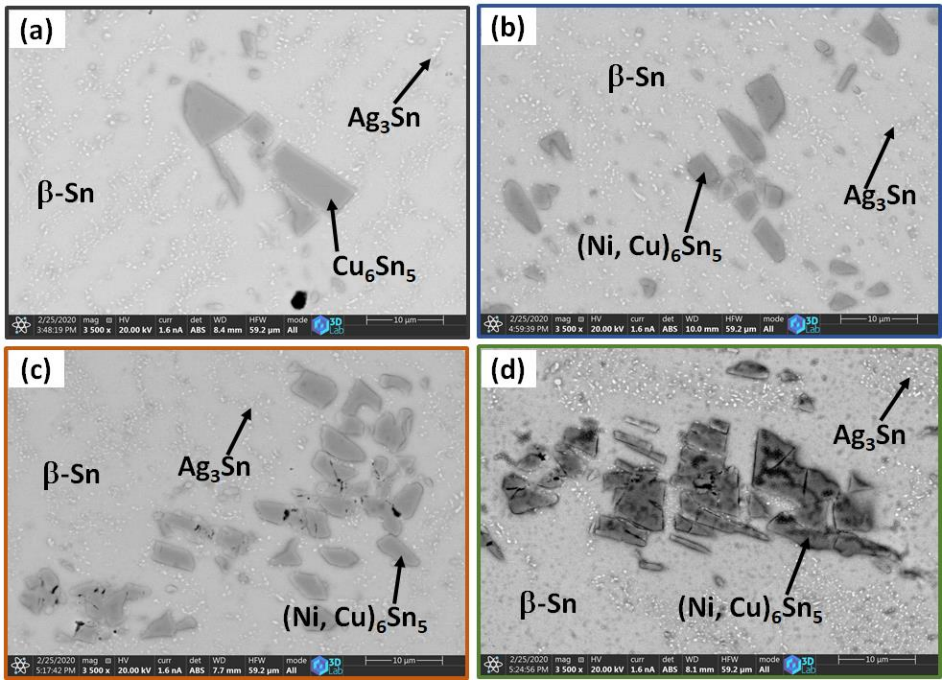


*Figure 4.4 Microstructure of SAC305/xSiC(Ni) solder composites after 100h aging (a) monolithic SAC305 (b) 0.5% (c)1.0% (d) 1.5%*

The reinforcement of SiC and SiC(Ni) particles affects the growth and size of the IMC in the solder matrix. Compared to the monolithic solder, the IMC size of the solder composite is smaller carrying 0.5wt.% and 1.0wt.%SiC and SiC(Ni) particles. Lin et al. **[101]** reported similar results in the refinement of IMCs growth. However, for the other composition (1.5%) of the solder composites, the IMCs size have homogeneous and it did not reduce with increasing of SiC and SiC(Ni). The refinement of the grain size can be attributed to the segregation and agglomeration of SiC and SiC(Ni) particles in bulk solder because the van der Waals forces cause the reinforcement particles to connect with each other. The morphology and size of the IMCs are a very important parameter to investigate the influence of the reinforcement in the solder composite. The IMCs were refined with the addition of the SiC and SiC(Ni) particles to the SAC305 solder. **Figure 4.3** and **Figure 4.4** shows the SEM image of the composite solder with the addition of the SiC and SiC(Ni); however, the development of the $Cu_6Sn_5$ (gray), $Cu_3Sn$, $Ag_3Sn$, and $(Ni, Cu)_6Sn_5$ (dark) IMCs are analyzed by EDS. The IMCs size is analyzed by ImageJ software and

approximately 100 particles are considered. The average size of $Ag_3Sn$ and $Cu_6Sn_5$ IMCs particles were identified as 1.0 to 2.5 μm and 2 to 4 μm in the SAC305/SiC lead–free composite solder. SiC particles were coated with nickel because the presence of IMCs in the SAC305/SiC alloy is not sufficient to provide alloy strength. The addition of small amounts (1%) of SiC(Ni) particles in the SAC305 solder alloys shows that the average size of IMCs ($Ag_3Sn$ and $Cu_6Sn_5$) grains were reduced and this is due to the strong adsorption effect of the reinforcing particles **[36]**. Decreasing the IMCs are followed by the theory of heterogeneous nucleation and adsorption effect **[24][28]**. Ni has a higher adsorption effect and it decreases the surface energy and therefore decreases the growth velocity of IMCs.

The reduction of IMCs grains in the composite solders also indicates the grain refining effect is caused only by the addition of nickel–coated silicon carbide. The average size of $Ag_3Sn$ and $Cu_6Sn_5$ grains were identified as 0.5 to 1.5μm and 1 to 2.5μm in the SAC305/SiC(Ni) lead–free composite solder. SiC particles provide the supplementary nucleation sites for the development of refined IMCs ($Ag_3Sn$ and $Cu_6Sn_5$) and it was observed that SiC particles and IMCs prevent dislocation slippage and thus helped to a strong strengthening effect in composite solder. Such IMCs are played a key role in the matrix since IMCs provide the strength of the matrix β–Sn **[33][29]**.

It is observed that the best morphology of the SAC305/SiC and SAC305/Ni–SiC are achieved at 1.0wt.% of reinforcements because it shows the fine refinement of the IMCs in the solder composites, after that the particle size of the IMCs are increased by 1.5wt.% **(Figure 4.3(c) and Figure 4.4(c)).** The SiC and Ni–coated SiC particles have been observed to be present in agglomerated form, causing cracks and pores to form in the composite, as shown by the enclosed areas. This can be related to the high amount of SiC and SiC(Ni) in the molten matrix (1.5wt.%), the distance between the particles decreases, and the particles get closer to the formation of agglomerates and are easily segregated.

#### *4.3.2 Microstructural evolution at solder/Cu interface*

The morphology of the interfacial IMCs is an important factor that significantly affects the reliability of the solder joint **[148]**. The formation of $Cu_6Sn_5$ on the interface in the solder joint is required to build a strong metallurgical bond and this is due to the interfacial reaction between Sn and Cu substrate during reflow. Several researchers **[149][150][151][152][153][154]** reported that the $Cu_3Sn$ would originate between $Cu_6Sn_5$ and Cu substrate during higher temperature and long

term aging process. The excessive growth of IMCs can weaken the strength of the solder joint during the reflow and aging process due to the brittle nature of IMCs **[155][156][157]**. Thus, the kinetics of the interfacial reaction between the solder and the Cu substrate is an important issue in evaluating the reliability of the solder**.**

Very few literature have reported on the played role of SiC reinforcements in lead-free solder played during the growth of IMCs in the solder matrix. It is known that SiC cannot react with the Cu because SiC is a non-reactive reinforcement but Ni is reactive and forms a $Cu_6Sn_5$ phase on the Cu–Sn interface. In general, the thickness of the interfacial IMCs increases continuously during thermal aging; however, interfacial IMCs mostly consists of a brittle nature, the large-scale growth of interfacial IMCs would serious problem for the reliability of solder joints. The development and growth of the IMCs ($Cu_6Sn_5$ and $Cu_3Sn$) layers in microstructural characterization were described after the reflow and aging process as shown in **Figure 4.5**

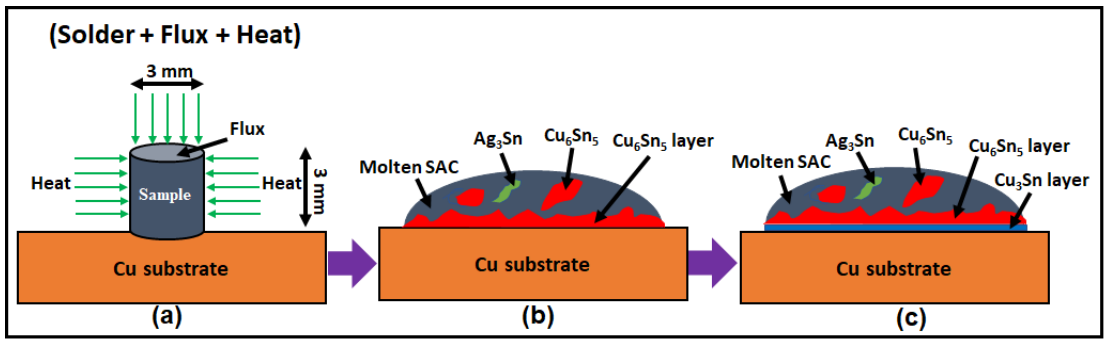


*Figure 4.5 Schematic diagram of the IMCs layers growth (a) solid SAC305 sample on the Cu substrate (b) diffusion of the SAC305 molten solder on substrate and formation of the $Cu_6Sn_5$ IMC after reflow (c) formation of the $Cu_3Sn$ (sandwich structure) layer exists between $Cu_6Sn_5$/Cu interfaces after aging*

**Figure 4.6 and Figure 4.8** show the SEM images of the Sn–3.0Ag–0.5Cu composite solder of the joint interface with the addition of SiC and SiC(Ni) after 100h aging. After aging, both IMCs ($Cu_6Sn_5$ and $Cu_3Sn$) layers are developed at the Sn-Cu interface. **Figure 4.7** is confirmed the $Cu_6Sn_5$ and $Cu_3Sn$ layers.

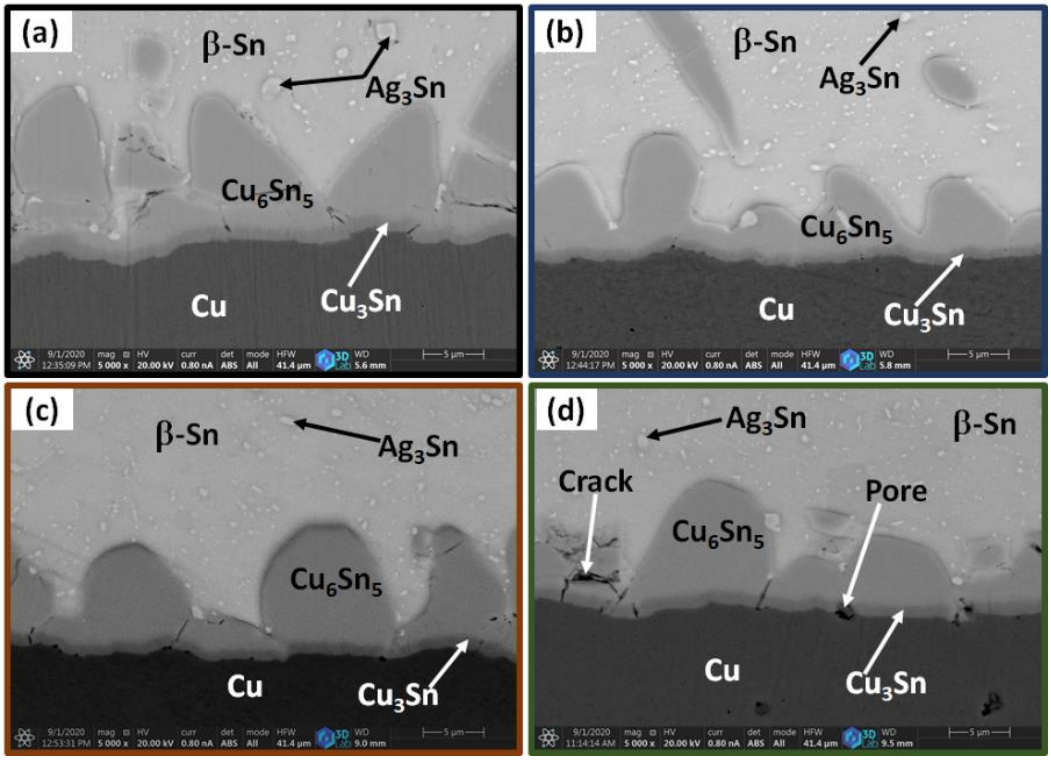


*Figure 4.6 SEM micrographs of SAC305/xSiC lead–free solder composites after 100h aging at 140 °C (a) monolithic SAC305 (b) 0.5% (c) 1.0% (d) 1.5%*

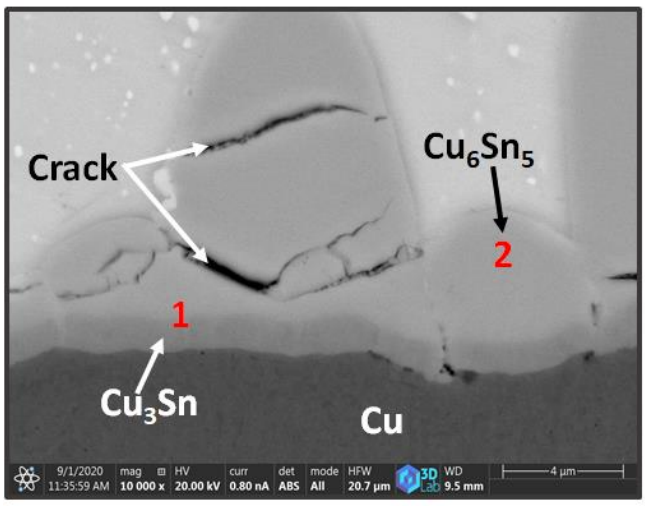


**Point-1**

| Element | Weight (%) |
|---|---|
| Sn L | 35.7 |
| Cu K | 64.3 |

**Point-2**

| Element | Weight (%) |
|---|---|
| Sn L | 59.9 |
| Cu K | 40.1 |

*Figure 4.7 Verification of the IMCs in the SAC305 solder composite with the addition of SiC*

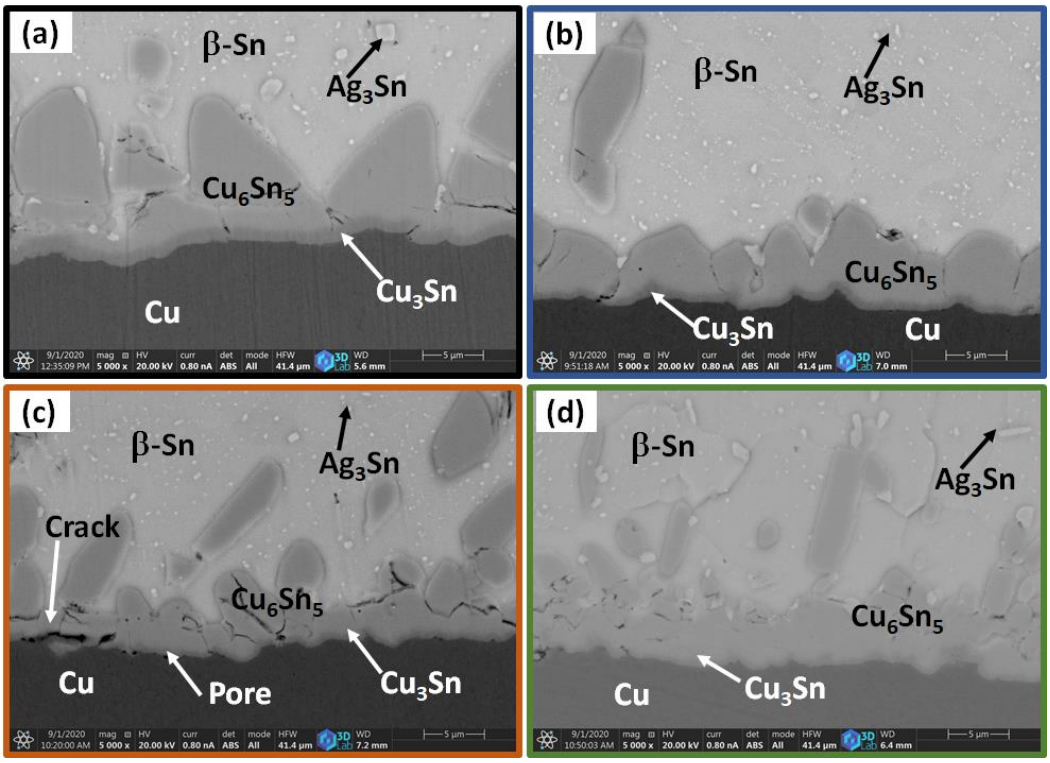


*Figure 4.8 SEM micrographs of SAC305/xSiC(Ni) lead–free solder composites after 100h aging at 140°C (a) monolithic SAC305 (b) 0.5% (c) 1.0% (d) 1.5%*

The average thickness of IMCs layers in the Sn–Cu interface in different conditions were determined by the SEM images. The irregular shape of $Cu_6Sn_5$ layer and thick plate-like $Cu_3Sn$ layer on the surface of the Cu as shown in schematic **Figure 4.9** and IMC thickness is measured by the ‘‘ImageJ’’ software. The average thickness ($x_t$) was calculated by the total area ($A$) of the individual IMC divided by the total length ($L$) of the layer, as shown in **Eq. (4.1)**:

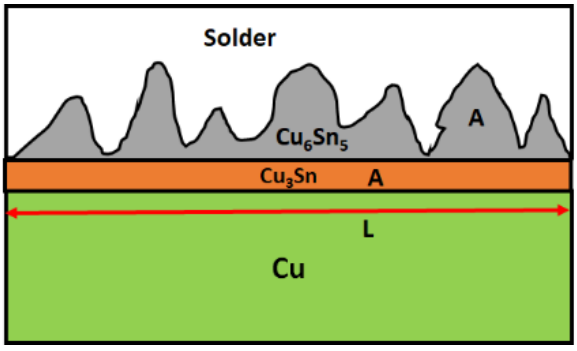


*Figure 4.9 Schematic diagram of interfacial microstructure on Cu substrate*

$$x_t = \frac{A}{L} \qquad Eq.(4.1)$$

Where, $x_t$ = Average thickness (µm),

$A$ = Total area of the individual IMCs and (µm$^2$),

$L$ = Total length of the IMCs layer (µm)

ImageJ is used for the analysis of the $Cu_6Sn_5$ and $Cu_3Sn$ layer thickness. **Figure 4.10 (a–c)** displays the segmented area of the $Cu_3Sn$, $Cu_6Sn_5$, and total layer ($Cu_3Sn$ + $Cu_6Sn_5$). The thickness of the IMCs layer is calculated from these areas of the IMCs divided by the length of the image.

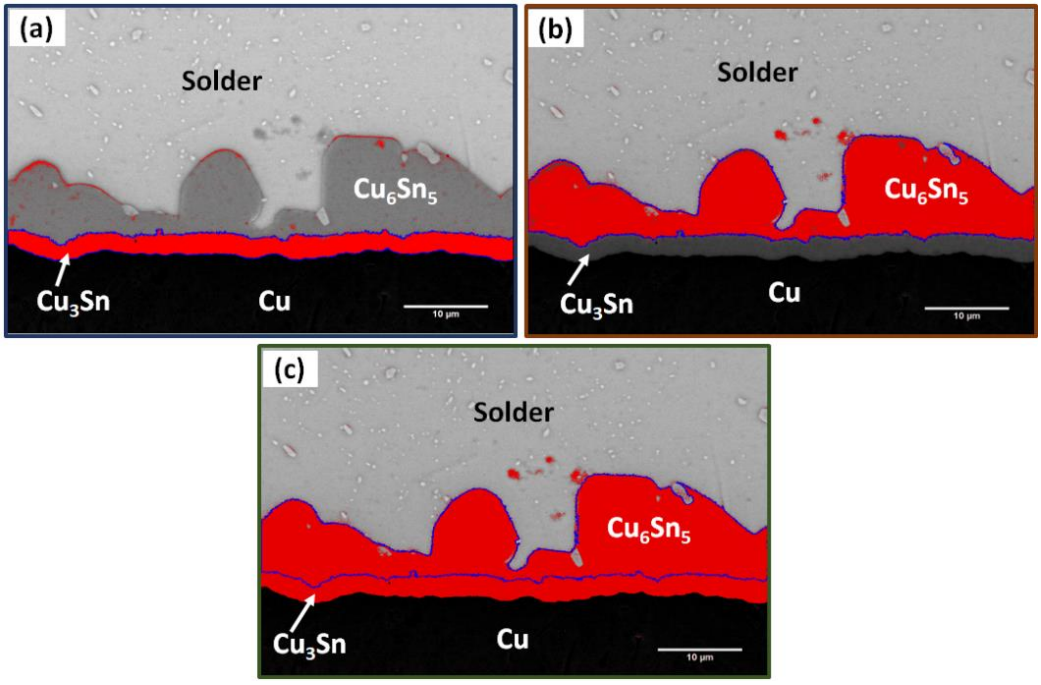


*Figure 4.10 Thickness analysis of the IMCs layer by ImageJ (a) segmented area of $Cu_3Sn$ (b) segmented area of $Cu_6Sn_5$ (c) total area of the IMCs*

The thickness results for all composite (SAC305/SiC and SAC305/SiC–Ni) solders are shown in **Table 4.4** and **Table 4.5** respectively.

*Table 4.4 Average thickness of $Cu_6Sn_5$ and $Cu_3Sn$ in lead–free solder composites with the addition of SiC*

| Composite solder | Aging temperature (°C) | Aging time (h) | IMC thickness layer (µm) | | |
|---|---|---|---|---|---|
| | | | $Cu_6Sn_5$ | $Cu_3Sn$ | Total |
| SAC305 | 140 | 100 | 7.57 | 1.21 | 8.78 |

| | | | | | |
|---|---|---|---|---|---|
| SAC305/0.5SiC | | | 6.08 | 1.01 | 7.09 |
| SAC305/1.0SiC | | | 4.24 | 0.73 | 4.97 |
| SAC305/1.5SiC | | | 5.27 | 0.96 | 6.23 |

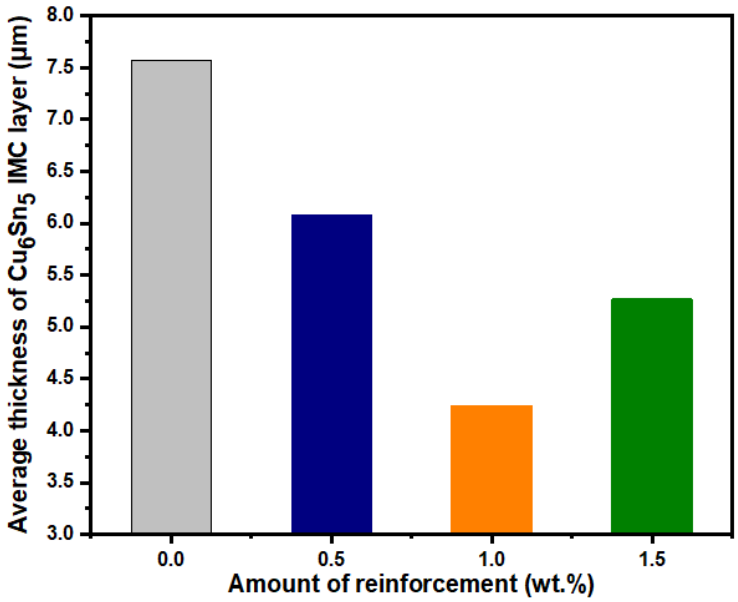


*Figure 4.11 Variation of $Cu_6Sn_5$ thickness in the SAC305 lead–free solder with the addition of SiC*

In the monolithic solder, the almost intermittent IMC morphology became smaller in size after the addition of different amounts of SiC and Ni–coated SiC particles. However, the almost intermittent IMC structures became thin and continuous after reinforcing particles were added to the SAC305. Most of the added particles are involved in the formation of the IMCs. The chemical reaction between SAC305 and the Cu substrate also induced the growth of a thin layer of the $Cu_3Sn$ phase. The growth of $Cu_6Sn_5$ and $Cu_3Sn$ layer thickness on the Cu substrate was suppressed by the addition of different amounts of reinforcement (SiC and Ni–coated SiC) particles in the solder matrix after 100h aging, as shown in **Figure 4.11, Figure 4.12, and Figure 4.13**. It was noticed that the minimum thickness of the IMC layer was obtained by the addition of 1% by weight of SiC and Ni–coated SiC particles. This was due to the added reinforcement particles in the solder matrix which were inhibited the Cu atom. Most of the Cu atoms came from the Cu substrate; however, a few percent came from the solder matrix **[158]**. This pathway of Cu atoms was retarded due to the formation of the Sn-Cu phase between molten solder and the Cu substrate during the reflow process.

*Table 4.5 Average thickness of Cu6Sn5 and $Cu_3Sn$ in SAC305 composites with the addition of SiC(Ni)*

| Composite solder | Aging temperature (°C) | Aging time (h) | IMC thickness layer (µm) | | |
|---|---|---|---|---|---|
| | | | $Cu_6Sn_5$ | $Cu_3Sn$ | Total |
| SAC305 | 140 | 100 | 7.57 | 1.21 | 8.78 |
| SAC305/0.5%SiC(Ni) | | | 5.44 | 0.85 | 6.29 |
| SAC305/1.0%SiC(Ni) | | | 3.78 | 0.53 | 4.31 |
| SAC305/1.5%SiC(Ni) | | | 4.95 | 0.80 | 5.75 |

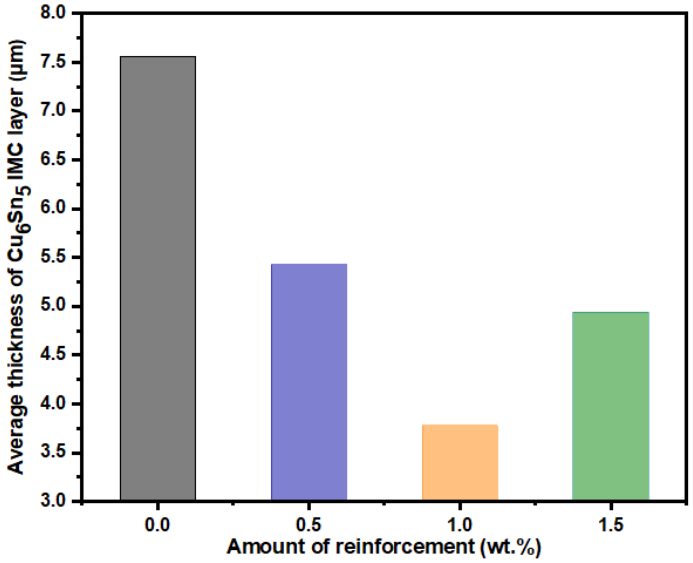


*Figure 4.12 Variation of $Cu_6Sn_5$ thickness in the SAC305 lead-free solder with the addition of SiC(Ni)*

The thickness of the $Cu_6Sn_5$ and $Cu_3Sn$ IMCs layer was decreased by 43.8% and 39.6% in the SAC/1%SiC; however, $Cu_6Sn_5$ and $Cu_3Sn$ IMCs layer was reduced by 50.06% and 56.19% in the SAC/1%SiC(Ni) composite solder. The outcome shows that the development of the $Cu_6Sn_5$ and $Cu_3Sn$ IMC layer on the Sn–Cu interface was suppressed by a small addition of SiC and SiC(Ni) particles. These reinforcement particles reduce the surface energy and inhibit the growth of IMC layers. Several researchers reported the same trend after using different types of reinforcements in the lead–free solders **[159][160][22][161][26][162][163][114][47][43][164][165][56]**.

However, with the reinforcement of 1.5wt%SiC and SiC(Ni) **(Figure 4.3d and Figure 4.4d),** coarse scallop type $Cu_6Sn_5$ particles were developed on the interfacial layer and the number of $Ag_3Sn$ IMC was not increased in the solder composite solder. Furthermore, the reduction of the

IMCs layer thickness was lesser than the other composition **(Figure 4.11, Figure 4.12, and Figure 4.13)** and this is due to the agglomeration and segregation of the reinforcement particles in the bulk solder. The segregation and agglomeration are happened due to the van der Waals forces and this force is entangled of the reinforcement particles as used of more amount (1.5%), therefore IMCs layer thickness and number of $Ag_3Sn$ grains are decreased **[159]**. Similar research is reported for the morphology of the bulk solder with the addition of SiC by Liu **[33].**

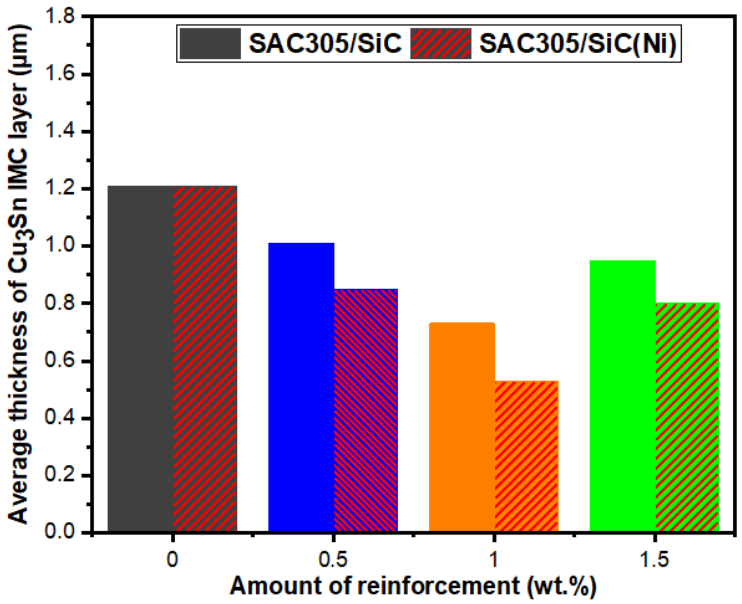


*Figure 4.13 Variation of $Cu_3Sn$ thickness in the SAC305 lead-free solder with the addition of SiC and SiC(Ni)*

### *4.3.3 Microhardness*

To estimate the effect of thermal aging on the microhardness of SiC and Ni–coated SiC reinforced composite solder with various composition was examined. Specifically, the microhardness test was performed with a Vickers hardness tester at room temperature; the details of the process are shown in a schematic diagram **(Figure 4.14)**.

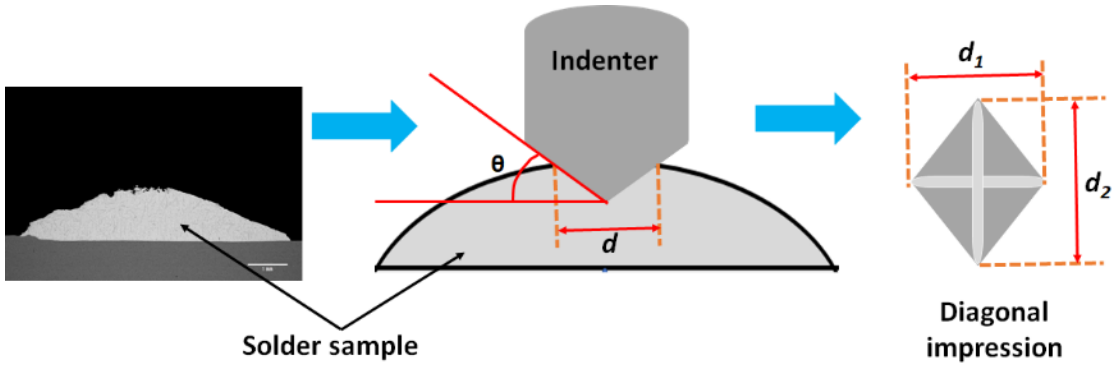


*Figure 4.14 Schematic diagram of a microhardness test*

During the hardness test, the applied load was 10g, while the dwell time was 10 seconds. For each solder sample, three points were tested by removing the minimum and maximum values. Using the size of the diagonals of the impression, the microhardness data of the different samples were calculated using **Eq. (4.2) and Eq. (4.3)**:

$$HV = 1.854 \times \frac{F}{d^2} \qquad Eq.(4.2)$$

$$d = \left(\frac{d_1 + d_2}{2}\right) \qquad Eq.(4.3)$$

Where, HV is the Vickers hardness, F is the applied load (g) and $d$ is the diameter of indentation (μm) and it can be calculated by the mean value of $d_1$ and $d_2$.

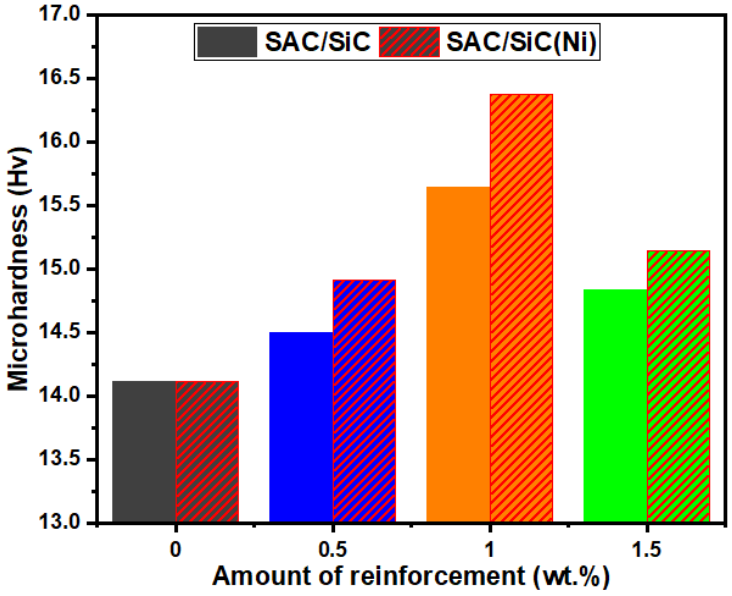


*Figure 4.15 Microhardness of monolithic SAC305, SAC305/SiC, and SAC305/SiC(Ni) composite solders*

The microhardness of monolithic SAC305, SAC305 and SAC305/Ni–coated SiC composite solder are shown in **Figure 4.15**. It is examined that the microhardness values of composite solders are increased as compared to that of the monolithic SAC305 solder. The higher values are 15.25 and 15.98Hv for SAC305/1.0%SiC and SAC305/1.0%SiC(%) composite solder. Compared to the monolithic SAC305 solder, these results show the ~10.8% and ~16.0% increment in the microhardness of composite solder with the addition of 1.0wt.%SiC and SiC(Ni). The reason for the improvement of microhardness is the finely distributed intermetallics ($Ag_3Sn$ and $Cu_6Sn_5$) in the composite solder **[107]**. The hard $Ag_3Sn$ IMCs can resist indentation more strongly than the monolithic SAC305 solder. This improvement can be related to (1) The existence of the harder SiC and Ni–coated SiC and (2) Reinforcements act as an obstruction to the localized matrix deformation and dislocation movement due to the presence of reinforcement **[45]**.

## 4.4 Wetting behavior of composite solder

Wetting concerning composite solders plays an important role in understanding the spreading behavior of the solder as a function of temperature, time. Besides time and temperature, in a composite solder wetting is affected by flux composition, reflow temperature, and surface roughness of solid. Here, as stated earlier, SiC and SiC(Ni) was chosen as the reinforcement in the SAC solder matrix to obtain the composite. The wettability was evaluated by measuring the spreading area on copper substrates and wetting angles. Solder specimen (3 mm × 3 mm) is placed on the center of the Cu plate with flux and melted in the furnace at a 260°C for 30min. For good wetting of solders, a perfect metallurgical bond must be established at the interface between the solder (liquid) and the Cu (solid) substrate. Due to interfacial reaction, the IMCs grains or the intermetallic layers are composed at the surface. **Figure 4.16** shows the schematic diagram for the evaluation of the relative spread area, contact angle, spread factor, and spread ratio.

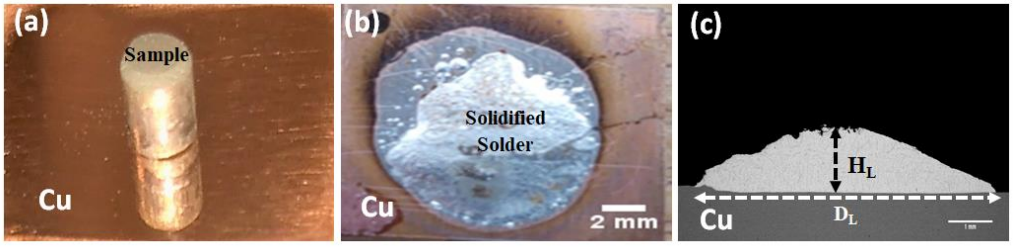

*Figure 4.16 Measuring process for the contact angle and spread ratio (a) solder sample (b) after melting (c) cross-section of the molten droplet on Cu substrate*

### *4.4.1 Contact angle (wettability) of composite solder*

The contact angle of the solder on the substrate changed as a function of the amount of reinforcements. The contact angles were calculated by using the following equation **Eq. (4.4) [166]**,

$$\sin\theta = \frac{2}{(d/h) + (h/d)} \qquad Eq.(4.4)$$

The variation of contact angles of composite solders was shown in **Figure 4.17**. The largest contact angle was observed of monolithic SAC305 solder. Initially, the contact angle is decreased from 30.87º to 19.80º for 1%SiC and 16.70 for 1%SiC(Ni), however, an increasing trend was seen afterward. These results verify that the improved wetting performance of the solder matrix at a limited composition can be achieved by marginally increasing the quantity of SiC particles. Non–uniform segregation and increased viscosity of melted solder on Cu have to lead to de-wetting **[45]**.

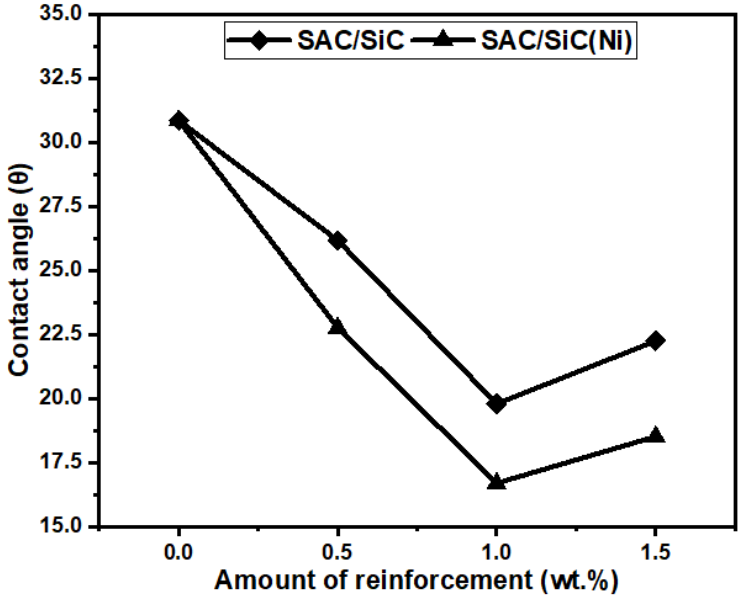


*Figure 4.17 Contact angle variation of SAC305 solder with the addition of Sic and SiC(Ni) on Cu substrate*

#### *4.4.2 Spread ratio and spread factor*

Spread ratio ($S_r$) is calculated by measuring the spherical area achieved by the melted solder specimen on the substrate. It is done by measuring the diameter ($d$) and height ($h$) of the cooled solder area on the substrate. Spread ratio is taken as the ratio of total plane area wetted by the molten solder on a solid substrate to the plane area of the original solder sample, which is expressed by **Eq. (4.5)** and **Eq. (4.6) [166]**.

$$S_r = \frac{Total\ plane\ area\ wetted\ by\ the\ molten\ solder\ on\ the\ solid\ substrate}{Plane\ area\ of\ the\ original\ spherical\ metal\ sample} \qquad Eq.(4.5)$$

$$S_r = \frac{4d^2/h^2}{[1+3d^2/h^2)]^{2/3}} \qquad Eq.(4.6)$$

Where, d is the diameter of the solder sample (mm) and h is the height (mm). Spread factor ($S_f$) is calculated as the consequence of spread ratio and is given in **Eq. (4.7)** and **Eq. (4.8):**

$$S_f = \frac{Diametre\ of\ the\ original\ solder\ sample\ (d) - \ Height\ of\ the\ spreaded\ molten\ metal\ (h)}{Diametre\ of\ the\ original\ solder\ sample\ (d)} \qquad Eq.(4.7)$$

$$S_f = 1 - \frac{1}{[1+3\,d^2/h^2]^{1/3}} \qquad Eq.(4.8)$$

**Figure 4.18** and **Figure 4.19** shows the variation of spread ratio ($S_r$) and spread factor ($S_f$) with the corresponding amount of reinforcements and it was observed that the spread ratio ($S_r$) and spread factor ($S_f$) of SAC305 solder increased at 1.0% with an addition of SiC and SiC(Ni). The lowest value obtained for the spread ratio and spread factor is 4.46 and 7.08 for monolithic SAC305 solder, whereas the maximum values were observed to be 6.12 and 7.84 for SAC305/1.0%SiC and 6.88 and 8.08 for SAC305/1.0%SiC(Ni) respectively.

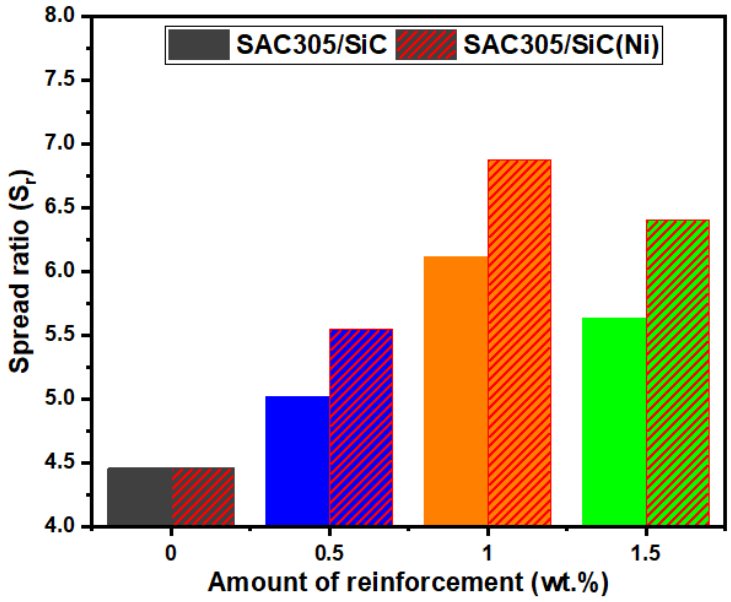


*Figure 4.18 Spread ratio factor trend of SAC305 solder composites with the addition of SiC and SiC(Ni)*

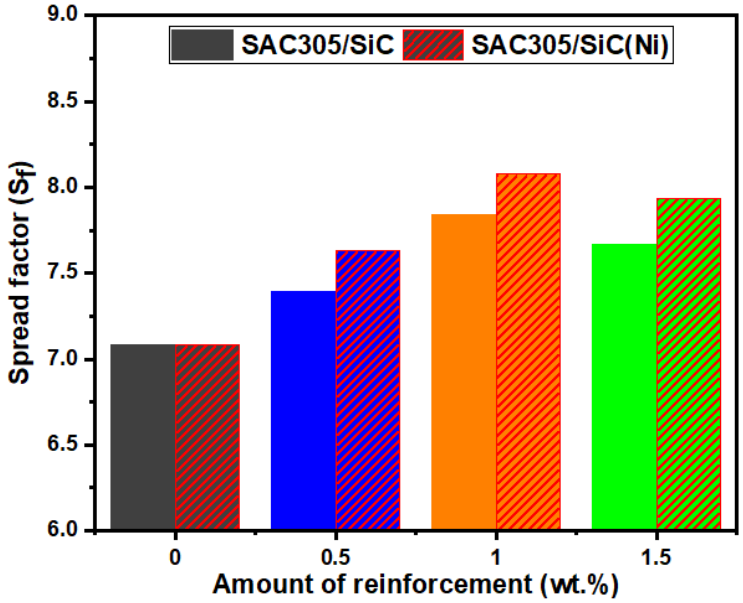


*Figure 4.19 Spread factor trend of SAC305 solder composites with the addition of SiC and SiC(Ni)*

It is noticed that SAC305/1.0%SiC and SAC305/1%SiC(Ni) has the maximum spreading ratio and spreading factor. The spreading ratio and spreading factor increases until 1.0% composition and then decreases. The higher amount of reinforcements interrupted the flow of the solder because it is increased the melt viscosity and decrease the spreading of the solders on the substrate **[9][45][107].**

## 4.5 Interfacial reactions between Sn–Ag–Cu solder and Cu substrate

SAC305/1%SiC composite solder is selected for examination of the thickness of the $Cu_6Sn_5$ and $Cu_3Sn$ at the different aged conditions and different times because this composition showed the best results as already discussed in chapter 3. The SAC305/1.0%SiC solder was reflowed for different temperatures (240$^o$C, 260$^o$C, 280$^o$C, 300$^o$C) at time (30min, 60min, 90min, 120min) and same composite solder was aged at different temperature (140$^o$C, 150$^o$C, 160$^o$C, 170$^o$C) at time (25h, 50h, 75h, 100h). **Figure 4.20(a–b)** shows the morphology of the reflow and aged solder sample, however, $Ag_3Sn$ grains are distributed on the $Cu_6Sn_5$ layer and in the bulk solder area and it is frequently widespread in the $Cu_6Sn_5$ surface layer with increasing aging time**. Figure 4.21** shows the morphology of the SAC305/1.0%SiC solder at the Cu substrate after various reflow temperature. The scallop–type $Cu_6Sn_5$ and plate-like $Cu_3Sn$ IMCs were observed at the Cu–Sn interface. Generally, $Cu_6Sn_5$ and $Cu_3Sn$ layers are formed in the Sn–based solder alloys at the Cu–Sn interface, and the thickness of these two layers are increased with increasing aging time. **Figure 4.21** shows the increasing thickness of IMCs with increasing time.

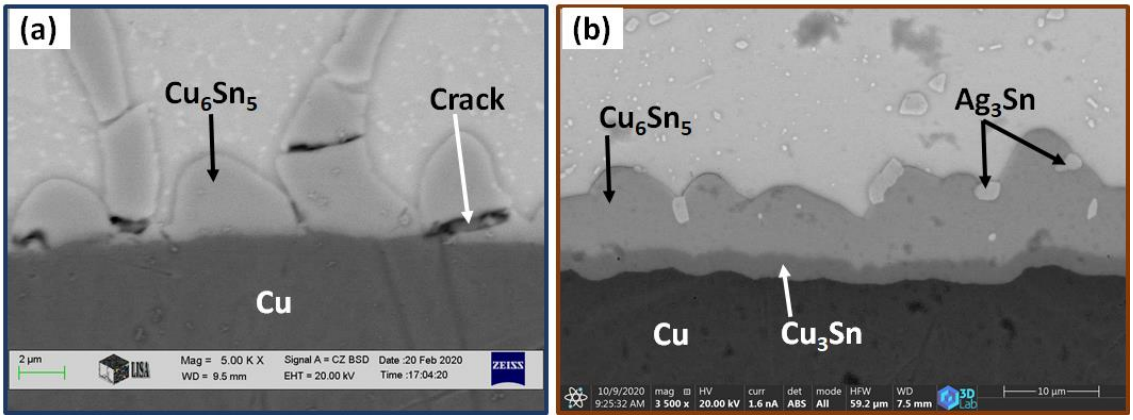


*Figure 4.20 SEM Image of composite solder after (a) reflow process and (b) aging*

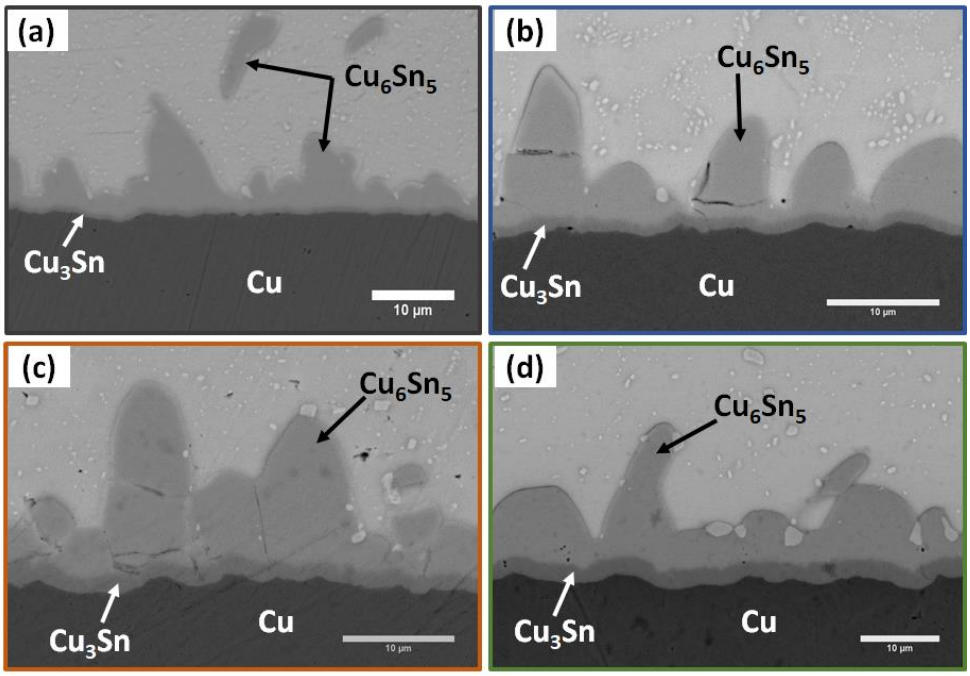


Figure 4.21 Morphology of SAC305/1%SiC composite solder at different reflow temperature (a) 240 °C (b) 260 °C (c) 280 °C (d) 300 °C

**Figure 4.22** shows the IMCs layer thickness of SAC305/1%SiC(Ni) composite solder after multiple reflow cycles. The diffusion rate is very quick at reflow temperature because the reflow process involves diffusion between modes of transport due to the melting of the solder particles.

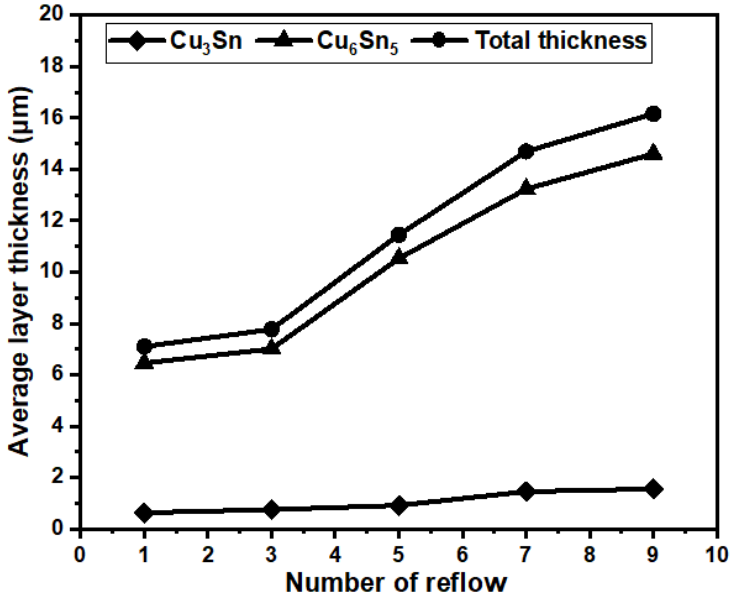


*Figure 4.22 IMCs layer thickness of SAC305/1%SiC(Ni) composite solder as a function of reflow number*

**Table 4.6** shows the effect of multiple reflows on the growth of the IMCs layer and it is thickness increased very fast. The average thickness of $Cu_6Sn_5$ and $Cu_3Sn$ IMCs layer grows from ~6.46 and ~0.64 μm after the first reflow cycle to a maximum of ~14.6 and 1.56 μm thickness after the ninth reflows.

*Table 4.6 Average layer thickness of the SAC305/1.0%SiC(Ni) composite solder with various reflow cycle*

| Composite solder | Reflow temperature (°C)/Time (min) | Number of reflows | IMC thickness layer (μm) | | |
|---|---|---|---|---|---|
| | | | $Cu_6Sn_5$ | $Cu_3Sn$ | Total |
| SAC305/1.0%SiC(Ni) | 260/30 | 1 | 6.46 | 0.64 | 7.10 |
| | | 3 | 7.01 | 0.76 | 7.77 |
| | | 5 | 10.53 | 0.92 | 11.45 |
| | | 7 | 13.23 | 1.46 | 14.69 |
| | | 9 | 14.6 | 1.56 | 16.16 |

The mean thickness of the IMCs layer in SAC305/1%SiC composite solder on Cu substrate at different reflow time and temperature are shown in **Table 4.7.** The thickness of the IMCs layer developed at the Cu–Sn interface was examined quantitatively as a function of aging time. To kinetics of the IMCs growth layer at the Sn/Cu interface, IMC growth was assumed to be controlled by volume diffusion, i.e., the growth rate is proportional to the square root of time. The IMC thickness as a function of time can be expressed by the Arrhenius **Eq. (4.9)**:

$$x_t = x_0 + Dt^n \qquad Eq.(4.9)$$

Where, $x_t$ = IMC layer thickness at time t (μm),

$t$ = aging time (s)

$x_0$ = Initial IMC layer thickness after aging (μm),

$D$ =Diffusion coefficient as a function of temperature ($\mu m^2/s$), and $n$ = Time exponent.

When plotting the thickness of the intermetallic layer ($x_t$) against the square root of the aging time ($t^{1/2}$) from **Eq. (4.10)**, the slope of the graph is equal to the square root of the diffusion coefficient ($D^{1/2}$). The diffusion coefficient was determined from a linear regression analysis of $x$ vs $t^{1/2}$, where the slope is $D^{1/2}$.

$$ln(x_t - x_0) = lnD - n.ln(t) \qquad Eq.(4.10)$$

Where, the exponent *n* is equal to the slope of the $ln(x_t - x_0)\ vs\ ln(t)$ curve. The value of *n* will be 1/2 when the IMC formation is controlled by the volume diffusion mechanism **[167]**. In this study, the value *n* under isothermal aging was 0.50, however, Shen et al. **[168]** reported for isothermal aging, thermal cycling, and thermal shock has considered 0.51, 0.6, and 0.62, respectively. When, plotting the thickness of the IMC layer ($x_t$) versus the aging time ($t^{1/2}$), the slope of the graph is equal to the square root of the diffusion coefficient ($D^{1/2}$). The thickness of the IMCs layer in SAC305/1%SiC composite solder on Cu substrate at different reflow time and temperature are shown in **Table 4.7.**

*Table 4.7 Thickness of IMCs layer of the SAC305/1%SiC composite solder at different reflow time and temperature*

| Reflow temperature (°C) | Reflow time (min) | IMCs thickness (µm) | | |
|---|---|---|---|---|
| | | $Cu_6Sn_5$ | $Cu_3Sn$ | $Cu_6Sn_5$ +$Cu_3Sn$ |
| 240 | 30 | 3.07 | 0.43 | 3.50 |
| | 60 | 5.06 | 0.59 | 5.66 |
| | 90 | 6.49 | 0.83 | 7.34 |
| | 120 | 7.71 | 0.96 | 8.66 |
| 260 | 30 | 3.81 | 0.55 | 4.32 |
| | 60 | 6.53 | 1.08 | 7.62 |
| | 90 | 8.22 | 1.30 | 9.52 |
| | 120 | 9.76 | 1.51 | 11.34 |
| 280 | 30 | 5.82 | 1.01 | 6.83 |
| | 60 | 8.42 | 1.42 | 9.84 |
| | 90 | 10.08 | 1.76 | 11.84 |
| | 120 | 12.41 | 2.15 | 14.56 |
| 300 | 30 | 6.75 | 1.35 | 8.10 |
| | 60 | 9.95 | 1.84 | 11.79 |
| | 90 | 12.38 | 2.39 | 14.77 |
| | 120 | 14.63 | 2.60 | 17.23 |

**Figure 4.23, Figure 4.24, and Figure 4.25** show the IMCs layer thickness ($Cu_6Sn_5$, $Cu_3Sn$, and total thickness) are developed on the Cu–Sn interface at different reflow time and temperatures. The thickness of the IMCs layers is increased with an increase of reflow time and temperature.

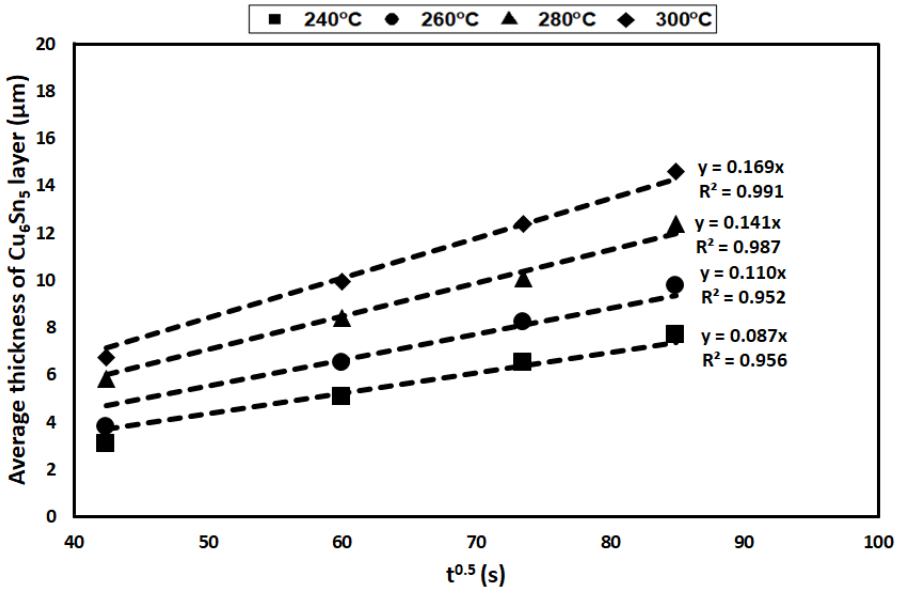


*Figure 4.23 Average thickness of $Cu_6Sn_5$ layer of SAC305/1%SiC composite solder at different reflow temperature*

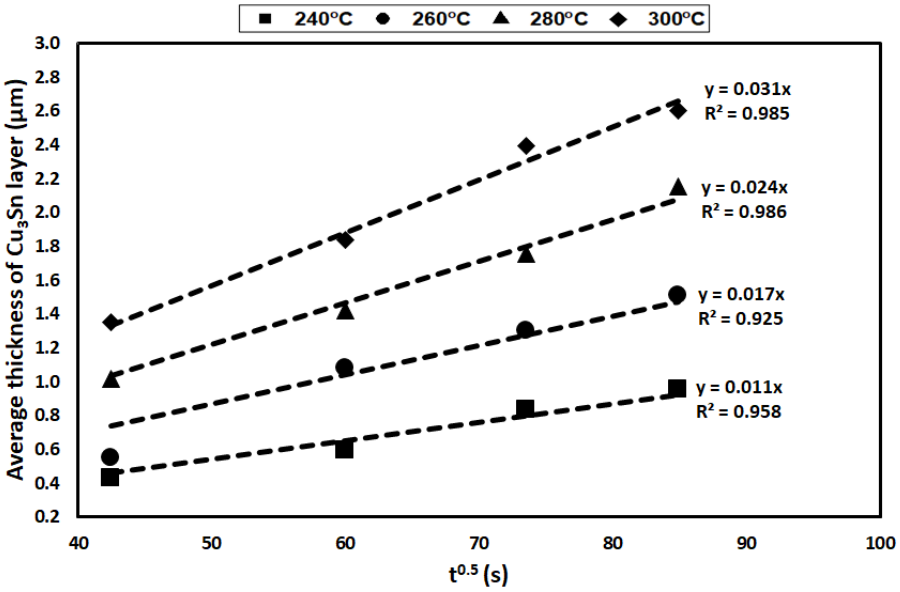


*Figure 4.24 Average thickness of $Cu_3Sn$ layer of SAC305/1%SiC composite solder at different reflow temperature*

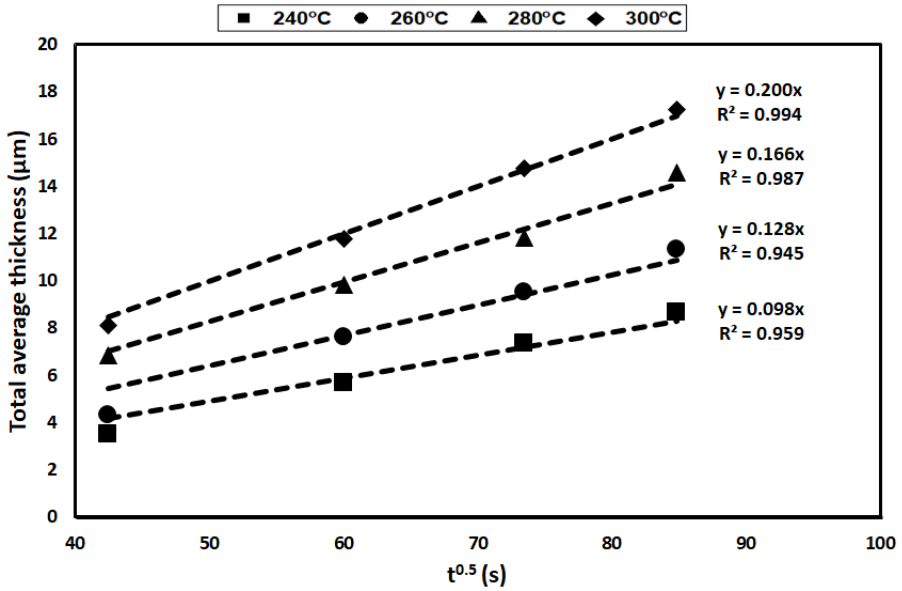


*Figure 4.25 Total Average thickness layer in SAC305/1%SiC composite solder at different reflow temperature*

The morphology of the SAC305/1%SiC composite solder after aging at different temperatures (140 °C, 150 °C, 160 °C, and 170 °C) is shown in **Figure 4.26** and the thickness of the IMCs layer at different aging time and temperature are shown in **Table 4.8.** The IMCs layer thickness is increased with an increase in time and temperature. **Figure 4.27, Figure 4.28, and Figure 4.29** show the IMCs layer thickness ($Cu_6Sn_5$, $Cu_3Sn$, and total thickness) developed at the Cu–Sn interface as a function of $t^{1/2}$ (aging time). The $Cu_6Sn_5$, $Cu_3Sn$, and total thickness layers enhanced linearly with the $t^{1/2}$. Moreover, the square root of the aging time sown that the enhanced IMCs layer thickness is a diffusion-driven process **[169]**.

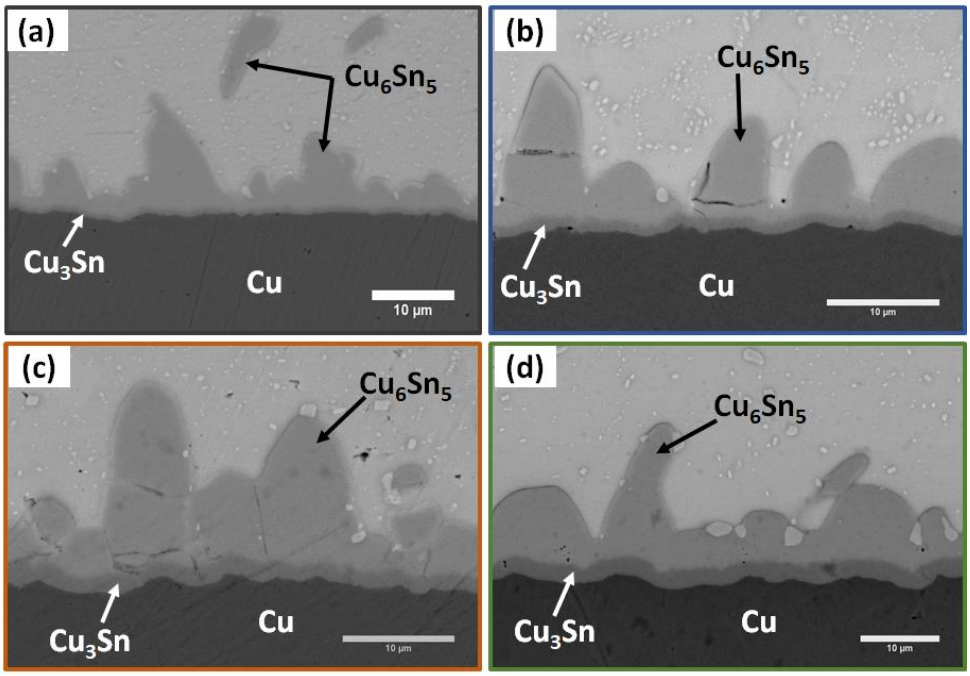


*Figure 4.26 Morphology of SAC305/1%SiC composite solder after 100h aging at different temperature (a) 140 °C (b) 150°C (c) 160°C (d) 170°C*

*Table 4.8 Thickness of IMCs layer of the SAC305/1%SiC composite at different aging time and temperature*

| Aging temperature (°C) | Aging time (h) | IMCs thickness (µm) | | |
|---|---|---|---|---|
| | | $Cu_6Sn_5$ | $Cu_3Sn$ | $Cu_6Sn_5$ +$Cu_3Sn$ |
| 140 | 25 | 3.99 | 0.47 | 4.46 |
| | 50 | 4.59 | 0.58 | 5.17 |
| | 75 | 5.31 | 0.73 | 6.04 |
| | 100 | 5.84 | 0.84 | 6.69 |
| 150 | 25 | 4.43 | 0.72 | 5.14 |
| | 50 | 4.91 | 1.06 | 5.97 |
| | 75 | 5.49 | 1.10 | 6.59 |
| | 100 | 5.80 | 1.21 | 7.01 |
| 160 | 25 | 6.06 | 0.93 | 6.99 |
| | 50 | 6.14 | 1.45 | 7.59 |
| | 75 | 6.34 | 1.48 | 7.82 |
| | 100 | 7.58 | 1.77 | 9.35 |
| 170 | 25 | 6.79 | 1.08 | 7.87 |
| | 50 | 6.90 | 1.66 | 8.56 |

| | | | | |
|---|---|---|---|---|
| | 75 | 7.62 | 1.69 | 9.31 |
| | 100 | 7.98 | 2.39 | 10.37 |

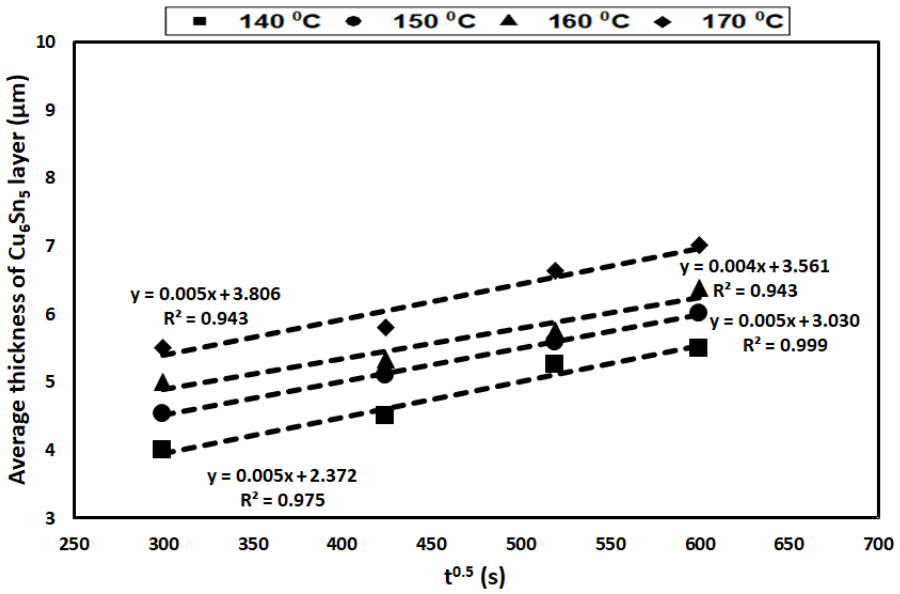


*Figure 4.27 Average thickness of $Cu_6Sn_5$ layer of SAC305/1%SiC composite solder at the different aging temperature*

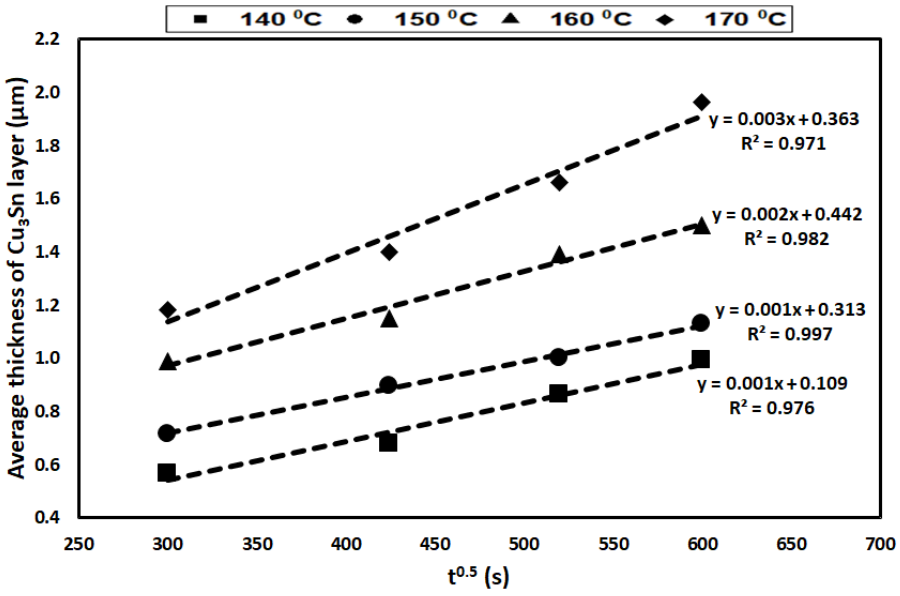


*Figure 4.28 Average thickness of $Cu_3Sn$ IMC layer of SAC305/1%SiC composite at the different aging temperature*

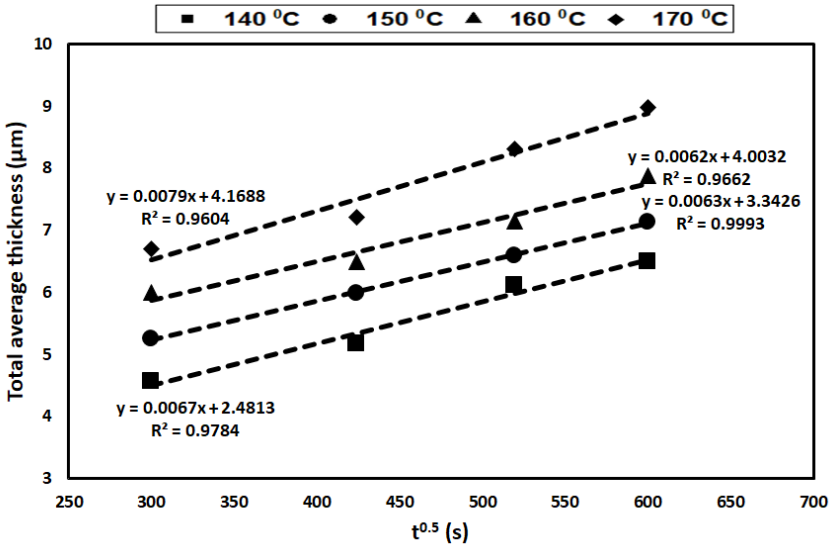


*Figure 4.29 Total Average thickness layer in SAC305/1%SiC composite solder at the different aging temperature*

The diffusion coefficient of the IMCs layer at the Cu–Sn interface is listed in **Table 4.9**. The diffusion coefficient of the IMC layers are varied with aging temperature and it is increased with increasing aging temperature. The diffusion coefficient of $Cu_3Sn$ IMC was higher than the $Cu_6Sn_5$ IMC at aging temperatures of 140 and 170°C, indicating that $Cu_3Sn$ IMC increased rapidly at high temperatures. $Cu_3Sn$ IMC enhanced slowly at low aging temperatures of 140°C, as shown in **Table 4.9**. The slopes of the curve can be considered as the diffusion coefficient of the IMC.

*Table 4.9 Diffusion coefficient of intermetallic phases of SAC305/1%SiC composite solder at the different aging temperature*

| Temperature (°C) | Intermetallic phase | Slope, $D^{1/2}$ ($m/s^{1/2}$) | D ($m^2/s$) |
|---|---|---|---|
| 140 | $Cu_6Sn_5$ | 3.00E-09 | 9.00E-18 |
| | $Cu_3Sn$ | 1.00E-09 | 1.00E-18 |
| | $Cu_6Sn_5$ +$Cu_3Sn$ | 4.00E-09 | 1.60E-17 |
| 150 | $Cu_6Sn_5$ | 4.00E-09 | 1.60E-17 |
| | $Cu_3Sn$ | 2.00E-09 | 4.00E-18 |
| | $Cu_6Sn_5$ +$Cu_3Sn$ | 6.00E-09 | 3.60E-17 |
| 160 | $Cu_6Sn_5$ | 8.00E-09 | 6.40E-17 |
| | $Cu_3Sn$ | 3.00E-09 | 9.00E-18 |
| | $Cu_6Sn_5$ +$Cu_3Sn$ | 1.00E-08 | 1.00E-16 |
| 170 | $Cu_6Sn_5$ | 9.00E-09 | 8.10E-17 |

| | | | |
|---|---|---|---|
| | $Cu_3Sn$ | 5.00E-09 | 2.50E-17 |
| | $Cu_6Sn_5$ +$Cu_3Sn$ | 1.00E-08 | 1.00E-16 |

To the development of the IMCs layer thickness, the growth process of the IMC needs to be understood. In the diffusion between lead-free solder and Cu, the development of the IMCs occurs in two ways. First is the interdiffusion and the second is an interfacial reaction. From the Sn–Cu phase diagrams, Sn can react with Cu to form the IMCs layer, while there is no interaction between SiC and Cu because Sic is non-reactive reinforcement and it is gathered in the solder matrix. It is clear from the Sn–Cu phase diagram that Cu has a concentration bandgap in each phase of the IMCs and the Cu concentration gradient must be in the IMCs layer during the solder–Cu interface. Chen et al**. [170]** and Chung et al. **[171]** reported that Cu is dominant in the Sn-Cu inter-diffusion process and Cu diffuses towards the Sn with a higher rate because Cu atoms have a lower atomic radius (0.128 nm) than Sn atoms (0.141nm). In the diffusion process, Cu gives sufficient Cu atoms for the origination of the IMCs. The $Cu_3Sn$ is developed by consuming $Cu_6Sn_5$, so kinetics IMCs are very important to solder reliability. The growth kinetics of IMC $Cu_6Sn_5$ is almost identical to the kinetics of all IMCs **[172]**. The chemical reaction allows the atoms to enter the IMC; however, the diffusion process gives the atoms for the reaction. **Figure 4.30** shows the development process for IMCs in the solder–Cu interface.

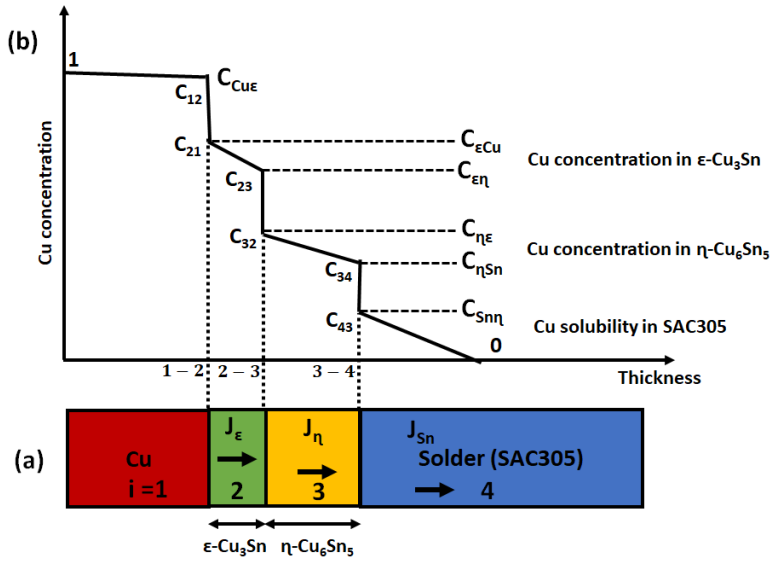


*Figure 4.30 Schematic diagram of the development of $Cu_3Sn$ and $Cu_6Sn_5$ layer between Cu and Sn during aging (1-2, 2-3 and 3-4)*

The interfacial reaction starts at the $Cu/Cu_3Sn$ interface and local chemical equilibrium is recognized at $C_{\varepsilon Cu}$ (phase 1–2), as shown in **Figure 4.30.** Cu atoms come from the substrate and enter into the $\varepsilon$ phase by chemical reaction expressed by **Eq. (4.11).** Some amount of them remain at the $Cu/Cu_3Sn$ interface and the others form the Cu diffusion flux ($J\varepsilon$), which is controlled by Cu concentration gradient in the ε-phase.

$$3Cu + Sn \leftrightarrow Cu_3Sn \qquad \textit{Eq. (4.11)}$$

Some amount of $J_\varepsilon$ reacts with $Cu_6Sn_5$ phase to develop the $Cu_3Sn$ phase at the $Cu_3Sn/Cu_6Sn_5$ interface, which is demonstrated by **Eq. (4.12)** and the remaining amount of $J_\varepsilon$ moves into the $\eta$ phase to develop diffusion flux ($J_\eta$) (phase 2–3).

$$9Cu + Cu_6Sn_5 \leftrightarrow 5\ Cu_3Sn \qquad \textit{Eq. (4.12)}$$

Some amount of $J_\eta$ moves at the $Cu_6Sn_5$/solder interface to develop the $Cu_6Sn_5$ and the remaining amount dissolves in the solder, which is shown by **Eq. (4.13).**

$$6Cu + 5Sn \leftrightarrow Cu_6Sn_5 \qquad \textit{Eq. (4.13)}$$

Shang et al. reported that the $Cu_3Sn$ phase develops through nucleation and growth at both sides of the interfaces ($Cu_6Sn_5/Cu_3Sn$ and $Cu/Cu_3Sn$). The Cu can react with $Cu_6Sn_5$ to form the $Cu_3Sn$ phase at the $Cu_3Sn/Cu_6Sn_5$ interface; however, Sn can react with $Cu_3Sn$ to form the $Cu_6Sn_5$ phase. This is the reversible process and it is expressed by the following **Eq. (4.14) [173]:**

$$Cu_6Sn_5 \quad \underset{Sn}{\overset{Cu}{\rightleftharpoons}} \quad Cu_3Sn \qquad \textbf{\textit{Eq. (4.14)}}$$

At the same time, Sn can diffuse across the volume or particle boundary to the $Cu/Cu_3Sn$ interface and react with Cu to form $Cu_3Sn$. Laurila et al. **[174]** reported that Sn is the main diffusing species in the $Cu_6Sn_5$ layer between 60 and 200ºC. Both Cu and Sn diffuse into the $Cu_3Sn$ layer, but Cu diffusion is about three times faster than Sn. Therefore, the reaction of the $Cu_6Sn_5/Cu_3Sn$ interface should influence the growth of the $Cu_3Sn$ layer **[174].**

### *4.5.1 Calculation of activation energy*

The diffusion coefficient at different temperatures was often expressed by Arrhenius **Eq. (4.15)**:

$$D = D_0\, e^{\left(\frac{-Q}{RT}\right)} \qquad Eq.(4.15)$$

Where, $D_0$ = Temperature-independent diffusion coefficient ($m^2/s$),

$Q$ = Activation energy (kJ/mol),

$R$ = Universal gas constant (8.3145 J/K mol),

$T$ = Absolute temperature (K)

The activation energy of the intermetallic phase can be determined by (**Eq. 4.15)** and the diffusion coefficient can be indicated as **Eq. (4.16)**:

$$ln(D) = ln(D_0) - \frac{Q}{R}\left(\frac{1}{T}\right) \qquad Eq.(4.16)$$

**Eq. 16** can be expressed as the linear equation $y = mx + c$, where, $y = ln(D)$, $m = (-Q/R)$ and $c = ln(D_0)$; however, $ln(D)$ is dependent and $(1/T)$ is independent variable. If the diffusion coefficient (D) is plotted against the aging temperature (1/T), the activation energy (Q) can be computed from the slope of the graph and the diffusion coefficient ($D_0$) can be determined from the intercept of the graph. **Table 4.10** and **Table 4.11** shows the diffusion coefficient and the activation energy of the intermetallic phase $Cu_3Sn$, $Cu_6Sn_5$, and ($Cu_6Sn_5$ + $Cu_3Sn$) after reflow and aging process.

*Table 4.10 Diffusion coefficient and activation energies of intermetallic phases after reflow*

| Intermetallic phases | Activation energy, Q (kJ/mol) | Diffusion coefficient, $D_0$ ($m^2/s$) |
|---|---|---|
| $Cu_6Sn_5$ | 54.57 | 2.73E-09 |
| $Cu_3Sn$ | 86.06 | 7.45E-08 |
| $Cu_3Sn$ + $Cu_6Sn_5$ | 58.83 | 9.51E-09 |

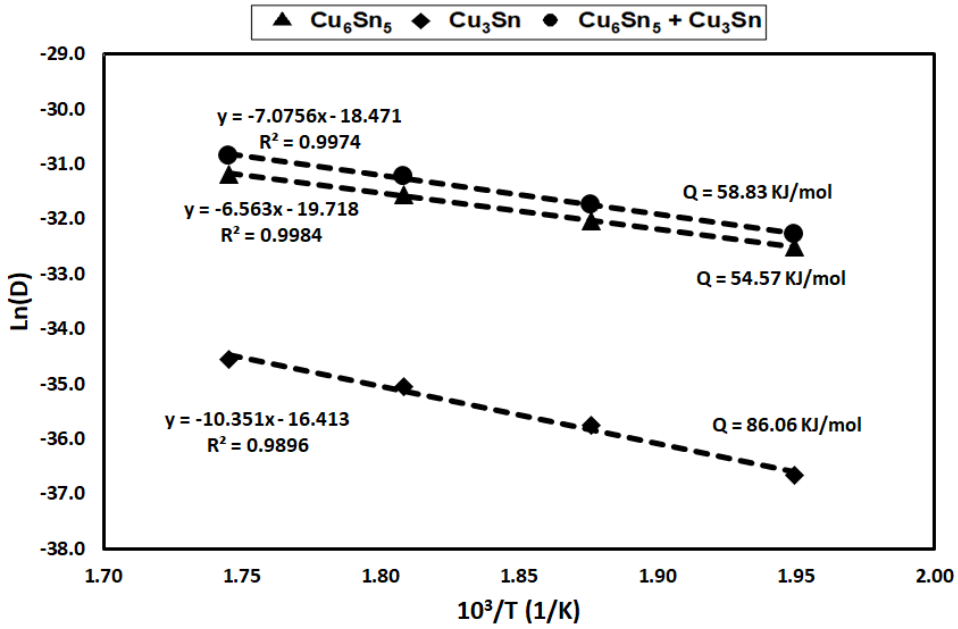


*Figure 4.31 Arrhenius plot for the growth of the IMCs layer after the reflow process*

*Table 4.11 Diffusion coefficient and activation energies of intermetallic phases after aging*

| Intermetallic phases | Activation energy, Q (kJ/mol) | Diffusion coefficient, $D_0$ ($m^2/s$) |
|---|---|---|
| $Cu_6Sn_5$ | 58.59 | 2.14E-10 |
| $Cu_3Sn$ | 91.74 | 4.52E-07 |
| $Cu_3Sn + Cu_6Sn_5$ | 68.62 | 7.46E-09 |

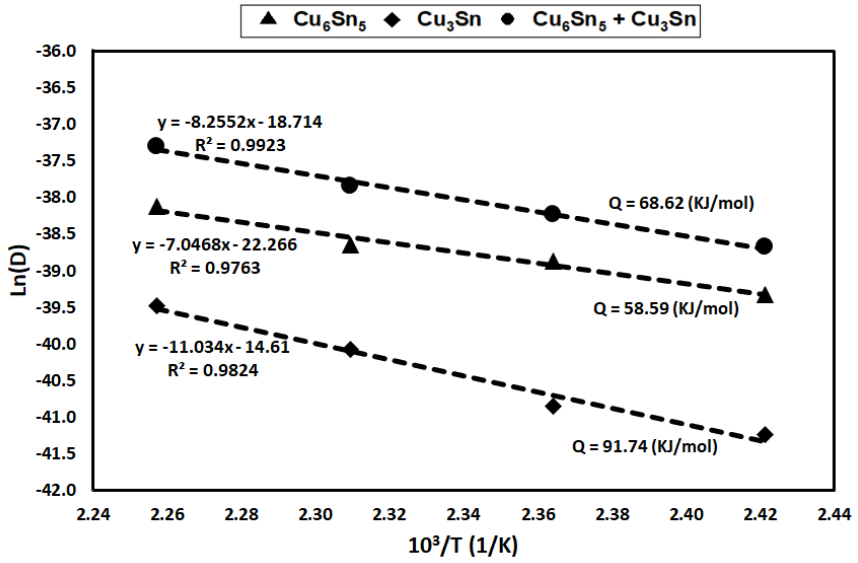


*Figure 4.32 Arrhenius plot for the growth of the IMCs layer after the aging process*

**Figure 4.31** and **Figure 4.32** shows the Arrhenius plots for the growth of the $Cu_6Sn_5$, $Cu_3Sn$, and total thickness layers formed at the solder joint after reflow and aging. The activation energies are 54.57, 86.06, and 58.8371kJ/mol for reflow and 91.74, 58.59, and 68.62kJ/mol for aging respectively. The activation energy of the $Cu_6Sn_5$ phase was created to be lower than that of the $Cu_3Sn$ phase. This states that the formation of the $Cu_6Sn_5$ layer is more thermodynamically stable than the $Cu_3Sn$ phase; however, the activation energy of the total ($Cu_6Sn_5$ + $Cu_3Sn$) layer found to be between $Cu_6Sn_5$ and $Cu_3Sn$ phases, which seems to be acceptable. Some researchers are reported the same trend with related literature **[150][175][169]. Table 4.12** shows the activation energies obtained by the other researchers and comparable with this study. This research shown that the activation energies are in acceptance with literature.

*Table 4.12 Comparison of activation energies obtained here to those from other literature studies*

| Solder/substrate | Soldering method | Aging Temperature (K) | Aging Time (s) | IMC Phases | Activation energy (kJ/mol) | Reference |
|---|---|---|---|---|---|---|
| Sn–3.0Ag–0.5Cu-SiC/ Cu | Reflow | 413–443 | 9.0E+04–3.6E+05 | $Cu_3Sn$ | 91.73 | Current work |
| | | | | $Cu_6Sn_5$ | 59.68 | |
| | | | | $Cu_3Sn + Cu_6Sn_5$ | 64.71 | |
| Sn–0.3Ag–0.7Cu/Cu | Dipping | 373–443 | 0–3.6E+6 | $Cu_3Sn$ | 119.04 | **[176]** |
| | | | | $Cu_6Sn_5$ | 51.59 | |
| | | | | $Cu_3Sn + Cu_6Sn_5$ | 80.65 | |
| Sn–3.8Ag–0.7Cu/CSP/OSP | Reflow | 373–423 | 0–3.6E+6 | $Cu_3Sn$ | 119.80 | **[169]** |
| Sn–3.5Ag | Dipping | 343–443 | 0–3.6E+6 | $Cu_6Sn_5$ | 58.59 | **[175]** |
| | | | | $Cu_3Sn + Cu_6Sn_5$ | 75.16 | |
| Sn–5Bi | Reflow | 343–443 | 0–2.6E+6 | $Cu_3Sn$ | 90.50 | **[177]** |
| | | | | $Cu_6Sn_5$ | 98.35 | |
| | | | | $Cu_3Sn + Cu_6Sn_5$ | 107.10 | |
| Sn–3.0Ag–0.5Cu/ CSP/OSP | Reflow | 373–443 | 0–5.2E+6 | $Cu_6Sn_5$ | 41.30 | **[178]** |
| | | | | $Cu_3Sn + Cu_6Sn_5$ | 79.90 | |
| Sn–3.0Ag–0.5Cu/Cu (THX) | Reflow | 373-443 | 0–5.2E+6 | $Cu_6Sn_5$ | 41.3 | **[169]** |
| | | | | $Cu_3Sn + Cu_6Sn_5$ | 79.9 | |

| | | | | | | |
|---|---|---|---|---|---|---|
| Sn–3.0Ag–0.5Cu/Cu (THO) | Reflow | 373-443 | 0–5.2E+6 | $Cu_6Sn_5$ | 49.7 | **[169]** |
| | | | | $Cu_3Sn + Cu_6Sn_5$ | 85.5 | |
| Sn-3.8Ag–0.7Cu/Cu | Reflow | 398–443 | 0–5.4E+6 | $Cu_3Sn + Cu_6Sn_5$ | 92.6 | **[179]** |
| Sn–3.5Ag–0.7Cu/Cu | Reflow | 393–463 | 0–3.6E+6 | $Cu_3Sn + Cu_6Sn_5$ | 88.2 | **[180]** |
| Sn–3.0Ag–0.5Cu/Cu | Reflow | 373-443 | 0–2.4E+6 | $Cu_3Sn + Cu_6Sn_5$ | 75.1 | **[169]** |

## 4.6 Summary

The solder joint microstructure is essential for the reliability of the solder joint and it is obtained through a metallurgical reaction. In this chapter, solder joint metallurgy, microstructure, wetting behavior and hardness evolution of two composite solders under thermal aging was comparatively studied. According to the experimental result, SiC and Ni–coated SiC reinforcements effectively suppress the growth of $Cu_6Sn_5$ and $Cu_3Sn$ IMCs under thermal aging and wetting properties are improved. In addition, Ni–coated SiC reinforcement improved the hardness of the SAC305 solder alloy to some extent. Fundamental concepts associated with IMCs formation and growth in solder joints have been presented in this chapter. These include diffusion, solid-state growth, and growth amongst others. The experimental procedure and methodology used for the study of IMCs layer formation and growth in SAC305 solder joint are presented in chapter 4.

# 5 CHAPTER 5: Thesis points

Based on the presented experimental results, the main conclusions are presented in the following thesis points:

***PM process***

(1) As increasing the amount of SiC, the relative density also increased due to the press of SiC into the large-sized solder grains by milling.

(2.a) Ni–coated SiC reinforced composite solder has a lower porosity than SAC305/SiC composites because the reinforcement particles distributed homogeneously. As a result of this homogeneous distribution, the SiC was less clustered, thus a reduced amount of porosity formed around the clusters.

(2.b) According to the lower porosity content, the changes in the compressive strength of the composite solders were observed and the SAC305/SiC(Ni) solder composite has higher compressive strength than the SAC305/SiC.

***Reflow process:***

(3) The RCP (relative contact perimeter) was increased in the Ni–coated SiC reinforced samples. In the case of non-coated samples, it was decreased. Higher RCP results in the homogenous distribution in the SiC(Ni)samples because the reinforcement grains can distribute better in the melt. Consequently, the average neighbour's particle shows that in the case of SiC(Ni) samples the clustering was less relevant than it is in SiC samples, i.e. reinforcements were homogeneously distributed in the SiC(Ni) samples vs. SiC samples.

(4) I have proved that SiC decreases, contact angle and increases the spread area, and application of Ni coating further reinforces this tendency. Think about why these parameters will be better if SiC is added and even these particles are coated with nickel?

***Kinetics***

(5) I have developed a method that can be used to simulate how the IMC layer changes during reflow under the influence of time and temperature (Fig. 5.1-5.3)

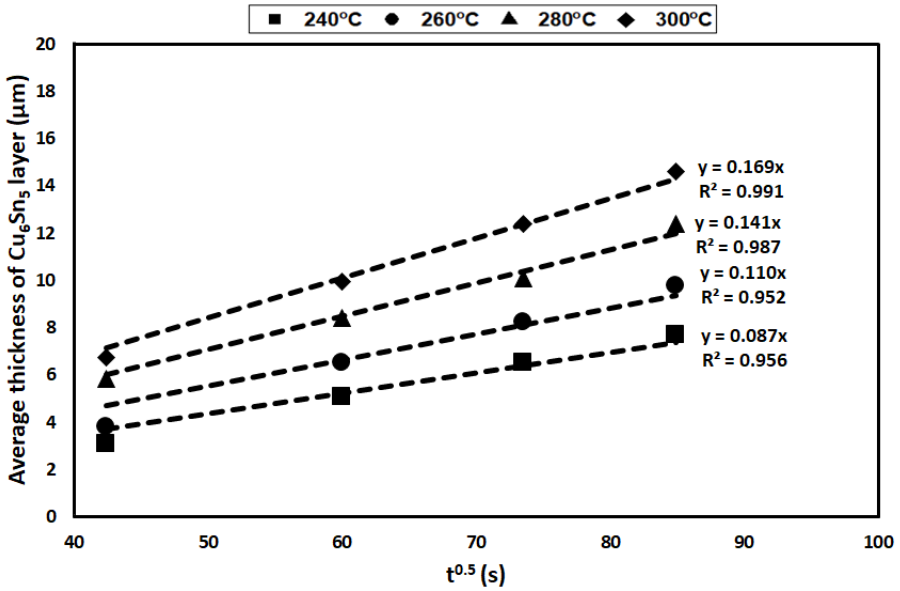


*Figure 5.1 Average thickness of $Cu_6Sn_5$ layer of SAC305/1%SiC composite solder at different reflow temperature*

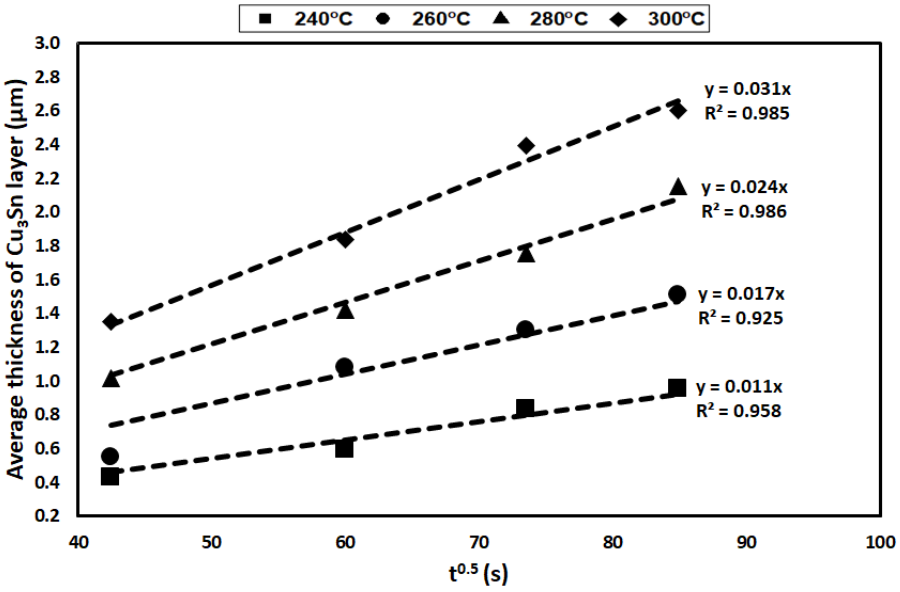


*Figure 5.2 Average thickness of $Cu_3Sn$ layer of SAC305/1%SiC composite solder at different reflow temperature*

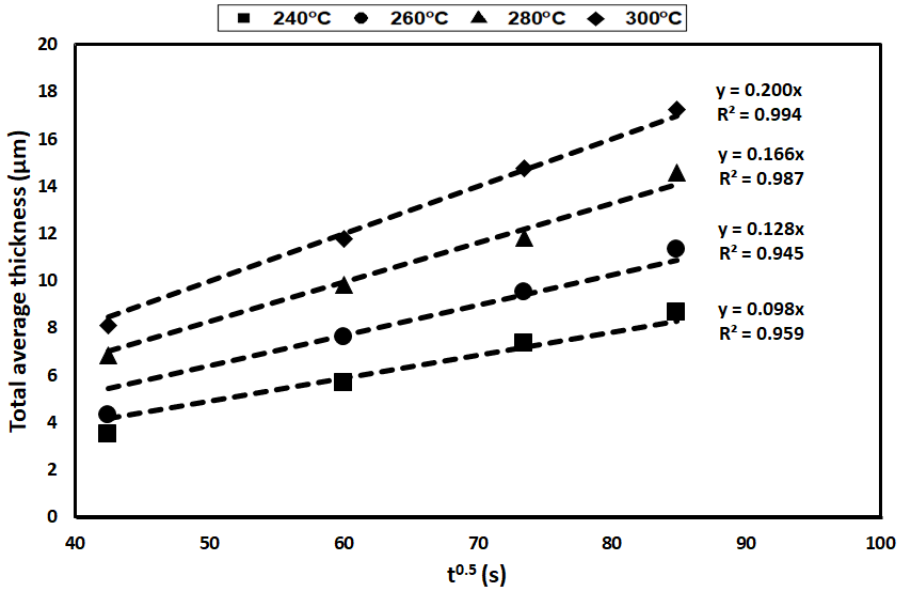


*Figure 5.3 Total Average thickness layer in SAC305/1%SiC composite solder at different reflow temperature*

(6) Using the procedure, I proved that the change in the thickness of the IMC layer is a diffusion process. I determined the diffusion coefficient and the activation energy, which can be used to estimate the layer thickness during the given technological process (Figure 5.4 and Figure 5.4).

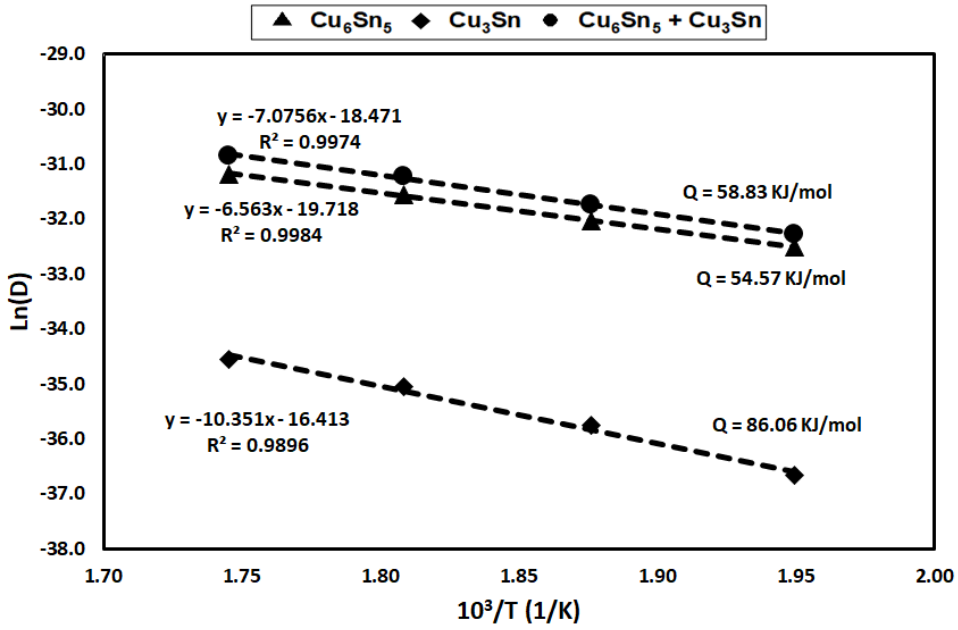


*Figure 5.4 Arrhenius plot for the growth of the IMCs layer after the reflow process*

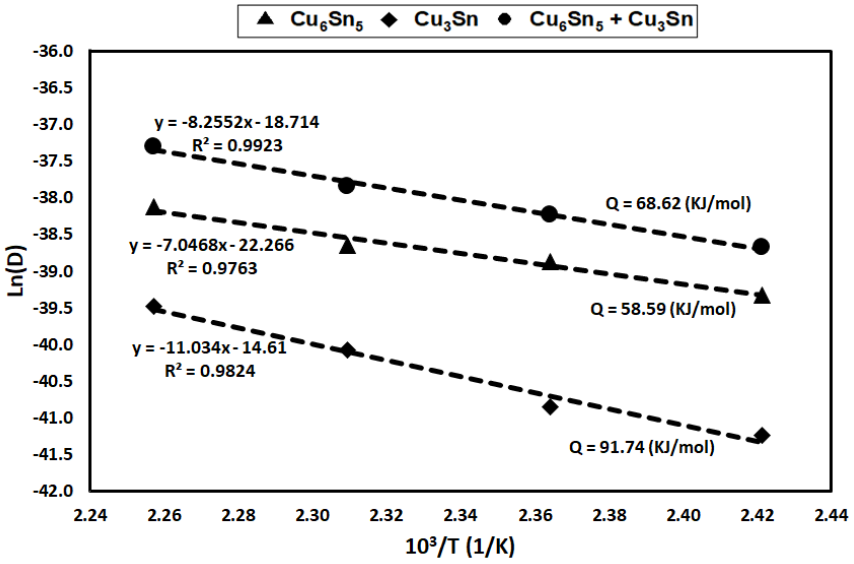


*Figure 5.5 Arrhenius plot for the growth of the IMCs layer after the aging process*

(7) I proved that the change in IMC layer thickness is a diffusion process. I determined the diffusion constant and the activation energy, which can be used to estimate the extent to how the IMC layer courses during aging (Fig. 5.6-5.8)

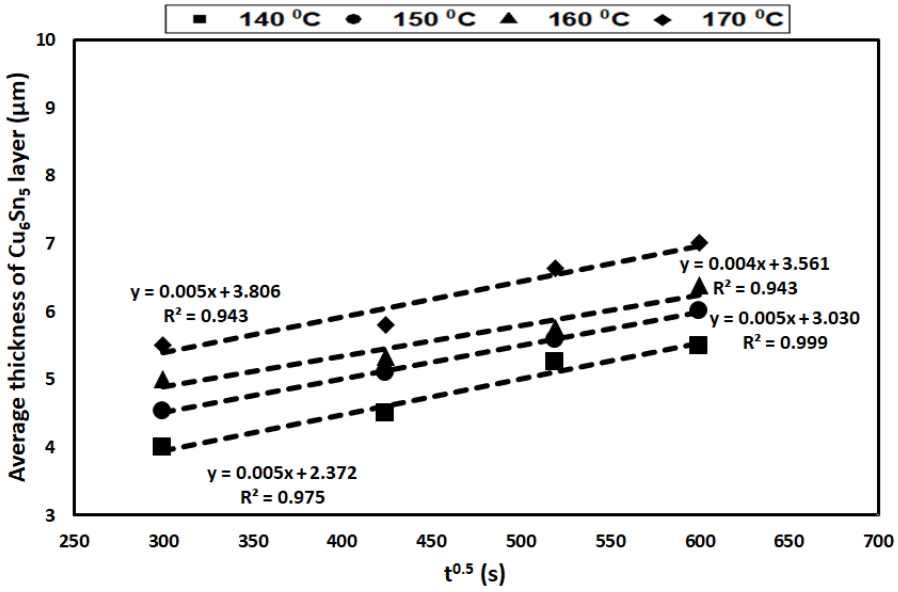


*Figure 5.6 Average thickness of $Cu_6Sn_5$ layer of SAC305/1%SiC composite solder at the different aging temperature*

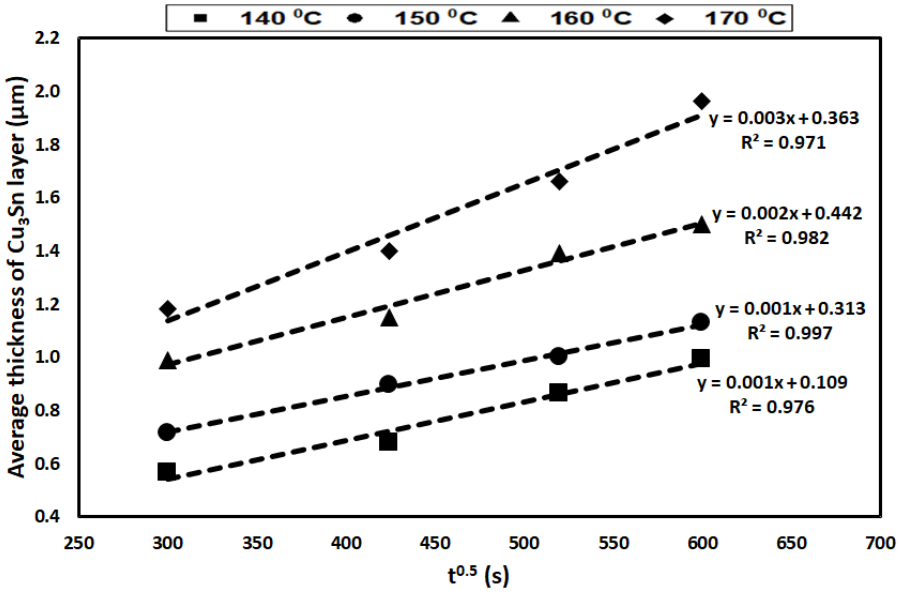


*Figure 5.7 Average thickness of $Cu_3Sn$ IMC layer of SAC305/1%SiC composite at the different aging temperature*

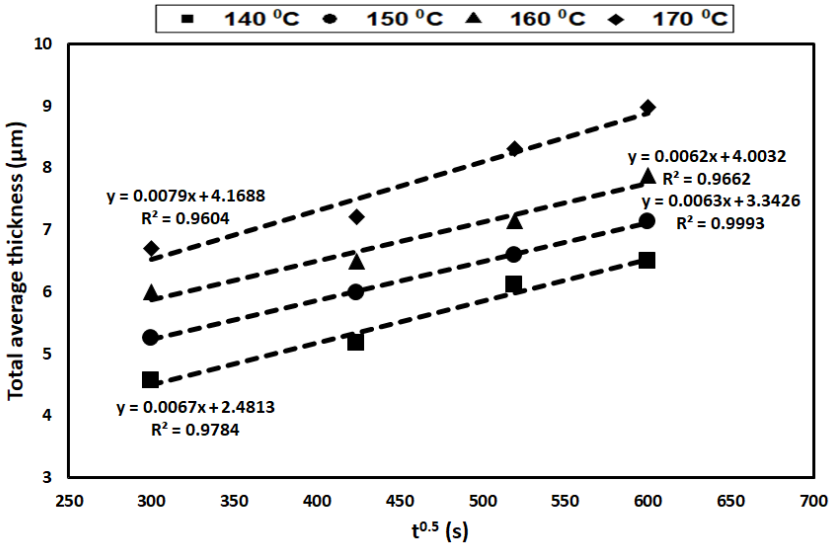


*Figure 5.8 Total Average thickness layer in SAC305/1%SiC composite solder at the different aging temperature*

## Acknowledgements

I would like to take this opportunity to express my sincere gratitude and deep appreciation to my supervisors, Prof. Zoltán Gácsi and Dr. Gergely Gréta at the University of Miskolc, for their valuable guidance, continuous support, and constructive suggestions throughout all my Ph.D. study period.

I am grateful to my independent assessor, Prof. George Kaptay, Prof. Török Tamás, and Dr. Peter Bamuli, for his advice and discussions for the Ph.D. period. Heartfelt thanks are given to the Institute of Physical Metallurgy, Metal Forming, and Nanotechnology for providing me with all the necessary laboratory and a good work environment for carrying out my research.

Deep gratitude is also expressed to "Antal Kerpely Doctoral School of Material Science and Technology" and Prof. Valeria Mertinger in the faculty of Materials Science for providing an opportunity to research the university of Miskolc. My gratitude extends to the I would like to thank Dr. Kovacs Arpad, Dr. Daniel Koncz-Horvath, and Dr. Anna Sycheva for their kind cooperation and scheduling of the SEM investigation.

A special thanks to Mrs. Aniko Markus and Mrs. Napsugar Bodnar for helping with both pre- and post-experimental sample preparation throughout my Ph.D. I show my appreciation to Mr. Dheeraj Varanasi, Dr. Tamas Miko, Zoltan David Gyoker, Dávid Angel, Tamás Bubonyi, Filep Ádám, Dr. Márton Benke, Dr. Zsolt Veres, Daniel Pethő, Mr. Tabish Aftab, and Mr. Raghawendra Pratap Singh Sisodia for their invaluable support. I would like to thanks Mrs. Judit Szabo, Mrs. Agnesz Solczi, Dr. Sveda Maria, Mrs. Nora Orosz-Forizs, and Mrs. Stumpf Eva for their continued and valuable support in the administrative work at the university. Finally, I would like to thank all my colleagues both Hungarian and International for helping, interacting, and supporting my thesis period.

I would like to show my appreciation for the Tempus Public Foundation and Stipendium Hungaricum scholarship program for selecting and providing financial assistance for my wonderful journey in Hungary and Europe. I would like to special thanks to my supervisor Prof. Zoltán Gácsi for providing me a part of nano-GINOP2.3.2-15-2016-00027 "Sustainable operation of the workshop of excellence for the research and development of crystalline and amorphous nanostructured materials" project implemented in the framework of the Szechenyi 2020 program. The realization of this project is supported by the European Union.

Finally, I am grateful for my wife (Mrs. Mamta Pal), daughter (Miss Samridhi Pal), who was a constant support system in my life. A special thanks to, Mrs. Neetu Bajaj and Dr. Vineet Bajaj who constantly support my Ph.D. duration and helped me in all kinds of supports.

## References:


[1] Y.W. Chang, S.H. Chiu, C. Chen, D.J. Yao, Effect of Si-die dimensions on electromigration failure time of flip-chip solder joints, Mater. Chem. Phys. 127 (2011) 85–90. doi:10.1016/j.matchemphys.2011.01.023.

[2] Y. Li, K.S. Moon, C.P. Wong, Electronics without lead, Science (80-. ). 308 (2005) 1419–1420. doi:10.1126/science.1110168.

[3] P.T. Vianco, D.R. Frear, Lead-Bearing Solders, (1993).

[4] M. Abtew, G. Selvaduray, Lead-free solders in microelectronics, Mater. Sci. Eng. R Reports. 27 (2000) 95–141. doi:10.1016/S0927-796X(00)00010-3.

[5] F. Omaç, D. Ozyurek, M. Erer, Investigation of the wetting properties of ternary lead-free solder alloys on copper substrate, Acta Phys. Pol. A. 131 (2017) 165–167. doi:10.12693/APhysPolA.131.165.

[6] A. Sharma, A.K. Srivastava, B. Ahn, Microstructure, Wetting, and Tensile Behaviors of Sn-Ag Alloy Reinforced with Copper-Coated Carbon Nanofibers Produced by the Melting and Casting Route, Metall. Mater. Trans. A Phys. Metall. Mater. Sci. 50 (2019) 5384–5394. doi:10.1007/s11661-019-05439-y.

[7] Binti Ida Umaya, No Titleالإلكتروني الابتزاز.. طفرة على تتغذى جرائم» ال التواصل«, Univ. Nusant. PGRI Kediri. 01 (2017) 1–7. doi:10.12739/NWSA.2017.12.4.2A0123.Erer.

[8] P. Zhang, S. Xue, J. Wang, P. Xue, S. Zhong, W. Long, Effect of nanoparticles addition on the microstructure and properties of lead-free solders: A review, Appl. Sci. 9 (2019). doi:10.3390/app9102044.

[9] A.K. Gain, Y.C. Chan, W.K.C. Yung, Microstructure, thermal analysis and hardness of a Sn-Ag-Cu-1 wt% nano-TiO2 composite solder on flexible ball grid array substrates, Microelectron. Reliab. 51 (2011) 975–984. doi:10.1016/j.microrel.2011.01.006.

[10] M.R. Harrison, M.O. Components, J.H. Vincent, H.A.H. Steen, To cite this document : Lead-free reflow soldering for electronics assembly, (2008).

[11] M. Amagai, Mechanical reliability in electronic packaging, Microelectron. Reliab. 42 (2002) 607–627. doi:10.1016/S0026-2714(02)00037-9.

[12] A.A. El-Daly, A.E. Hammad, Development of high strength Sn-0.7Cu solders with the addition of small amount of Ag and in, J. Alloys Compd. 509 (2011) 8554–8560. doi:10.1016/j.jallcom.2011.05.119.

[13] K. Suganuma, Advances in lead-free electronics soldering, Curr. Opin. Solid State Mater. Sci. 5 (2001) 55–64. doi:10.1016/S1359-0286(00)00036-X.

[14] J. Lau, W. Dauksher, J. Smetana, R. Horsley, D. Shangguan, T. Castello, I. Menis, D. Love, B. Sullivan, Design for lead-free solder joint reliability of high-density packages, Solder. Surf. Mt. Technol. 16 (2004). doi:10.1108/09540910410517013.

[15] G.G. Sozhamannan, S.B. Prabu, Influence of interface compounds on interface bonding characteristics of aluminium and silicon carbide, Mater. Charact. 60 (2009) 986–990. doi:10.1016/j.matchar.2009.04.005.

[16] D. Shangguan, A. Achari, W. Green, Application of Lead-Free Eutectic Sn-Ag Solder in No-Clean Thick Film Electronic Modules, 17 (1994) 603–611.

[17] D. Shang-, Leading the Lead-Free Transition A look at how lead free is changing the assembly landscape . CO IO IT ID IN IT CU IS IO, (n.d.).

[18] A. Fawzy, S.A. Fayek, M. Sobhy, E. Nassr, M.M. Mousa, G. Saad, Effect of ZnO nanoparticles addition on thermal, microstructure and tensile properties of Sn–3.5 Ag–0.5 Cu (SAC355) solder alloy, 24 (2013) 3210–3218. doi:10.1007/s10854-013-1230-2.

[19] J. Shen, Y.C. Chan, Effect of metal/ceramic nanoparticle-doped fluxes on the wettability between Sn-Ag-Cu solder and a Cu layer, J. Alloys Compd. 477 (2009) 909–914. doi:10.1016/j.jallcom.2008.11.015.

[20] L. Wang, D.Q. Yu, S.Q. Han, H.T. Ma, H.P. Xie, The evaluation of the new composite lead free solders with the novel fabricating process, (2004) 50–56.

[21] T.H. Chuang, M.W. Wu, S.Y. Chang, S.F. Ping, L.C. Tsao, Strengthening mechanism of nano-Al 2O 3 particles reinforced Sn3.5Ag0.5Cu lead-free solder, J. Mater. Sci. Mater. Electron. 22 (2011) 1021–1027. doi:10.1007/s10854-010-0253-1.

[22] L.C. Tsao, R.W. Wu, T.H. Cheng, K.H. Fan, R.S. Chen, Effects of nano-Al2O3particles on microstructure and mechanical properties of Sn3.5Ag0.5Cu composite solder ball grid array joints on Sn/Cu pads, Mater. Des. 50 (2013) 774–781. doi:10.1016/j.matdes.2013.03.045.

[23] L.C. Tsao, S.Y. Chang, C.I. Lee, W.H. Sun, C.H. Huang, Effects of nano-Al2O3 additions on microstructure development and hardness of Sn3.5Ag0.5Cu solder, Mater. Des. 31 (2010) 4831–4835. doi:10.1016/j.matdes.2010.04.033.

[24] X. Wang, Y.C. Liu, C. Wei, H.X. Gao, P. Jiang, L.M. Yu, Strengthening mechanism of SiC-particulate reinforced Sn-3.7Ag-0.9Zn lead-free solder, J. Alloys Compd. 480 (2009) 662–

665. doi:10.1016/j.jallcom.2009.02.002.

[25] L.C. Tsao, S.Y. Chang, Effects of Nano-TiO2 additions on thermal analysis, microstructure and tensile properties of Sn3.5Ag0.25Cu solder, Mater. Des. 31 (2010) 990–993. doi:10.1016/j.matdes.2009.08.008.

[26] M.I.I. Ramli, N. Saud, M.A.A.M. Salleh, M.N. Derman, R.M. Said, Microelectronics Reliability Effect of TiO 2 additions on Sn-0 . 7Cu-0 . 05Ni lead-free composite solder, MR. 65 (2016) 255–264. doi:10.1016/j.microrel.2016.08.011.

[27] Y. Wen, X. Zhao, Z. Chen, Y. Gu, Y. Wang, Z. Chen, X. Wang, Reliability enhancement of Sn-1 . 0Ag-0 . 5Cu nano-composite solders by adding multiple sizes of TiO 2 nanoparticles, J. Alloys Compd. 696 (2017) 799–807. doi:10.1016/j.jallcom.2016.12.037.

[28] A.A. El-Daly, A. Fawzy, S.F. Mansour, M.J. Younis, Novel SiC nanoparticles-containing Sn-1.0Ag-0.5Cu solder with good drop impact performance, Mater. Sci. Eng. A. 578 (2013) 62–71. doi:10.1016/j.msea.2013.04.022.

[29] A.A. El-Daly, A. Fawzy, S.F. Mansour, M.J. Younis, Thermal analysis and mechanical properties of Sn-1.0Ag-0.5Cu solder alloy after modification with SiC nano-sized particles, J. Mater. Sci. Mater. Electron. 24 (2013) 2976–2988. doi:10.1007/s10854-013-1200-8.

[30] F. Authors, SAC – xTiO 2 nano-reinforced lead-free solder joint characterizations in ultra-fi ne package assembly, (2018). doi:10.1108/SSMT-04-2017-0011.

[31] P.B.Æ.S.M.L.N.Æ.M. Gupta, Development of lead-free Sn-3 . 5Ag / SnO 2 nanocomposite solders, (2009) 571–576. doi:10.1007/s10854-008-9767-1.

[32] S.M.L. Nai, J.V.M. Kuma, M.E. Alam, X.L. Zhong, P. Babaghorbani, M. Gupta, Using Microwave-Assisted Powder Metallurgy Route and Nano-size Reinforcements to Develop High-Strength Solder Composites, 19 (2010) 335–341. doi:10.1007/s11665-009-9481-z.

[33] P. Liu, P. Yao, J. Liu, Effect of SiC nanoparticle additions on microstructure and microhardness of Sn-Ag-Cu solder alloy, J. Electron. Mater. 37 (2008) 874–879. doi:10.1007/s11664-007-0366-3.

[34] K.M. Kumar, V. Kripesh, A.A.O. Tay, Single-wall carbon nanotube ( SWCNT ) functionalized Sn – Ag – Cu lead-free composite solders, 450 (2008) 229–237. doi:10.1016/j.jallcom.2006.10.123.

[35] B. Zhong, X. Li, M. Gupta, High Strength Lead-Free Composite Solder Materials using, (2005) 1049–1054. doi:10.1002/adem.200500109.

[36] J. Shen, Y.C. Liu, Y.J. Han, Y.M. Tian, H.X. Gao, Strengthening Effects of ZrO 2 Nanoparticles on the Microstructure and Microhardness of, 2006.

[37] T. Fouzder, A. Kumar, Y.C. Chan, A. Sharif, W.K.C. Yung, Microelectronics Reliability Effect of nano Al 2 O 3 additions on the microstructure , hardness and shear strength of eutectic Sn – 9Zn solder on Au / Ni metallized Cu pads, Microelectron. Reliab. 50 (2010) 2051–2058. doi:10.1016/j.microrel.2010.06.013.

[38] Y. Wang, X. Zhao, X. Xie, Y. Gu, Y. Liu, Effects of nano-SiO2 particles addition on the microstructure, wettability, joint shear force and the interfacial IMC growth of Sn3.0Ag0.5Cu solder, J. Mater. Sci. Mater. Electron. 26 (2015) 9387–9395. doi:10.1007/s10854-015-3151-8.

[39] H. Peng, G. Chen, L. Mo, Y.C.C. Fengshun, An investigation on the ZnO retained ratio , microstructural evolution , and mechanical properties of ZnO doped Sn3 . 0Ag0 . 5Cu composite solder joints, J. Mater. Sci. Mater. Electron. 27 (2016) 9083–9093. doi:10.1007/s10854-016-4943-1.

[40] M. Qu, T. Cao, Y. Cui, Z. Jiao, F. Liu, Effect of ZnO micron-particles on properties and intermetallic compound, (2019) 0–7.

[41] T. Fouzder, Y.C.C. Daniel, Influence of cerium oxide ( CeO 2 ) nanoparticles on the microstructure and hardness of tin – silver – copper ( Sn – Ag – Cu ) solders on silver ( Ag ) surface-finished copper ( Cu ) substrates, (2014) 5375–5387. doi:10.1007/s10854-014-2316-1.

[42] T. Fouzder, I. Shafiq, Y.C. Chan, A. Sharif, W.K.C. Yung, Influence of SrTiO 3 nano-particles on the microstructure and shear strength of Sn – Ag – Cu solder on Au / Ni metallized Cu pads, J. Alloys Compd. 509 (2011) 1885–1892. doi:10.1016/j.jallcom.2010.10.081.

[43] Y. Tang, G.Y. Li, Y.C. Pan, joints in reflow process, 554 (2013) 195–203. doi:10.1016/j.jallcom.2012.12.019.

[44] G. Chen, H. Peng, V. V. Silberschmidt, Y.C. Chan, C. Liu, F. Wu, Performance of Sn-3.0Ag-0.5Cu composite solder with TiC reinforcement: Physical properties, solderability and microstructural evolution under isothermal ageing, J. Alloys Compd. 685 (2016) 680–689. doi:10.1016/j.jallcom.2016.05.245.

[45] A. Sharma, B.G. Baek, J.P. Jung, Influence of La2O3 nanoparticle additions on

microstructure, wetting, and tensile characteristics of Sn-Ag-Cu alloy, Mater. Des. 87 (2015) 370–379. doi:10.1016/j.matdes.2015.07.137.

[46] S. Chellvarajoo, M.Z. Abdullah, Microstructure and mechanical properties of Pb-free Sn-3.0Ag-0.5Cu solder pastes added with NiO nanoparticles after reflow soldering process, Mater. Des. 90 (2016) 499–507. doi:10.1016/j.matdes.2015.10.142.

[47] S. Chellvarajoo, M.Z. Abdullah, Z. Samsudin, Effects of Fe2NiO4 nanoparticles addition into lead free Sn–3.0Ag–0.5Cu solder pastes on microstructure and mechanical properties after reflow soldering process, Mater. Des. 67 (2015) 197–208. doi:10.1016/j.matdes.2014.11.025.

[48] A.A. El-Daly, W.M. Desoky, T.A. Elmosalami, M.G. El-Shaarawy, A.M. Abdraboh, Microstructural modifications and properties of SiC nanoparticles-reinforced Sn-3.0Ag-0.5Cu solder alloy, Mater. Des. 65 (2015) 1196–1204. doi:10.1016/j.matdes.2014.08.058.

[49] G. Chen, F. Wu, C. Liu, V. V. Silberschmidt, Y.C. Chan, Microstructures and properties of new Sn-Ag-Cu lead-free solder reinforced with Ni-coated graphene nanosheets, J. Alloys Compd. 656 (2016) 500–509. doi:10.1016/j.jallcom.2015.09.178.

[50] Z.X. Wang, Thermomechanical response of a lead-free solder reinforced with a shape memory alloy, 54 (2006) 627–632. doi:10.1016/j.scriptamat.2005.10.037.

[51] S.M.L. Nai, J. Wei, M. Gupta, Influence of ceramic reinforcements on the wettability and mechanical properties of novel lead-free solder composites, Thin Solid Films. 504 (2006) 401–404. doi:10.1016/j.tsf.2005.09.057.

[52] S.M.L. Nai, J. Wei, M. Gupta, Lead-Free Solder Reinforced with Multiwalled Carbon Nanotubes, 35 (2006) 1518–1522.

[53] S.M.L. Nai, J. Wei, M. Gupta, Development of lead-free solder composites containing nanosized, 111 (2006) 59–62. doi:10.4028/www.scientific.net/SSP.111.59.

[54] X.L. Zhong, M. Gupta, Development of lead-free Sn-0.7Cu/Al2O3 nanocomposite solders with superior strength, J. Phys. D. Appl. Phys. 41 (2008). doi:10.1088/0022-3727/41/9/095403.

[55] R.S.- Solder, Z.N. Izzati, A.M. Al-bakri, M.A.A.M. Salleh, R. Ahmad, Microstructure and Mechanical Properties of Geopolymer Ceramic Microstructure and Mechanical Properties of Geopolymer Ceramic Reinforced Sn-0 . 7Cu Solder, (2020) 0–5. doi:10.1088/1757-899X/864/1/012041.

[56] L. Wang, Effect of Y 2 O 3 particles on microstructure formation and shear properties of Sn-58Bi solder, (2010) 1046–1054. doi:10.1007/s10854-009-0025-y.

[57] A. Sharma, S. Bhattacharya, S. Das, Fabrication of Sn-Ag / CeO 2 Electro-Composite Solder by Pulse Electrodeposition, 44 (2013) 5587–5601. doi:10.1007/s11661-013-1894-5.

[58] Z. Zhao, L. Liu, H. Seok, J. Cai, Q. Wang, Y. Wang, G. Zou, Microelectronics Reliability Effect of nano-Al 2 O 3 reinforcement on the microstructure and reliability of Sn – 3 . 0Ag – 0 . 5Cu solder joints, MR. 60 (2016) 126–134. doi:10.1016/j.microrel.2016.03.005.

[59] Y. Gu, X. Zhao, Y. Li, Y. Liu, Y. Wang, Z. Li, Effect of nano-Fe 2 O 3 additions on wettability and interfacial intermetallic growth of low-Ag content Sn – Ag – Cu solders on Cu substrates, 627 (2015) 39–47. doi:10.1016/j.jallcom.2014.12.024.

[60] G. Chen, H. Peng, V. V Silberschmidt, Y.C. Chan, C. Liu, F. Wu, Performance of Sn e 3 . 0Ag e 0 . 5Cu composite solder with TiC reinforcement : Physical properties , solderability and microstructural evolution under isothermal ageing, J. Alloys Compd. 685 (2016) 680–689. doi:10.1016/j.jallcom.2016.05.245.

[61] T.T. Dele-afolabi, M.A.A. Hanim, O.J. Ojo-kupoluyi, R. Calin, Impact of different isothermal aging conditions on the IMC layer growth and shear strength of MWCNT-reinforced Sn e 5Sb solder composites on Cu substrate, J. Alloys Compd. 808 (2019) 151714. doi:10.1016/j.jallcom.2019.151714.

[62] H. Sun, Y.C. Chan, F. Wu, Materials Science & Engineering A Effect of CNTs and Ni coated CNTs on the mechanical performance of Sn57 . 6Bi0 . 4Ag BGA solder joints, Mater. Sci. Eng. A. 656 (2016) 249–255. doi:10.1016/j.msea.2016.01.045.

[63] D. Ma, P. Wu, Improved microstructure and mechanical properties for Sn58Bi0 . 7Zn solder joint by addition of graphene nanosheets, J. Alloys Compd. 671 (2016) 127–136. doi:10.1016/j.jallcom.2016.02.093.

[64] M. Yang, H. Ji, S. Wang, Y. Ko, C. Lee, J. Wu, M. Li, Effects of Ag content on the interfacial reactions between liquid Sn e Ag e Cu solders and Cu substrates during soldering, J. Alloys Compd. 679 (2016) 18–25. doi:10.1016/j.jallcom.2016.03.177.

[65] S.K. Das, A. Sharif, Y.C. Chan, N.B. Wong, W.K.C. Yung, Influence of small amount of Al and Cu on the microstructure , microhardness and tensile properties of Sn – 9Zn binary eutectic solder alloy, 481 (2009) 167–172. doi:10.1016/j.jallcom.2009.03.017.

[66] B. Ali, M. Faizul, M. Sabri, I. Jauhari, N.L. Sukiman, Microelectronics Reliability Impact

toughness , hardness and shear strength of Fe and Bi added, MR. 63 (2016) 224–230. doi:10.1016/j.microrel.2016.05.004.

[67] Q.B. Tao, L. Benabou, L. Vivet, V.N. Le, F.B. Ouezdou, Materials Science & Engineering A Effect of Ni and Sb additions and testing conditions on the mechanical properties and microstructures of lead-free solder joints, 669 (2016) 403–416. doi:10.1016/j.msea.2016.05.102.

[68] Q.B. Tao, L. Benabou, V.N. Le, H. Hwang, D.B. Luu, Viscoplastic characterization and post-rupture microanalysis of a novel lead-free solder with small additions of Bi , Sb and Ni, 694 (2017) 892–904. doi:10.1016/j.jallcom.2016.10.025.

[69] Z.L. Ma, S.A. Belyakov, C.M. Gourlay, Effects of cobalt on the nucleation and grain re fi nement of Sn-3Ag- 0 . 5Cu solders, 682 (2016) 326–337. doi:10.1016/j.jallcom.2016.04.265.

[70] L. Zhang, J. Han, Y. Guo, C. He, Materials Science & Engineering A Effect of rare earth Ce on the fatigue life of SnAgCu solder joints in WLCSP device using FEM and experiments, Mater. Sci. Eng. A. 597 (2014) 219–224. doi:10.1016/j.msea.2013.12.098.

[71] L. Gao, S. Xue, L. Zhang, Z. Sheng, F. Ji, W. Dai, S.L. Yu, G. Zeng, Effect of alloying elements on properties and microstructures of SnAgCu solders, Microelectron. Eng. 87 (2010) 2025–2034. doi:10.1016/j.mee.2010.04.007.

[72] Z. Yang, W. Zhou, P. Wu, Effects of Ni-coated Carbon Nanotubes addition on the electromigration of Sn – Ag – Cu solder joints, J. Alloys Compd. 581 (2013) 202–205. doi:10.1016/j.jallcom.2013.07.058.

[73] L. Xu, X. Chen, H. Jing, L. Wang, J. Wei, Y. Han, Materials Science & Engineering A Design and performance of Ag nanoparticle-modi fi ed graphene / SnAgCu lead-free solders, Mater. Sci. Eng. A. 667 (2016) 87–96. doi:10.1016/j.msea.2016.04.084.

[74] J. Liu, C. Andersson, Y. Gao, Q. Zhai, supfaearmagnetism , pexuitraor b anda, in: 2008.

[75] L. Ma, Y. Zuo, S. Liu, F. Guo, A. Lee, K.N. Subramanian, Whisker growth behaviors in POSS-silanol modi fi ed Sn3 . 0Ag0 . 5Cu composite solders, J. Alloys Compd. 657 (2016) 400–407. doi:10.1016/j.jallcom.2015.09.266.

[76] K. Abdullahi, A.S. Hakeem, C. Suryanarayana, T. Laoui, S. Nouari, Synthesis , characterisation and mechanical properties of SiC reinforced Al based nanocomposites processed by MA and SPS, 56 (2013) 149–157. doi:10.1179/1743290112Y.0000000029.

[77] A.A. El-daly, M. Abdelhameed, M. Hashish, A.M. Eid, Synthesis of Al / SiC nanocomposite and evaluation of its mechanical properties using pulse echo overlap method, J. Alloys Compd. 542 (2012) 51–58. doi:10.1016/j.jallcom.2012.07.102.

[78] K.D. Woo, D.L. Zhang, Fabrication of Al – 7wt % Si – 0 . 4wt % Mg / SiC nanocomposite powders and bulk nanocomposites by high energy ball milling and powder metallurgy, 4 (2004) 175–178. doi:10.1016/j.cap.2003.11.002.

[79] L.C. Tsao, An investigation of microstructure and mechanical properties of novel Sn3 . 5Ag0 . 5Cu – X TiO 2 composite solders as functions of alloy composition and cooling rate, Mater. Sci. Eng. A. 529 (2011) 41–48. doi:10.1016/j.msea.2011.08.053.

[80] O. Mokhtari, A. Roshanghias, R. Ashayer, H.R. Kotadia, F. Khomamizadeh, A.H. Kokabi, M.P. Clode, M. Miodownik, S.H. Mannan, Disabling of nanoparticle effects at increased temperature in nanocomposite solders, J. Electron. Mater. 41 (2012) 1907–1914. doi:10.1007/s11664-012-1976-y.

[81] Z. Yang, W. Zhou, P. Wu, Effects of Ni-coated Carbon Nanotubes addition on the electromigration of Sn-Ag-Cu solder joints, J. Alloys Compd. 581 (2013) 202–205. doi:10.1016/j.jallcom.2013.07.058.

[82] Z. Yang, W. Zhou, P. Wu, Effects of Ni-coated carbon nanotubes addition on the microstructure and mechanical properties of Sn-Ag-Cu solder alloys, Mater. Sci. Eng. A. 590 (2014) 295–300. doi:10.1016/j.msea.2013.10.008.

[83] Z. Fathian, A. Maleki, B. Niroumand, Synthesis and characterization of ceramic nanoparticles reinforced lead-free solder, Ceram. Int. 43 (2017) 5302–5310. doi:10.1016/j.ceramint.2017.01.067.

[84] C. Suryanarayana, N. Al-Aqeeli, Mechanically alloyed nanocomposites, Prog. Mater. Sci. 58 (2013) 383–502. doi:10.1016/j.pmatsci.2012.10.001.

[85] C. Suryanarayana, Mechanical alloying and milling, in: Mech. Alloy. Milling, 2004: pp. 1–472. doi:10.4150/kpmi.2006.13.5.371.

[86] C. Suryanarayana, E. Ivanov, V. V. Boldyrev, The science and technology of mechanical alloying, Mater. Sci. Eng. A. 304–306 (2001) 151–158. doi:10.1016/S0921-5093(00)01465-9.

[87] A. Upadhyaya, G. Sethi, Effect of heating mode on the densification and microstructural homogenization response of premixed bronze, 56 (2007) 469–472.

doi:10.1016/j.scriptamat.2006.11.031.

[88] M. Gupta, W.L.E. Wong, Enhancing overall mechanical performance of metallic materials using two-directional microwave assisted rapid sintering, 52 (2005) 479–483. doi:10.1016/j.scriptamat.2004.11.006.

[89] W.L.E. Wong, S. Karthik, M. Gupta, Development of high performance Mg – Al 2 O 3 composites containing Al 2 O 3 in submicron length scale using microwave assisted rapid sintering, 21 (2005) 1063–1071. doi:10.1179/174328405X51758.

[90] H. Mavoori, S. Jin, New , Creep-Resistant , Low Melting Point Solders with Ultrafine Oxide Dispersions, 27 (1998) 1216–1222.

[91] Y. Shi, J. Liu, Y. Yan, Z. Xia, Y. Lei, F.U. Guo, X. Li, Creep Properties of Composite Solders Reinforced with Nano- and Microsized Particles, 37 (2008) 507–514. doi:10.1007/s11664-007-0208-3.

[92] A.A. El-Daly, A. Fawzy, S.F. Mansour, M.J. Younis, Novel SiC nanoparticles-containing Sn-1.0Ag-0.5Cu solder with good drop impact performance, Mater. Sci. Eng. A. 578 (2013) 62–71. doi:10.1016/j.msea.2013.04.022.

[93] Z. Fathian, A. Maleki, B. Niroumand, Synthesis and characterization of ceramic nanoparticles reinforced lead-free solder, Ceram. Int. 43 (2017) 5302–5310. doi:10.1016/j.ceramint.2017.01.067.

[94] H. Kaser, A. Taherizadeh, A. Maleki, A. Ghaei, Development of an aluminum / amorphous nano-SiO 2 composite using powder metallurgy and hot extrusion processes, Ceram. Int. 43 (2017) 14582–14592. doi:10.1016/j.ceramint.2017.06.057.

[95] J.S.Æ.Y.C.L.Æ.H.X. Gao, In situ nanoparticulate-reinforced lead-free Sn – Ag composite prepared by rapid solidification, (2007) 463–468. doi:10.1007/s10854-006-9056-9.

[96] S. Hwang, J. Lee, Z. Lee, Microstructure of a Lead-Free Composite Solder Produced by an In-Situ Process, 31 (2002) 5–9.

[97] G. Kumar, K.N. Prabhu, Review of non-reactive and reactive wetting of liquids on surfaces, 133 (2007) 61–89. doi:10.1016/j.cis.2007.04.009.

[98] S. Vaynman, M.E. Fine, DEVELOPMENT OF FLUXES FOR LEAD-FREE SOLDERS CONTAINING ZINC, 41 (1999) 1269–1271.

[99] J.I.D. Bernardin, I. Mudawar, F. Christopher, E.I. Fransesi, Contact angle temperature dependence for water droplets on practical aluminum surfaces, 40 (1997) 1017–1033.

[100] V.H. López, A.R. Kennedy, Flux-assisted wetting and spreading of Al on TiC, 298 (2006) 356–362. doi:10.1016/j.jcis.2005.12.040.

[101] D.C. Lin, G.X. Wang, T.S. Srivatsan, M. Al-hajri, M. Petraroli, Influence of titanium dioxide nanopowder addition on microstructural development and hardness of tin – lead solder, 57 (2003) 3193–3198. doi:10.1016/S0167-577X(03)00023-5.

[102] S.M.L. Nai, J. Wei, M. Gupta, Effect of Carbon Nanotubes on the Shear Strength and Electrical Resistivity of a Lead-Free Solder, 37 (2008) 515–522. doi:10.1007/s11664-008-0379-6.

[103] M. Science, E.A. Interactive, No Title, n.d.

[104] D. Lin, G.X. Wang, T.S. Srivatsan, M. Al-hajri, M. Petraroli, The inf luence of copper nanopowders on microstructure and hardness of lead – tin solder, 53 (2002) 333–338.

[105] S. Zhang, Q. Chen, Composites : Part B Fabrication of MWCNT incorporated Sn – Bi composite, Compos. PART B. 58 (2014) 275–278. doi:10.1016/j.compositesb.2013.10.044.

[106] Y. Lei, Æ.F. Guo, Æ.X. Li, Creep property of composite solders reinforced by nano-sized particles, (2008) 349–356. doi:10.1007/s10854-007-9327-0.

[107] A. Sharma, H.R. Sohn, J.P. Jung, Effect of Graphene Nanoplatelets on Wetting, Microstructure, and Tensile Characteristics of Sn-3.0Ag-0.5Cu (SAC) Alloy, Metall. Mater. Trans. A Phys. Metall. Mater. Sci. 47 (2016) 494–503. doi:10.1007/s11661-015-3214-8.

[108] A. Sharma, A.K. Srivastava, B. Ahn, Microstructure, Wetting, and Tensile Behaviors of Sn-Ag Alloy Reinforced with Copper-Coated Carbon Nanofibers Produced by the Melting and Casting Route, Metall. Mater. Trans. A. 50 (2019) 5384–5394. doi:10.1007/s11661-019-05439-y.

[109] J. Lee, D. Park, J. Heo, Y. Lee, D. Shin, Y. Kim, REFLOW CHARACTERISTICS OF Sn-Ag MATRIX IN-SITU COMPOSITE SOLDERS, 42 (2000) 827–831.

[110] S.M.L. Nai, J. Wei, M. Gupta, Improving the performance of lead-free solder reinforced with multi-walled carbon nanotubes, 423 (2006) 166–169. doi:10.1016/j.msea.2005.10.072.

[111] M.A.A.M. Salleh, S.D. Mcdonald, C.M. Gourlay, H. Yasuda, K. Nogita, Suppression of Cu 6 Sn 5 in TiO 2 reinforced solder joints after multiple re fl ow cycles, 108 (2016) 418–428. doi:10.1016/j.matdes.2016.06.121.

[112] X. Zhao, Y. Wen, Y. Li, Y. Liu, Y. Wang, Journal of Alloys and Compounds, 662 (2016) 272–282. doi:10.1016/j.jallcom.2015.11.213.

[113] E.A. Eid, A.N. Fouda, E.M. Duraia, Materials Science & Engineering A Effect of adding 0 . 5 wt % ZnO nanoparticles , temperature and strain rate on tensile properties of Sn – 5 . 0 wt % Sb – 0 . 5 wt % Cu ( SSC505 ) lead free solder alloy, Mater. Sci. Eng. A. 657 (2016) 104–114. doi:10.1016/j.msea.2016.01.081.

[114] S. Xu, Y. Cheong, K. Zhang, K.C. Yung, Interfacial intermetallic growth and mechanical properties of carbon nanotubes reinforced Sn3 . 5Ag0 . 5Cu solder joint under current stressing, J. Alloys Compd. 595 (2014) 92–102. doi:10.1016/j.jallcom.2014.01.083.

[115] Y.D. Han, H.Y. Jing, S.M.L. Nai, L.Y. Xu, C.M. Tan, J. Wei, Effect of Ni-coated carbon nanotubes on interfacial intermetallic layer growth, Proc. Electron. Packag. Technol. Conf. EPTC. (2009) 292–295. doi:10.1109/EPTC.2009.5416534.

[116] S. Chellvarajoo, M.Z. Abdullah, C.Y. Khor, Effects of diamond nanoparticles reinforcement into lead-free Sn-3.0Ag-0.5Cu solder pastes on microstructure and mechanical properties after reflow soldering process, Mater. Des. 82 (2015) 206–215. doi:10.1016/j.matdes.2015.05.065.

[117] L. Zhang, K.N. Tu, Structure and properties of lead-free solders bearing micro and nano particles, Mater. Sci. Eng. R Reports. 82 (2014) 1–32. doi:10.1016/j.mser.2014.06.001.

[118] M. Amagai, A study of nanoparticles in Sn – Ag based lead free solders, 48 (2008) 1–16. doi:10.1016/j.microrel.2007.05.004.

[119] D.Q. Yu, L. Wang, C.M.L. Wu, C.M.T. Law, The formation of nano-Ag 3 Sn particles on the intermetallic compounds during wetting reaction, 389 (2005) 153–158. doi:10.1016/j.jallcom.2004.08.017.

[120] A.A. El-daly, A.E. Hammad, A. Fawzy, D.A. Nasrallh, Microstructure , mechanical properties , and deformation behavior of Sn – 1 . 0Ag – 0 . 5Cu solder after Ni and Sb additions, J. Mater. 43 (2013) 40–49. doi:10.1016/j.matdes.2012.06.058.

[121] A.K. Gain, L. Zhang, Materialia The effects of TiO 2 nanoparticles addition on the thermal shock resistance , shear strength and IMC layer growth of SAC305 alloy, Materialia. 3 (2018) 64–73. doi:10.1016/j.mtla.2018.10.009.

[122] M. Schaefer, R.A. Fournelle, J.I.N. Liang, Theory for Intermetallic Phase Growth Between Cu and Liquid Sn-Pb Solder Based on Grain Boundary Diffusion Control, di (1998) 1167–1176.

[123] Z. Wu, L. Liu, B. Shen, Y. Wu, Y. Deng, C. Zhong, W. Hu, Mechanical behavior of α-

Al2O3-coated SiC particle reinforced nickel matrix composites, J. Alloys Compd. 570 (2013) 81–85. doi:10.1016/j.jallcom.2013.03.125.

[124] R. Kolenak, M. Chachula, P. Sebo, M. Kolenakova, Wettability and shear strength of active Sn2Ti solder on Al 2O3 ceramics, Solder. Surf. Mt. Technol. 23 (2011) 224–228. doi:10.1108/09540911111169066.

[125] Y. Tang, G.Y. Li, Y.C. Pan, Effects of TiO2 nanoparticles addition on microstructure, microhardness and tensile properties of Sn-3.0Ag-0.5Cu-xTiO2 composite solder, Mater. Des. 55 (2014) 574–582. doi:10.1016/j.matdes.2013.10.033.

[126] M.I.I. Ramli, N. Saud, M.A.A.M. Salleh, M.N. Derman, R.M. Said, Effect of TiO2 additions on Sn-0.7Cu-0.05Ni lead-free composite solder, Microelectron. Reliab. 65 (2016) 255–264. doi:10.1016/j.microrel.2016.08.011.

[127] I. Martin, Precipitation Hardening, (n.d.).

[128] H. Mughrabi, 1 Introductory Chapter : Microstructure and Mechanical Properties, (n.d.).

[129] C. Yu, J. Lee, W. Chen, J. Duh, Enhancement of the impact toughness in Sn – Ag – Cu / Cu solder joints via modifying the microstructure of solder alloy, Mater. Lett. 119 (2014) 20–23. doi:10.1016/j.matlet.2013.12.088.

[130] X. Hu, T. Xu, L.M. Keer, Y. Li, X. Jiang, Materials Science & Engineering A Microstructure evolution and shear fracture behavior of aged Sn3Ag0 . 5Cu / Cu solder joints, Mater. Sci. Eng. A. 673 (2016) 167–177. doi:10.1016/j.msea.2016.07.071.

[131] X. Tu, D. Yi, J. Wu, B. Wang, In fl uence of Ce addition on Sn-3 . 0Ag-0 . 5Cu solder joints : Thermal behavior , microstructure and mechanical properties, J. Alloys Compd. 698 (2017) 317–328. doi:10.1016/j.jallcom.2016.12.191.

[132] J.W.S. Xue, Recent progress of Sn – Ag – Cu lead-free solders bearing alloy elements and nanoparticles in electronic packaging, J. Mater. Sci. Mater. Electron. 27 (2016) 12729–12763. doi:10.1007/s10854-016-5407-3.

[133] L.C. Tsao, R.W. Wu, T. Cheng, K. Fan, R.S. Chen, Effects of nano-Al 2 O 3 particles on microstructure and mechanical properties of Sn3 . 5Ag0 . 5Cu composite solder ball grid array joints on Sn / Cu pads, 50 (2013) 774–781. doi:10.1016/j.matdes.2013.03.045.

[134] D.Q. Yu, H.P. Xie, L. Wang, Investigation of interfacial microstructure and wetting property of newly developed Sn – Zn – Cu solders with Cu substrate, 385 (2004) 119–125. doi:10.1016/j.jallcom.2004.04.129.

[135] N.S.M. Zaimi, M.A.A.M. Salleh, A.M. Mustafa Al Bakri, R.M. Said, N. Saud, Influence of non-metallic particles addition on wettability, intermetallic compound formation and microhardness of sn-0.7cu lead free solder paste, Solid State Phenom. 280 SSP (2018) 169–174. doi:10.4028/www.scientific.net/SSP.280.169.

[136] R.M. Said, N. Saud, M. Arif, A. Mohd, M.N. Derman, M. Izrul, I. Ramli, N.M. Nasir, Effect of SiC Particles Addition on the Wettability and Intermetallic Compound Layer Formation of Sn-Cu-Ni ( SN100C ) Solder Paste, (2015) 546–550. doi:10.4028/www.scientific.net/AMM.754-755.546.

[137] M.R. Vaezi, S.K. Sadrnezhaad, L. Nikzad, Electrodeposition of Ni – SiC nano-composite coatings and evaluation of wear and corrosion resistance and electroplating characteristics, 315 (2008) 176–182. doi:10.1016/j.colsurfa.2007.07.027.

[138] E.A. Pavlatou, M. Stroumbouli, P. Gyftou, N. Spyrellis, Hardening effect induced by incorporation of SiC particles in nickel electrodeposits, (2006) 385–394. doi:10.1007/s10800-005-9082-y.

[139] A.F. Zimmerman, G. Palumbo, K.T. Aust, U. Erb, Mechanical properties of nickel silicon carbide nanocomposites, 328 (2002) 137–146.

[140] Z. Ahmad, Z. Ahmad, Chapter 7 – Coatings, in: Princ. Corros. Eng. Corros. Control, 2006: pp. 382–437. doi:10.1016/B978-075065924-6/50008-8.

[141] G. Jiaqiang, L. Lei, W. Yating, S. Bin, H. Wenbin, Electroless Ni – P – SiC composite coatings with superfine particles, 200 (2006) 5836–5842. doi:10.1016/j.surfcoat.2005.08.134.

[142] H. Arik, Effect of mechanical alloying process on mechanical properties of α-Si3N4 reinforced aluminum-based composite materials, Mater. Des. 29 (2008) 1856–1861. doi:10.1016/j.matdes.2008.03.010.

[143] No Title, (2016).

[144] No Title, n.d.

[145] X.L. Zhong, M. Gupta, Development of lead-free Sn – 0 . 7Cu / Al 2 O 3 nanocomposite solders with superior strength X L Zhong and M Gupta, 095403 (n.d.). doi:10.1088/0022-3727/41/9/095403.

[146] P.A. Karnezis, G. Durrant, B. Cantor, Composites Characterization of Reinforcement Distribution inCast Al-Alloy / SiC p, Mater. Charact. 40 (1998) 97–109.

[147] C. Igathinathane, L.O. Pordesimo, E.P. Columbus, W.D. Batchelor, S.R. Methuku, Shape identification and particles size distribution from basic shape parameters using ImageJ, Comput. Electron. Agric. 63 (2008) 168–182. doi:10.1016/j.compag.2008.02.007.

[148] T.Y. Kang, Y.Y. Xiu, C.Z. Liu, L. Hui, J.J. Wang, W.P. Tong, Bismuth segregation enhances intermetallic compound growth in SnBi/Cu microelectronic interconnect, J. Alloys Compd. 509 (2011) 1785–1789. doi:10.1016/j.jallcom.2010.10.040.

[149] K.N. Tu, C u / S n interfacial reactions' thin-film case versus bulk c a s e, 46 (1996) 217–223.

[150] P.T. Vianco, P.F. Hlava, A.C. Kilgo, Intermetallic Compound Layer Formation Between Copper and Hot-Dipped 100In, 501n-50Sn, 100Sn, and 63Sn-37Pb Coatings, 23 (1994).

[151] D.R. Flanders, E.G. Jacobs, R.F. Pinizzotto, Activation Energies of Intermetallic Growth of Sn-Ag Eutectic Solder on Copper Substrates, 26 (1997).

[152] S. Choi, T.R. Bieler, J.P. Lucas, K.N. Subramanian, Characterization of the Growth of Intermetallic Interfacial Layers of Sn-Ag and Sn-Pb Eutectic Solders and Their Composite Solders on Cu Substrate During Isothermal Long-Term Aging, (1999) 1209–1215.

[153] J. Gong, C. Liu, P. Conway, V. V Silberschmidt, Initial formation of CuSn intermetallic compounds between molten SnAgCu solder and Cu substrate, Scr. Mater. 60 (2009) 333–335. doi:10.1016/j.scriptamat.2008.10.029.

[154] T.Y. Kang, Y.Y. Xiu, L. Hui, J.J. Wang, W.P. Tong, C.Z. Liu, Effect of Bismuth on Intermetallic Compound Growth in Lead Free Solder/Cu Microelectronic Interconnect, J. Mater. Sci. Technol. 27 (2011) 741–745. doi:10.1016/S1005-0302(11)60136-9.

[155] C.H. Raeder, L.E. Felton, V.A. Tanzi, The Effect of Aging on Microstructure , Room Temperature Deformation , and Fracture of Sn-Bi / Cu Solder Joints, 23 (1994).

[156] H.L.J. Pang, K.H. Tan, X.Q. Shi, Z.P. Wang, Microstructure and intermetallic growth effects on shear and fatigue strength of solder joints subjected to thermal cycling aging, 307 (2001) 42–50.

[157] K. Chang, K. Chiang, Aging Study on Interfacial Microstructure and Solder-Ball Shear Strength of a Wafer-Level Chip-Size Package with Au / Ni Metallization on a Cu Pad, 33 (2004) 1373–1380.

[158] A.K. Gain, Y.C. Chan, Growth mechanism of intermetallic compounds and damping properties of Sn-Ag-Cu-1 wt% nano-ZrO2composite solders, Microelectron. Reliab. 54

(2014) 945–955. doi:10.1016/j.microrel.2014.01.026.

[159] J.C. Leong, L.C. Tsao, C.J. Fang, C.P. Chu, Effect of nano-TiO 2 addition on the microstructure and bonding strengths of Sn3 . 5Ag0 . 5Cu composite solder BGA packages with immersion Sn surface finish, (2011) 1443–1449. doi:10.1007/s10854-011-0327-8.

[160] L.C.T.M.W.W.S.Y. Chang, Effect of TiO 2 nanoparticles on the microstructure and bonding strengths of Sn0 . 7Cu composite solder BGA packages with immersion Sn surface finish, (2012) 681–687. doi:10.1007/s10854-011-0471-1.

[161] M.A.A. Mohd Salleh, A.M. Mustafa Al Bakri, H. Kamarudin, M. Bnhussain, M. h. Zan Hazizi, F. Somidin, Solderability of Sn-0.7Cu/Si3N4 lead-free composite solder on Cu-substrate, Phys. Procedia. 22 (2011) 299–304. doi:10.1016/j.phpro.2011.11.047.

[162] M. Qu, T. Cao, Y. Cui, Z. Jiao, F. Liu, Effect of ZnO micron-particles on properties and intermetallic compound layers of a Sn3.0Ag0.5Cu solder, Jpn. J. Appl. Phys. 58 (2019) SHHA04. doi:10.7567/1347-4065/ab1e38.

[163] S.M.L. Nai, J. Wei, M. Gupta, Interfacial intermetallic growth and shear strength of lead-free composite solder joints, J. Alloys Compd. 473 (2009) 100–106. doi:10.1016/j.jallcom.2008.05.070.

[164] Y. Gu, X. Zhao, Y. Li, Y. Liu, Y. Wang, Z. Li, Effect of nano-Fe2O3 additions on wettability and interfacial intermetallic growth of low-Ag content Sn-Ag-Cu solders on Cu substrates, J. Alloys Compd. 627 (2015) 39–47. doi:10.1016/j.jallcom.2014.12.024.

[165] S. Kao, Y. Lin, J. Duh, Controlling Intermetallic Compound Growth in SnAgCu / Ni-P Solder Joints by Nanosized Cu 6 Sn 5 Addition, 35 (2006) 486–493.

[166] D.M. Jacobson, Principles of soldering, 2004. doi:10.5860/choice.42-1581.

[167] S. Kondo, Influence of third elements on growth of Nb3Sn compounds and on global pinning force, 21 (1986) 1509–1516.

[168] J. Shen, Y.C. Chan, S.Y. Liu, Growth mechanism of Ni 3 Sn 4 in a Sn / Ni liquid / solid interfacial reaction, Acta Mater. 57 (2009) 5196–5206. doi:10.1016/j.actamat.2009.07.021.

[169] J. Yoon, B. Noh, Y. Lee, H. Lee, S. Jung, Microelectronics Reliability Effects of isothermal aging and temperature – humidity treatment of substrate on joint reliability of Sn – 3 . 0Ag – 0 . 5Cu / OSP-finished Cu CSP solder joint OSP finished Cu SMD ( Solder Mask Define ) type, Microelectron. Reliab. 48 (2008) 1864–1874. doi:10.1016/j.microrel.2008.07.065.

[170] L.D. Chen, M.L. Huang, S.M. Zhou, Effect of electromigration on intermetallic compound

formation in line-type Cu/Sn/Cu interconnect, J. Alloys Compd. 504 (2010) 535–541. doi:10.1016/j.jallcom.2010.05.158.

[171] C.K. Chung, J.G. Duh, C.R. Kao, Direct evidence for a Cu-enriched region at the boundary between Cu 6Sn5 and Cu3Sn during Cu/Sn reaction, Scr. Mater. 63 (2010) 258–260. doi:10.1016/j.scriptamat.2010.04.011.

[172] C.Z.L.Æ.W. Zhang, Bismuth redistribution induced by intermetallic compound growth in SnBi / Cu microelectronic interconnect, (2009) 149–153. doi:10.1007/s10853-008-3118-8.

[173] M. Yang, M. Li, C. Wang, Intermetallics Interfacial reactions of eutectic Sn3 . 5Ag and pure tin solders with Cu substrates during liquid-state soldering, Intermetallics. 25 (2012) 86–94. doi:10.1016/j.intermet.2012.02.023.

[174] T. Laurila, V. Vuorinen, J.K. Kivilahti, Interfacial reactions between lead-free solders and common base materials, Mater. Sci. Eng. R Reports. 49 (2005) 1–60. doi:10.1016/j.mser.2005.03.001.

[175] K.H. Prakash, T. Sritharan, INTERFACE REACTION BETWEEN COPPER AND MOLTEN TIN – LEAD SOLDERS, 49 (2001) 2481–2489.

[176] N. Mookam, K. Kanlayasiri, Evolution of Intermetallic Compounds between Sn-0.3Ag-0.7Cu Low-silver Lead-free Solder and Cu Substrate during Thermal Aging, J. Mater. Sci. Technol. 28 (2012) 53–59. doi:10.1016/S1005-0302(12)60023-1.

[177] P.T. Vianco, J.A. Rejent, P.F. Hlava, Solid-State Intermetallic Compound Layer Growth Between Copper and 95 . 5Sn-3 . 9Ag-0 . 6Cu Solder, 33 (2004) 991–1004.

[178] J.F. Li, P.A. Agyakwa, C.M. Johnson, Interfacial reaction in Cu/Sn/Cu system during the transient liquid phase soldering process, Acta Mater. 59 (2011) 1198–1211. doi:10.1016/j.actamat.2010.10.053.

[179] T.Y. Lee, W.J. Choi, K.N. Tu, Morphology , kinetics , and thermodynamics of solid-state aging of eutectic SnPb and Pb-free solders ( Sn – 3 . 5Ag , (2002) 291–301.

[180] N. Metals, Effects of bismuth on growth of intermetallic compounds in Sn-Ag-Cu Pb-free solder joints, (2006) 1–5.

## Author publications

### Journal papers

1. **Pal, M. K.**, Gergely, G., Horváth, D. K., & Gácsi, Z, Microstructural investigations and mechanical properties of pure lead-free (Sn–3.0Ag–0.5Cu and Sn–4.0Ag–0.5Cu) solder alloy. **Metallurgical and Materials Engineering**, 24 (1) **(2018)**, 27–36.
2. **Pal, M. K.,** Gergely, G., Horváth, D. K., & Gácsi, Z., influence of ceramic particles on the microstructure and mechanical properties of SAC305 lead-free soldering material, **Arch. Metall. Mater.** 64 (2) **(2019)**, 603–606.
3. Koncz-Horvath, D., Molnar, A., Gergely, G., **Pal, M. K**., & Gacsi, Z., Examination the effect of thermal shock test on SAC solder joints fabricated by THRS and multi-wave soldering techniques. **Resolution and Discovery**, 4(1) **(2019)**, 1–6.
4. **Pal, M. K.**, Gergely, G., Horváth, D. K., & Gácsi, Z., Investigation of the electroless nickel plated SiC particles in SAC305 solder matrix, **Powder metallurgy and metal ceramics**, 58(9–10) **(2020)**, 529–537.
5. **Pal, M. K.,** Gergely, G., Horváth, D. K., & Gácsi, Z., Characterization of the interface between ceramics reinforcement and lead-free solder matrix, **Surfaces and Interfaces**, 20(3) **(2020),** 100576.
6. **Pal, M. K.**, Gergely, G., Horváth, D. K., & Gácsi, Z., Distribution and microstructure analysis of ceramic particles in the lead-free solder matrix, **Crystal Research and Technology**, 55(10) **(2020)**, 2000123**.**
7. **Pal, M. K.**, Gergely, G., Horváth, D. K., & Gácsi, Z., Investigation of microstructure and wetting behavior of Sn-3.0Ag-0.5Cu (SAC305) lead–free solder with additions of 1.0 wt. % SiC on copper substrate, **Intermetallics**,128 **(2021)** 106991.

### Conference presentations

1. **Pal, M. K**., Gergely, G., Horváth, D. K., & Gácsi, Z., Comparison of different SAC solders, XXI. Tavaszi Szél Konferencia 2018 május 03. – 2018. május 6, Széchenyi István Egyetem, Győr, Hungary **(Oral).**

2. **Pal, M. K.**, Gergely, G., Horváth, D. K., & Gácsi, Z., Fabrication of solder material by powder metallurgy route, XXI. Tavaszi Szél Konferencia 2018 május 03. – 2018. május 6, Széchenyi István Egyetem, Győr, Hungary **(Oral)**.
3. **Pal, M. K.**, Gergely, G., Horváth, D. K., & Gácsi, Z., Investigating the microstructural and mechanical properties of pure lead-free soldering materials (SAC305 & SAC405), XVI.PhD–2018, Conference organized by Professors for European Hungary Association, Budapest **(Oral)**.
4. **Pal, M. K.**, Gergely, G., Horváth, D. K., & Gácsi, Z., Influence of ceramic nanoparticles on the microstructure and Mechanical Properties of SAC305 & SAC405, 15th International Symposium on Novel and Nano Materials, July 1(Sun.)-July 6(Fri.), 2018, Tivoli Oriente, Lisbon, Portugal **(Oral)**.
5. **Pal, M. K.**, Gergely, G., Horváth, D. K., & Gácsi, Z., Preparation of Ni-coated SiC ceramic powders by electroless plating method, 7th International Scientific Conference on Advances in Mechanical Engineering (ISCAME), 7-8 November 2019, Debrecen, Hungary **(Oral)**.
6. **Pal, M. K.**, Gergely, G., Horváth, D. K., & Gácsi, Z., Investigation of the electroless Nickel-plated SiC particles in SAC305 solder matrix, $11^{th}$ international conference on materials science & engineering, 13-16 March 2019, Organised by Transylvania University Brasov, Romania **(Oral)**.